

1986

## Tectonics of the Juan Fernandez Microplate and Nazca-Antarctic Plate Boundary

Sandra Anderson-Fontana  
*University of Rhode Island*

Follow this and additional works at: <https://digitalcommons.uri.edu/theses>

Terms of Use

All rights reserved under copyright.

---

### Recommended Citation

Anderson-Fontana, Sandra, "Tectonics of the Juan Fernandez Microplate and Nazca-Antarctic Plate Boundary" (1986). *Open Access Master's Theses*. Paper 1172.  
<https://digitalcommons.uri.edu/theses/1172>

This Thesis is brought to you by the University of Rhode Island. It has been accepted for inclusion in Open Access Master's Theses by an authorized administrator of DigitalCommons@URI. For more information, please contact [digitalcommons-group@uri.edu](mailto:digitalcommons-group@uri.edu). For permission to reuse copyrighted content, contact the author directly.

TECTONICS OF THE JUAN FERNANDEZ MICROPLATE  
AND NAZCA-ANTARCTIC PLATE BOUNDARY  
IN THE SOUTHEASTERN PACIFIC

BY

SANDRA ANDERSON-FONTANA

A THESIS SUBMITTED IN PARTIAL FULFILLMENT OF THE  
REQUIREMENT FOR THE DEGREE OF  
MASTER OF SCIENCE  
IN  
OCEANOGRAPHY

UNIVERSITY OF RHODE ISLAND

1986

MASTER OF SCIENCE THESIS

OF

SANDRA ANDERSON-FONTANA

APPROVED

Thesis Committee

Major Professor

Robert H. Larson

Robert S. Platt

Richard H. Foulds

A. Amick

DEAN OF THE GRADUATE SCHOOL

UNIVERSITY OF RHODE ISLAND

1986

## ABSTRACT

In the first part of this study, magnetic and bathymetric data from an R/V Endeavor survey are combined with earthquake mechanism studies to produce a tectonic model for the Juan Fernandez microplate at the Pacific-Nazca-Antarctic triple junction. Using rate data from the East Ridge of the microplate, a Nazca-Juan Fernandez best fit pole was determined. As is suggested by the fanning of anomalies, this pole is just north of the ridge. The other two poles were determined by closure. Plate motion data for the four-plate system were inverted to define present-day plate motions and rotation poles. The resulting tectonic model predicts that the northern boundary of the Juan Fernandez microplate is a zone of compression and that the West Ridge and southwestern boundary are spreading obliquely. The southeastern boundary is predicted to be obliquely divergent, but present data fail to constrain its geometry. A schematic evolutionary model was also constructed to illustrate the migration and evolution of the triple junction, and relates the formation of the Juan Fernandez microplate to differential spreading rates at the triple junction. Possibilities for the future evolution of the four-plate system are included as part of the model.

In the second part of this study, bathymetric data collected by the Endeavor were used to construct a new contour map of the Chile transform system, a major part of the Nazca-Antarctic boundary, from  $100^{\circ}\text{W}$  to its termination at the East Ridge of the Juan Fernandez microplate at  $34^{\circ}30'\text{S}$ ,  $109^{\circ}15'\text{W}$ . Geophysical data from along this boundary had been extremely limited until the Endeavor survey. A generally continuous lineated bathymetric trend can be followed through the entire region,

with the transform valley being relatively narrow and well-defined from  $109^{\circ}\text{W}$  to approximately  $104^{\circ}30'\text{W}$ . The fracture zone-parallel topography then widens eastward, with at least two probable en echelon offsets to the south at  $104^{\circ}$  and  $102^{\circ}\text{W}$ . This bathymetric data, along with new earthquake mechanism data from the transform system and additional data from the Nazca-Antarctic boundary to the east, have been compiled into a new, larger data set for this boundary. Inversion of this data set has produced a new best fit pole for the Nazca-Antarctic plate pair, providing better constraints on the relative motion along this boundary. This new best fit pole matches the data better than the best fit pole calculated from old data, though some discrepancies still remain. Additional data, particularly from the western portion of the boundary, are needed to further refine the pole location.

## ACKNOWLEDGEMENT

First I thank Dr. Roger Larson, my major professor, for his guidance and support throughout this study. I also thank Dr. Robert Detrick for helpful discussions and reviews of the manuscript, and for serving on my thesis committee. I also benefited from discussions with Dr. P. Jeff Fox. I am grateful to Dr. Reinhard Frohlich for serving on my thesis committee and Dr. O. Don Hermes for serving as chairman of my defense committee. Drs. Seth Stein, Northwestern University, and Joseph Engeln, University of Missouri, provided many valuable suggestions and constructive criticisms which improved the manuscripts.

I am particularly grateful to Michael Sundvik for his invaluable assistance during the data reduction phase of this work, for helping me greatly with revisions of the projection and magnetic modeling programs, and for many valuable discussions. Nancy Adams also provided aid and suggestions during data reduction. I thank Claire Sherman for her willing help and support, and for always seeming to be available when needed. I have enjoyed and appreciated the company of all the students associated with the Marine Geophysical Laboratory and all my friends at the Graduate School of Oceanography. Finally, due credit goes to my husband, Dave, whose unending humor and moral support were instrumental in my successful completion of this work.

I gratefully acknowledge the financial support provided by National Science Foundation grant OCE 8308894 during all phases of this work.

## PREFACE

The format of this thesis follows the manuscript option. Two manuscripts are included which form the text of the thesis. Two appendices are also included which discuss data collection and reduction and the plate motion inversion technique which was used in both parts of this study. I was responsible for all the bathymetric and magnetic data reduction and interpretation, with the earthquake analyses and plate motion inversions carried out by coauthors J. F. Engeln, P. Lundgren, and S. Stein. The final tectonic and evolutionary models were jointly constructed.

Manuscript I (Tectonics and evolution of the Juan Fernandez micro-plate at the Pacific-Nazca-Antarctic triple junction) has been published in the Journal of Geophysical Research, volume 91. Coauthors are Joseph F. Engeln (University of Missouri, Columbia), Paul Lundgren (Northwestern University, Evanston, Illinois), Roger L. Larson (Graduate School of Oceanography, University of Rhode Island), and Seth Stein (Northwestern University). The text follows AGU style.

Manuscript II (Tectonics of the Nazca-Antarctic plate boundary) will be submitted to Earth and Planetary Science Letters with Joseph F. Engeln, Seth Stein, and Roger L. Larson as coauthors. The text follows EPSL style which differs from the AGU style of Manuscript I.

TABLE OF CONTENTS

	Page
ABSTRACT.....	ii
ACKNOWLEDGEMENT.....	iv
PREFACE.....	v
TABLE OF CONTENTS.....	vi
LIST OF TABLES.....	viii
LIST OF FIGURES.....	ix
 MANUSCRIPTS	
I. TECTONICS AND EVOLUTION OF THE JUAN FERNANDEZ MICROPLATE AT THE PACIFIC-NAZCA-ANTARCTIC TRIPLE JUNCTION.....	1
Abstract.....	2
Introduction.....	3
Earthquake Studies.....	4
Magnetic Anomaly Data.....	6
Bathymetric Data.....	9
Present-Day Tectonics.....	12
Discussion.....	15
Acknowledgments.....	22
References.....	24
Tables.....	28
Figures.....	35
II. TECTONICS OF THE NAZCA-ANTARCTIC PLATE BOUNDARY.....	59
Abstract.....	60
Introduction.....	61



Bathymetry and Seismicity.....	62
Earthquake Studies.....	66
Tectonics of the Nazca-Antarctic Boundary.....	68
Discussion.....	70
References.....	73
Tables.....	75
Figures.....	78
APPENDIX A: Data Collection and Reduction.....	98
APPENDIX B: Plate Motion Inversion.....	101
BIBLIOGRAPHY.....	104

LIST OF TABLES

Page

MANUSCRIPT I.

Table 1.	Source Parameters of Juan Fernandez Microplate Earthquakes.....	28
Table 2a.	Sea Floor Spreading Rates Along the East Ridge Averaged from 0 m.y. to Indicated Anomaly.....	29
Table 2b.	Sea Floor Spreading Rates Along the East Ridge Measured During Indicated Anomaly Interval.....	30
Table 3.	Plate Motion Data: Juan Fernandez Four Plate System.....	31
Table 4.	Euler Vectors: Juan Fernandez Four Plate System.....	34

MANUSCRIPT II.

Table 1.	Source Parameters of Chile Transform System Earthquakes.....	75
Table 2.	Plate Motion Data: Nazca-Antarctic Plates.....	76
Table 3.	Euler Vectors: Nazca-Antarctic Motion.....	77

## LIST OF FIGURES

Figure	Page
<b>MANUSCRIPT I.</b>	
1. Location map with bathymetry, seismicity, and focal mechanisms.....	35
2. Focal mechanisms from the western boundary of the Juan Fernandez microplate.....	37
3. Focal mechanisms from the northern boundary of the Juan Fernandez microplate.....	39
4. Map of regional magnetic lineations.....	41
5. East Ridge magnetic anomaly profiles.....	43
6. Southernmost magnetic anomaly profiles from the East Ridge with corresponding model profiles.....	45
7. Graph of age versus distance from the spreading axis for East Ridge profiles.....	47
8. East Ridge bathymetric and magnetic anomaly profiles.....	49
9. Southern Juan Fernandez microplate bathymetry plotted along ship tracks.....	51
10. Schematic present-day tectonic model of the Juan Fernandez microplate.....	53
11. Past evolutionary model for the Pacific-Nazca- Antarctic-Juan Fernandez four-plate system.....	55
12. Future evolutionary models for the Pacific- Nazca-Antarctic-Juan Fernandez system.....	57

MANUSCRIPT II.

1. Location map with bathymetry, seismicity, and focal mechanisms.....	78
2. Contoured bathymetric map of the Chile transform system.....	80
3. Projected bathymetric profiles.....	82
4. Bathymetric map of the Chile transform system with earthquake epicenter locations shown.....	84
5. First motions and surface wave amplitude patterns for three Chile Transform events.....	86
6. First motions and surface wave amplitude patterns for three Chile Transform events.....	88
7. Normal fault mechanism from the northern end of the Chile Rise.....	90
8. Euler Pole determinations for Nazca-Antarctic relative motion.....	92
9. Relative motions on the Nazca-Antarctic plate boundary.....	94
10. Predicted transform trends superimposed on the Chile Transform bathymetry.....	96

ABSTRACT

In this study, geologic and geophysical data from an air-seismic survey are combined with satellite geodesy to provide a tectonic model for the Juan Fernandez arc region at the South American Antarctic tectonic junction. We study the region along the Chile Ridge in the mid-Pacific east of the South American Plate and the Nazca Plate.

**TECTONICS AND EVOLUTION**  
**OF THE JUAN FERNANDEZ MICROPLATE**  
**AT THE PACIFIC-NAZCA-ANTARCTIC TRIPLE JUNCTION**

Interplate tectonics along the Chile Ridge and the Nazca Ridge are examined using satellite geodesy and seismicity. The resulting tectonic model shows the Juan Fernandez microplate is a tectonic plate that is bounded by a transform fault to the west, a subduction zone to the east, and a transform fault to the south. The microplate is shown to be a remnant of a larger plate that was once part of the Pacific Plate. The microplate is shown to be a tectonic plate that is bounded by a transform fault to the west, a subduction zone to the east, and a transform fault to the south. Its geometry, in the present is consistent with a model in which the microplate is a remnant of a larger plate that was once part of the Pacific Plate. The microplate is shown to be a tectonic plate that is bounded by a transform fault to the west, a subduction zone to the east, and a transform fault to the south.

## ABSTRACT

In this study, magnetic and bathymetric data from an R/V Endeavor survey are combined with earthquake mechanism studies to produce a tectonic model for the Juan Fernandez microplate at the Pacific-Nazca-Antarctic triple junction. Magnetic lineations along the East Ridge of the microplate fan to the south, indicating that the Nazca-Juan Fernandez pole is near the northern end of this feature. Relative motions of the Juan Fernandez-Pacific-Nazca-Antarctic four-plate system are determined using relative plate motion inversions. The resulting tectonic model predicts that the northern boundary of the Juan Fernandez microplate is a zone of compression and that the West Ridge and southwestern boundary are spreading obliquely. The southeastern boundary is predicted to be obliquely divergent, but present data fail to constrain its geometry. We also present a schematic evolutionary model which relates the formation of the Juan Fernandez microplate to differential spreading rates at the triple junction, and discuss related complexities. The future evolution of the four-plate system depends on whether one or both ridges remain active.



## INTRODUCTION

The existence of a small plate at the intersection of the Nazca, Antarctic, and Pacific plates, just north of the Chile Fracture Zone (Figure 1), was proposed independently by Herron [1972a] and Forsyth [1972] on the basis of anomalous seismicity. Earthquake epicenters outline the region, called the "lower plate" by Herron [1972a], and fault plane solutions [Forsyth, 1972] are inconsistent with the expected Pacific-Nazca relative motion. Stover [1973] noted that the epicenter distribution from  $31^{\circ}$  to  $35^{\circ}$ S could be interpreted to include one or two small plates, although plate boundaries could not be clearly identified. He concluded that this anomalous seismic activity is the result of a reorientation of the ridge axis. Additional fault plane solution data by Anderson et al. [1974] supported the interpretation of this region as a microplate. They noted a solution along the west boundary of the proposed plate near  $33^{\circ}$ S showing a large component of normal faulting, which they suggested was evidence for slow to intermediate spreading.

During a recent Sea Beam survey of the microplate region, Craig et al. [1983] mapped an eastern and a western ridge along the East Pacific Rise (EPR) between  $31^{\circ}$  and  $35^{\circ}$ S. They interpreted this region as a microplate, which they named the "Juan Fernandez microplate." Our subsequent geophysical survey on the R/V Endeavor in early 1984, with the objective of describing the present-day configuration and recent tectonic evolution of the triple junction, was designed to complement the Sea Beam survey and further define the eastern, southern, and northern boundaries of the proposed microplate.

Both geophysical data and fault plane solutions are needed to realistically model the present day tectonics of this region due to its complexity and rapid tectonic evolution. The Easter microplate further north demonstrates this, as the tectonic model constructed by Anderson et al. [1974], based mainly on focal mechanism studies because of the extremely limited marine geophysical data existing at the time, has since been modified significantly as more geophysical data became available [Engeln and Stein, 1984; R. N. Hey et al., unpublished manuscript, 1985; D. F. Naar and R. N. Hey, unpublished manuscript, 1985]. In this paper, we present magnetic and bathymetric data from the R/V Endeavor survey and focal mechanism studies for earthquakes on two of the Juan Fernandez microplate boundaries. We then combine these data and invert them using the technique of Minster et al. [1974] to define present-day plate motions and rotation poles. Finally, we propose a present-day tectonic model and a possible evolutionary model for the region consistent with our data, and discuss some of the complexities of this area.

#### EARTHQUAKE STUDIES

The seismicity of the Chile Rise and Chile Fracture Zone defines the Nazca-Antarctic plate boundary, with the Juan Fernandez microplate indicated by a ring in the seismicity at the western end of the Chile Fracture Zone (Figure 1). We studied four earthquakes (Figures 1, 2, and 3) on two boundaries of the Juan Fernandez microplate to provide data on present motions. In addition, we studied six events on the



Chile Fracture Zone to provide additional constraints on Nazca-Antarctic motion, a key to Juan Fernandez tectonics. Details of these six events can be found elsewhere [Engeln, 1985; S. Anderson-Fontana et al., unpublished manuscript, 1985]. All events were studied using P wave first motions and Rayleigh wave spectral amplitudes. For the Juan Fernandez events, P and SH waveform modeling [Fukao, 1970; Langston and Helmberger, 1975; Kanamori and Stewart, 1976] using the algorithm of G. C. Kroeger and R. J. Geller (unpublished manuscript, 1985) was used. The parameters of the four Juan Fernandez events are listed in Table 1. Three of these events are nearly pure strike-slip. Only the April 24, 1972, event has a large dip-slip component.

Two events large enough for detailed analysis occurred on the western boundary of the Juan Fernandez microplate. One (December 29, 1966) was studied by Anderson et al. [1974], who proposed a mechanism combining normal and strike-slip components. Our results (Figure 2) indicate nearly pure strike-slip motion. The first motion polarities analyzed in this study allow only determination of the general trend of the nodal planes, but SH wave analysis provides stricter constraints on the mechanism. Some of the results from the P and SH wave modeling are shown, indicating the good agreement of the data and the synthetic waveforms. First motions for the June 16, 1965, earthquake are similar to those for the December 29, 1966, event. Poor station coverage limits the usefulness of the SH waves, but three lobes of the Rayleigh wave radiation pattern are evident and agree with the mechanism shown.

Two events which occurred along the northern boundary of the Juan Fernandez microplate were large enough for mechanism determination (Figure 3). For both events the northeast trending nodal planes were constrained by the first motions. For the October 12, 1964 earthquake the other nodal plane could also be determined. SH waves place additional constraints on the mechanisms; they agree with the first motion data for the October 1964 event and constrain the mechanism of the April 24, 1972 earthquake to be very near the geometry shown. The Rayleigh wave data, although poor, provide near minimum misfits at the fault geometries shown.

#### MAGNETIC ANOMALY DATA

Total intensity magnetic measurements were made aboard the R/V Endeavor in the region around the Pacific-Nazca-Antarctic triple junction. These data were reduced to anomaly form by subtracting the 1980 International Geomagnetic Reference Field [Peddie, 1982] from each data point. The magnetic anomaly data, along with the bathymetric data, were then merged with navigational data and plotted along the ship's tracks. In order to improve the regional field manipulations, residual trends were removed from selected anomaly profiles which were then interpolated to a 0.5 km data spacing for subsequent projection.

The locations of the magnetic anomaly profiles we examined are shown in Figure 4. We present the data in Figure 5, along with a synthetic profile for comparison based on approximate spreading rates from profile A. These profiles have been projected to an azimuth of  $097^{\circ}$ , normal to

the trend of the ridge axis. The location of the central anomaly can be clearly seen on these profiles, but older anomalies become increasingly difficult to identify towards the north. This is apparently due to the rapid northward convergence of the magnetic lineations, which is more extreme on the west flank than on the east. To further support this interpretation of northward convergence, we illustrate in Figure 6 the three southernmost magnetic anomaly profiles (A, B, and C) with their respective synthetic profiles. Note the good correlation between the synthetic and actual profiles in each case. If there were a constant spreading rate along the ridge, the model for profile A should also match profiles B and C. However, examination of the data and model profiles show that this is not the case, and that models with decreasing spreading rates northward are necessary to match the data. The converging lineations produced imply rotation about a nearby pole.

We measured approximate half-opening rates averaged from anomaly 2 to the present for the east and west flanks. These are unusually large,  $10.4^{\circ}/\text{m.y.}$  for the west flank and  $6.9^{\circ}/\text{m.y.}$  for the east flank. These rates are more than twice the rates calculated for the north and south flanks of the Magellan spreading system, where a nearby Euler pole also produced asymmetric, fanning anomalies [Tamaki et al., 1979], and more than 10 times the rotational half-opening rates for the Pacific of  $0.5^{\circ}$  to  $0.69^{\circ}/\text{m.y.}$  [Lancelot and Larson, 1975]. Such asymmetric and extremely rapid rotation rates may suggest instability of the spreading system [Tamaki et al., 1979].



Anomalies out to 2A time (and anomaly 3 on the east flank of profile A) can be identified on all profiles except E, F, and the west flank of D. The time scale of LaBrecque et al. [1977] was used to calculate spreading rates (Figure 7, Tables 2a and 2b). Two trends occur: (1) a decrease in rates to the north and (2) a general decrease in rates over time. Spreading along the East Ridge has been asymmetric, with the asymmetry increasing northward, but the nature of the asymmetry has been inconsistent, suggesting complications in the spreading process. Profiles A and B indicate faster spreading on the west flank than on the east since Jaramillo time, conflicting with the previously observed general trend of faster east flank spreading at other locations on the EPR south of  $13.5^{\circ}\text{S}$  [Rea, 1977, 1981; Hey et al., 1985]. These two profiles show an increase in rates on the west flank during the Jaramillo to Brunhes-Matuyama time interval, followed by a decrease to the present time. A similar fluctuation was noted by Rea [1977] on the EPR at  $31^{\circ}\text{S}$ , but confined to the east flank of the rise, and at  $9.5^{\circ}$  to  $12^{\circ}\text{S}$  on the west flank only [Rea, 1976a]. Present whole spreading rates on the East Ridge decrease northward from 5.5 cm/year. North of profile B, however, our inability to identify anomalies younger than anomaly 2 prevents calculation of present spreading rates. Two crossings made by R/V Endeavor over the West Ridge between  $33^{\circ}$  and  $34^{\circ}\text{S}$ , extending west to approximately  $116.5^{\circ}\text{W}$ , failed to reveal any identifiable anomalies. These crossings verified previous findings of confused magnetics produced by the West Ridge (J. Francheteau, personal communication, 1983; D. W. Handschumacher, personal communication, 1984), and led us to focus

the Endeavor survey on the East Ridge and northern and southern plate boundaries.

Spreading rates directly north of the microplate at  $31^{\circ}\text{S}$ , averaged over the last 2.41 m.y., have been estimated at 8.6 cm/year for the east flank and 7.7 cm/year for the west flank of the EPR, with symmetric spreading over the last 0.7 m.y. at 16.2 cm/year (whole rate) [Rea, 1977]. The discontinuity of anomaly J at  $31^{\circ}\text{S}$  (Figure 4) may suggest complications in the spreading process at that time [Rea, 1977, 1981]. On the Pacific-Antarctic Rise directly south of the region, Handschumacher [1976] estimated whole rates at 10 to 10.5 cm/year, and identified anomalies out to 5A on the Nazca plate at about  $33^{\circ}\text{S}$ ,  $103^{\circ}\text{W}$  (Figure 4). These anomalies correlate and are continuous with the newly identified anomalies produced by the East Ridge, implying that this ridge has been spreading for at least 11.5 m.y.

#### BATHYMETRIC DATA

The bathymetric profiles across the East Ridge have also been projected to an azimuth of  $097^{\circ}$  and interpolated to a 0.5 km spacing (Figure 8). The East Ridge displays typical rift valley topography characteristic of a slow spreading center. The trend of this ridge is approximately  $\text{N}7^{\circ}\text{E}$ , the southern limit intersecting orthogonally with the Chile Fracture Zone which extends to the east. The central anomaly coincides with the rift valley on profiles A, B, E, and possibly F. The exact location of the rift valley is less clear on profiles C and D. However, since analysis of the magnetic anomalies does not show shifting

or jumping of the ridge axis at those locations (Figures 5 and 6), we feel that the location of the spreading center is accurately shown by the dashed line in Figure 8. The significance of the depressions greater than 4000 m in depth on the west flanks of profiles C and D cannot be determined based on our present data set. Similar depressions of uncertain origin have also been mapped along the EPR at 6°S [Rea, 1976b]. In addition, a large depression can be seen on the west flank near the ridge tip (profile F). The maximum width of this depression is approximately 35 km, with a local relief of 3200 m and a maximum water depth of approximately 5100 m. It is a localized feature, is teleseismically quiet, and has no apparent magnetic signature. The tectonic significance of this depression and its location relative to the spreading axis are unclear. Topographic deeps have been observed both at propagating rift tips and at ridge-transform intersections, but are generally not of this magnitude [Macdonald et al., 1979; Fox and Gallo, 1984; D. F. Naar and R. N. Hey, unpublished manuscript, 1985]. A depression of similar dimensions has, however, been mapped near the northern tip of the East Ridge on the Easter microplate [Mammerickx and Smith, 1978; Hey et al., 1985].

A topographic boundary is evident on the east and west flanks of the East Ridge, particularly on profiles A, B, and C (Figure 8). The topography changes from rough to smooth approaching the axis, with the boundary coinciding with anomaly 2A or 3 on profiles A and B. The local relief is approximately 1000 m for the rough basement in contrast to less than 300 m for the smooth basement. The topography becomes rougher



again as the ridge axis is approached. Profile C shows a possible slope reversal also coinciding with anomaly 2A, but the northward spreading rate decrease results in generally rougher topography, making it difficult to accurately identify a boundary.

Ship crossings were also made at the probable locations of the northern and southern boundaries of the proposed microplate. The northern crossings indicated a region of rough, unlineated topography 110 km wide from about  $110^{\circ}$  to  $111.5^{\circ}$ W. Rough topography in this area was also observed in the 1983 Sea Beam survey (J. Francheteau, personal communication, 1983). Rea [1977] reported a region of disturbed topography extending from  $31.7^{\circ}$ S,  $111.5^{\circ}$ W to  $34.7^{\circ}$ S,  $112.9^{\circ}$ W, and a large scarp trending  $098^{\circ}$  at about  $31.8^{\circ}$ S which he defined as the northern limit of this rough topography. Crossings of the southwest boundary (Figure 9) indicate a lineated feature with fracture zone topography trending approximately  $102^{\circ}$ , nearly parallel to the trend of the Chile Fracture Zone east of the East Ridge determined from R/V Endeavor bathymetric data. This feature has a depth ranging from 3400 to 4000 m and a relief of 800 to 1500 m. On the westernmost profile in this region, a flat feature can be identified that may be a lava plateau. Its north-south extent is about 42.5 km, and it has an average depth of 2500 m with a high peak to the north of approximately 1600 m depth.

Another curious zone of lineated topography was identified on these same profiles north of the lineated feature described above (Figure 9). This zone appears to have an arcuate shape and consists of an apparently linear depression 3500 to 4500 m in depth with an associated high

directly south 1300 to 2000 m in depth. The significance of this feature is unknown, although its lack of seismicity implies that it may be a relict feature. Finally, crossings of the supposed southeast boundary, also seen in Figure 9, indicate relatively smooth topography in this region.

#### PRESENT-DAY TECTONICS

The seismicity (Figure 1) near the Juan Fernandez microplate is clustered in a ring which defines the supposed plate boundaries, suggesting that the nearly aseismic area in the center of the plate is behaving rigidly. To test whether rigid plate tectonics adequately describes the region, we inverted the relative motion data for the four-plate (Pacific-Nazca-Antarctic-Juan Fernandez) system using the Minster et al. [1974] algorithm. The data, listed in Table 3, included the data used in model RM2 [Minster and Jordan, 1978] for the Pacific-Nazca and Pacific-Antarctic boundaries (minus those slip vectors now known to be on the Pacific-Easter and Pacific-Juan Fernandez boundaries), rate data along the Juan Fernandez East Ridge from this study, and slip vectors from the four Juan Fernandez events. We also used a new data set for the Nazca-Antarctic boundary which includes the RM2 data, slip vectors from Engeln [1985], transform azimuth and rate data from Herron et al. [1981], and EN-112 transform azimuth data. Engeln [1985] showed that these data produced a best fit pole much closer to the RM2 Nazca-Antarctic pole which matched the data much better than a best fit pole produced using only RM2 data.



Using only the rate data from anomaly 2 to the present along the East Ridge and assuming orthogonal spreading, we determined a Nazca-Juan Fernandez best fit pole. As is suggested by the fanning of anomalies, this pole is just north of the ridge (Table 4; Figure 10, dots). The Pacific-Juan Fernandez and Antarctic-Juan Fernandez poles were determined by closure. Based on the locations of these poles, we assumed that the northeast trending nodal planes were the fault planes for the events on the plate boundaries. These slip vectors were added to the data for use in the four plate inversions. The slip vectors for the three strike-slip events seem suitable for this purpose; use of the event with a large dip-slip component is more questionable. The consistency of the results with the rates-only inversion (and the very sparse data set) appear to justify this use and the choice of fault planes.

Four inversions were carried out using different subsets of the Juan Fernandez data (Table 4). We assigned the rate data uncertainties of 50 mm/year and the slip vectors on the Juan Fernandez boundaries  $20^{\circ}$  uncertainties. The poles vary only slightly based on which data were used. Poles determined using the spreading rates from anomaly 2 (the most recent that can be identified on all three of the profiles used for the rate data) to the present are shown in Figure 10. The dots indicate the poles determined by an inversion in which the only data from the Juan Fernandez microplate were the rate data from the East Ridge. The stars indicate the poles determined by inversion of the entire data set, with their 95% confidence limits indicated by the ellipses; these poles

were used to generate the relative motion vectors shown. The good fit of the data (summarized in Table 3) offers some confidence in the locations of the rotation poles for the four plate system. If the Nazca-Juan Fernandez pole were at a great distance, it would be inconsistent with the decrease in spreading rate along this boundary or the slip vectors on the other two Juan Fernandez boundaries. The small 95% confidence ellipses shown in Figure 10 indicate the internal consistency of the data, although they underestimate the true uncertainty in these poles' determinations. One possible problem is presented by the two earthquakes along the northern plate boundary; if this is a broad zone of deformation, the compressional axes may be more important to the tectonic interpretation than the slip vectors of these events.

The spreading rate along the East Ridge increases almost linearly from north to south because of the proximity of the pole. This pole's location requires that most of the northern boundary of the Juan Fernandez plate be in compression unless the boundary geometry is very different from that shown. The rough topography of this region may be a result of this compression, with the young age of the lithosphere probably preventing subduction (or obduction) from occurring.

The West Ridge is predicted to be a fast spreading ridge (greater than 100 mm/year), but must be spreading obliquely if the slip vectors from the earthquakes along this boundary and the interpretation of ridge strike [Craig et al., 1983; J. Francheteau, personal communication, 1983] are correct. This oblique spreading, along with the rough topography to the west of the ridge observed on the two EN-112 ship cross-

ings, would most likely contribute to the lack of identifiable magnetic anomaly patterns in this area. The transforms shown are schematic and are not bathymetrically defined; they have the predicted trend and the correct sense of offset, but their lengths are not well constrained. The southwestern boundary is also an obliquely spreading ridge if the trend mapped from EN-112 data indicates the boundary, or is a series of ridge segments offset by transforms. The remaining boundary, Antarctic-Juan Fernandez, is predicted to have slow, divergent motion across it. However, the details of its geometry are totally unconstrained.

It is important to recognize that this tectonic model is limited by the sparse data. Nonetheless, it is internally consistent and testable, facilitating future investigations.

#### DISCUSSION

Given the limited data along the Juan Fernandez microplate boundaries, only a general outline of its evolution is possible at present. The age continuity of the magnetics to the east of the East Ridge (Figure 4) out to anomaly 5A indicates that this has been an active spreading center for at least 11 million years. The distance between the East and West Ridges indicates that if the West Ridge has not jumped since its formation, it was formed approximately 3 m.y. B.P. This interpretation does not rely on the assumption that the Juan Fernandez microplate is rigid, but only on the internal rigidity of the Pacific, Nazca, and Antarctic plates such that the angular rotation between those plates is preserved. The absence of anomalies on the west flank of the East Ridge



older than anomaly 2A, and the topographic boundary coincident with 2A on this flank, support this age interpretation. This topographic change may mark the boundary between crust created by the East Ridge and crust created by the West Ridge. In addition, the change in orientation of anomalies eastward of the East Ridge and another topographic boundary possibly related to this rotational effect also occur at 3 to 4 m.y. B.P. If the West Ridge is the result of successive ridge jumps or rift propagation, or if the ridge was formed far from the East Ridge, this is an upper limit to its age.

The question arises as to whether these topographic boundaries represent pseudofaults created by ridge propagation [e.g., Hey, 1977; Hey and Wilson, 1982]. We feel this is not the case for the East Ridge for several reasons. First, this boundary occurs at approximately the same location temporally from south to north (Figure 8) rather than cutting across and truncating magnetic lineations as pseudofaults do. Second, in a pure ridge propagation model with spreading about a distant pole, the spreading rate is essentially constant along the strike of the ridge. As was shown earlier (Figure 6), spreading rates are not constant along the East Ridge, and we interpret the anomaly fanning to be the result of spreading about a nearby Euler pole. Third, the continuity of the magnetics to the east of the East Ridge argues against a newly formed ridge in this area. Thus although the topographic boundaries on the east and west flanks may initially appear analogous to pseudofaults, analysis of the magnetic lineations argues against pure ridge propagation. This does not, however, preclude the possibility of

some northward growth of the East Ridge, with or without northward migration of the Nazca-Juan Fernandez rotation pole over time.

The near alignment of anomaly 3A east and north of the Juan Fernandez microplate (Figure 4) requires that the northern part of the East Ridge was almost continuous with the East Pacific Rise to the north 5 m.y. ago. The East Ridge has thus migrated 260 km eastward relative to the EPR segment to the north since anomaly 3A time. This can be the result of one or both of two factors. Asymmetric spreading with more crust being added to the plate to the west of the ridge would cause the ridge to migrate relatively eastward and the offsetting transform to lengthen. Alternatively, the start of spreading on the West Ridge causes the East Ridge to move relative to the Pacific plate at the full rate of the West Ridge plus the rate of accretion on the western limb of the East Ridge; unless the spreading is extremely asymmetric on the East Ridge, this ridge will move eastward relative to the EPR. Because the asymmetry on the East Ridge is not large, the inception of spreading on a West Ridge presumably caused the eastward migration of the East Ridge relative to the EPR (as the simplified model in Figure 11 shows).

At the Pacific-Nazca-Antarctic triple junction, relative motion is essentially collinear, with Pacific-Nazca much faster than Pacific-Antarctic motion (Figure 1). As spreading is nearly symmetric, the Pacific-Nazca Ridge moves eastward with respect to the Pacific-Antarctic Ridge with time. The geometry of the triple junction thus changes with time and may, in an overall sense, be responsible for the formation of the Juan Fernandez microplate. Without trying to match the details of

the tectonics of the Juan Fernandez microplate, we show a schematic evolutionary model to illustrate the migration and evolution of the triple junction.

This model (Figure 11) has a variety of simplifying assumptions to show the basic points without complications due to second-order geometric considerations. The poles are at infinity (as opposed to the nearby poles shown in Figure 10), thus reducing the complexities of the model by making this a plane problem. All spreading is assumed to be orthogonal and symmetric (which is not strictly true for the East Ridge), and the rates shown for each time remain constant for the next time interval (all changes in rate occur instantaneously). The time scale and velocities have been chosen to approximate the situation at the Pacific-Antarctic-Nazca triple junction, but are not intended as an actual reconstruction. In this model, plates A, B, C, and D can be equated in general to the Pacific, Nazca, Antarctic, and Juan Fernandez plates, respectively. We use the letter names throughout the discussion to emphasize that our model is extremely simplified and is only a first step toward an actual reconstruction. Plate A is shown fixed. The spreading rate between A and B is 160 mm/year; that between A and C is 100 mm/year. Both of these rates remain constant over the entire time illustrated. The original configuration (4 m.y. B.P.) includes a F-R-F triple junction with the A-C ridge east of the first A-B ridge segment north of the triple junction.

One million years later (3 m.y. B.P.) the two ridges are aligned, producing, for an instant only, a R-R-F triple junction. Another mil-



1100 years later (2 m.y. B.P.), the southern A-B ridge segment has migrated to the east of the A-C ridge. At this point a new ridge forms either by rift propagation or a ridge jump to form a new plate, D, with the A-C-D triple junction a R-R-F junction. This new ridge instantaneously starts spreading at 60 mm/year. As time progresses, plate D widens at 80 mm/year, resulting in the migration of the old A-B (now D-B) ridge section to the east. The western ridge of microplate D lags in eastward migration relative to the other ridges due to its slower spreading rate, leading to an alignment of the A-B and A-D ridge segments at the present.

It is interesting to consider three of the many paths the system might follow in its future evolution (Figure 12). In one case (Figure 12, top), the microplate continues to grow as a separate entity. In another case (Figure 12, middle), the eastern ridge of microplate D dies, allowing the triple junction to reestablish a geometry somewhat similar to that four million years ago. The only evidence for the existence of the small plate would be doubled magnetic anomalies indicating a previous ridge. Alternatively (Figure 12, bottom), when the spreading rate on the B-D ridge equals the relative motion on the B-C transform, no motion occurs across the former D-C transform and plate D becomes part of plate C (this possibility was suggested to us by E. Okal, personal communication, 1985). It is worthwhile noting that if the microplate is incorporated into either of the major plates, the new plate geometry is similar to the initial geometry shown, and similar evolution can occur in the future.

These tectonic cartoons are very simplified, yet contain a number of similarities to the Juan Fernandez microplate. The relative spreading rates used are similar to the real situation. The alignment and formation of a new ridge to the west of the existing ridge and the East Ridge migration relative to that of the next ridge segment to the north both appear to have occurred at the Juan Fernandez microplate. The present near alignment of the West Ridge and the Pacific-Nazca Ridge segment to the north is also observed.

The gradual rather than the instantaneous evolution of spreading processes probably accounts for most of the additional complexity near the Juan Fernandez plate. The development over a few million years of a new ridge-transform system with nearby Euler poles results in the along-strike velocity variations and gradual spreading rate changes with time shown by the data. Such complications are seen most easily in the east-west trending boundaries which are transforms in the simple model. In our tectonic interpretation of the Juan Fernandez microplate (Figure 10), the southeast and southwest boundaries are predicted to be zones of slow, oblique spreading. The slow compression along the northern boundary also results from the proximity of the poles. The rapid change in spreading rates along the East Ridge results in oblique motion along the West Ridge. In the simple model, the entire ridge could spread orthogonally; on the West Ridge of the Juan Fernandez microplate, either the mapped trends or the slip vectors are incorrectly interpreted or spreading is extremely oblique.



This simple model illustrates several possibilities for the future evolution of the Pacific-Nazca-Antarctic triple junction consistent with rigid plate tectonics. If the East Ridge dies, as suggested by the observed slowing over the past 4 to 5 m.y., the presence of two formerly active ridges should be obvious in the doubled anomaly pattern, though complicated by the along-strike variations in spreading rate. The geometry which would result if the East Ridge dies is similar to that which may have existed prior to the formation of the Juan Fernandez microplate (Figure 11), suggesting that this process may be cyclic. Alternatively, if both ridges continue to spread, the Juan Fernandez microplate would either be incorporated into the Antarctic plate or grow to a large plate. The former is reminiscent of Weissel et al.'s [1977] proposal that magnetic anomalies show northward growth of the Antarctic plate at the expense of the Nazca plate and that the Pacific-Nazca-Antarctic triple junction has jumped northward several times over the past 20 m.y., resulting in the "splitting of a segment of the Pacific-Nazca ridge into two separating spreading segments." If both ridges of the Juan Fernandez microplate remain active, the microplate may be a transitory feature in this northward migration of the triple junction. Another possibility, if neither ridge dies, is that the Juan Fernandez microplate will grow into a major plate. Hilde et al. [1976] suggested that the Pacific plate was formed in a somewhat similar manner in the late Jurassic.

Understanding the Juan Fernandez plate should provide crucial insights into past and present major plate boundary reorganizations.

Evidence for microplates similar to the Juan Fernandez and Easter plates appears to be preserved in marine magnetic anomalies. For example, between 8.2 and 6.5 million years ago, a small plate existed between the EPR and the then-active Galapagos Rise [Rea, 1978; Mammerickx et al., 1980]. After the extinction of the Galapagos Rise, this microplate became part of the Nazca plate. Cande et al. [1982] proposed that a plate which existed at the Farallon-Aluk-Antarctic-Pacific junction about 45 million years ago formed by rift propagation and was transferred from the Pacific to the Antarctic plate. Microplates such as the Juan Fernandez and Easter microplates may thus play an important role in spreading center evolution [Engeln and Stein, 1984]. Planned detailed marine geophysical work in the area should provide a better picture of both the present kinematics and the past evolution of the Juan Fernandez microplate.

Acknowledgments. We thank Captain Tate and the crew of R/V Endeavor for professional assistance at sea, and the government of Chile and the people of Easter Island for their support and hospitality. J. Francheteau generously provided unpublished Sea Beam and magnetics data prior to the cruise. We also thank R. Gordon, D. Wiens, E. Okal, R. Hey, R. Detrick, J. Mutter, and M. Sundvik for useful discussions, and N. Adams for valuable assistance. Reviews by D. K. Rea and an anonymous referee improved this manuscript. The plate motion inversion program was written by R. Gordon and S. Stein. This research was supported by NSF grants OCE 8308894, EAR 8407510, EAR 8206381, and NASA Crustal Dynamics

Contract NAS5-27238. Acknowledgment for partial support is also made to the donors of the Petroleum Research Fund, administered by the American Chemical Society.

## REFERENCES

- Anderson, R.N., D.W. Forsyth, P. Molnar, and J. Mammerrickx, Fault plane solutions on the Nazca Plate boundaries and the Easter Plate, Earth Planet. Sci. Lett., 24, 188-202, 1974.
- Cande, S.C., E.M. Herron, and B.R. Hall, The early Cenozoic history of the southeast Pacific, Earth Planet. Sci. Lett., 56, 63-74, 1982.
- Craig, H., K.-R. Kim, and J. Francheteau, Active ridge crest mapping on the Juan Fernandez micro-plate: The use of SEABEAM-controlled hydrothermal plume surveys, Eos Trans. AGU, 64, 45, 1983.
- Engeln, J.F., Seismological studies of the tectonics of divergent plate boundaries, Ph.D. thesis, 138 pp., Northwestern Univ., Evanston, Ill., 1985.
- Engeln, J.F., and S. Stein, Tectonics of the Easter plate, Earth Planet. Sci. Lett., 68, 259-270, 1984.
- Forsyth, D.W., Mechanisms of earthquakes and plate motions in the East Pacific, Earth Planet. Sci. Lett., 17, 189-194, 1972.
- Fox, P.J., and D.G. Gallo, A tectonic model for ridge-transform-ridge plate boundaries: Implications for the structure of oceanic lithosphere, Tectonophysics, 104, 205-242, 1984.
- Fukao, Y., Focal process of a deep-focus earthquake as deduced from long period P and S waves, Bull. Earthquake Res. Inst., 48, 707-727, 1970.
- Handschumacher, D.W., Post-Eocene tectonics of the Eastern Pacific, in The Geophysics of the Pacific Ocean Basin and Its Margin, Geophys.



- Monogr. Ser., vol. 19, edited by G.H. Sutton, M.H. Manghni, and R. Moberly, pp. 117-202, AGU, Washington, D.C., 1976.
- Herron, E.M., Two small crustal plates in the South Pacific near Easter Island, Nature Phys. Sci., 240, 35-37, 1972a.
- Herron, E.M., Sea-floor spreading and the Cenozoic history of the East-Central Pacific, Geol. Soc. Am. Bull., 83, 1671-1692, 1972b.
- Herron, E.M., S.C. Cande, and B.R. Hall, An active spreading center collides with a subduction zone: A geophysical survey of the Chile Margin triple junction, Geol. Soc. Am. Mem., 154, 683-702, 1981.
- Hey, R.N., A new class of "pseudofaults" and their bearing on plate tectonics: A propagating rift model, Earth. Planet. Sci. Lett., 37, 321-325, 1977.
- Hey, R.N., and D.S. Wilson, Propagating rift explanation for the tectonic evolution of the northeast Pacific--The pseudomovie, Earth. Planet. Sci. Lett., 58, 167-188, 1982.
- Hey, R.N., D.F. Naar, M.C. Kleinrock, W.J. Phipps Morgan, E. Morales, and J.-G. Schilling, Microplate tectonics along a superfast seafloor spreading system near Easter Island, Nature, 317, 320-325, 1985.
- Hilde, T.W.C., S. Uyeda, and L. Kroenke, Tectonic history of the Western Pacific, in Geodynamics Progress and Prospects, edited by C.L. Drake, pp. 1-15, AGU, Washington, D.C., 1976.
- Kanamori, H., and G.S. Stewart, Mode of the strain release along the Gibbs Fracture Zone, Phys. Earth Planet. Inter., 11, 312-332, 1976.

- LaBrecque, J.L., D.V. Kent, S.C. Cande, Revised magnetic polarity time scale for Late Cretaceous and Cenozoic time, Geology, 5, 330-335, 1977.
- Lancelot, Y., and R.L. Larson, Sedimentary and tectonic evolution of the Northwestern Pacific, in Initial Reports of the Deep-Sea Drilling Project, vol. 32, edited by R.L. Larson et al., pp. 925-939, 1975.
- Langston, C.A., and D.V. HelMBERGER, A procedure for modelling shallow dislocation sources, Geophys. J. R. Astron. Soc., 42, 117-130, 1975.
- Macdonald, K.D., K. Kastens, S. Miller, and F.N. Spiess, Deep-tow studies of the Tamayo transform fault, Mar. Geophys. Res., 4, 37-70, 1979.
- Mammerickx, J., and S.M. Smith, Bathymetry of the Southeast Pacific, Geol. Soc. Am. Map Chart Ser., MC-26 442, 194, 1978.
- Mammerickx, J., E. Herron, and L. Dorman, Evidence for two fossil spreading ridges in the southeast Pacific, Geol. Soc. Am. Bull., 91, 263-271, 1980.
- Minster, J.B., and T.H. Jordan, Present-day plate motions, J. Geophys. Res., 83, 5331-5354, 1978.
- Minster, J.B., T.H. Jordan, P. Molnar, and E. Haines, Numerical modeling of instantaneous plate tectonics, Geophys. J. R. Astron. Soc., 36, 541-576, 1974.
- Peddie, N.W., International geomagnetic reference field: The third generation, J. Geomag. Geoelec., 34, 309-326, 1982.

- Rea, D.K., Analysis of a fast-spreading rise crest: The East Pacific Rise,  $9^{\circ}$  to  $12^{\circ}$  South, Mar. Geophys. Res., 2, 291-313, 1976a.
- Rea, D.K., Changes in the axial configuration of the East Pacific Rise near  $6^{\circ}$ S during the past 2 m.y., J. Geophys. Res., 81, 1495-1504, 1976b.
- Rea, D.K., Local axial migration and spreading rate variations, East Pacific Rise,  $31^{\circ}$ S, Earth Planet. Sci. Lett., 34, 78-84, 1977.
- Rea, D.K., Evolution of the East Pacific Rise between  $3^{\circ}$ S and  $13^{\circ}$ S since the middle Miocene, Geophys. Res. Lett., 5, 561-564, 1978.
- Rea, D.K., Tectonics of the Nazca-Pacific divergent plate boundary, Geol. Soc. Am. Mem., 154, 27-62, 1981.
- Stover, C.W., Seismicity and tectonics of the East Pacific Ocean, J. Geophys. Res., 78, 5209-5220, 1973.
- Tamaki, K., M. Joshima, and R.L. Larson, Remanent Early Cretaceous spreading center in the Central Pacific Basin, J. Geophys. Res., 84, 4501-4510, 1979.
- Weissel, J.K., D.E. Hayes, and E.M. Herron, Plate tectonics synthesis: the displacements between Australia, New Zealand, and Antarctica since the late Cretaceous, Mar. Geol., 25, 231-277, 1977.

TABLE 1: Source Parameters of Juan Fernandez Microplate Earthquakes

Date	Time	Latitude	Longitude	$M_s$	$m_b$	$M_o$	Mechanism*
10/12/64	2155:33	-31.40	-110.84	6.1	5.9	$2.0 \times 10^{25}$	243/88/348
4/24/72	0120:48	-31.36	-111.06	6.1	5.8	$5.3 \times 10^{25}$	230/82/40
12/29/66	2216:22	-32.80	-111.70	6.0	5.4	$1.6 \times 10^{25}$	220/78/10
6/16/65	0243:08	-34.40	-112.22	5.8	5.7	$1.4 \times 10^{25}$	215/88/1

\* Strike, dip, and slip angles using Kanamori and Stewart [1976] conventions.



TABLE 2a: Sea Floor Spreading Rates Along the East Ridge Averaged From 0 m.y. to Indicated Anomaly

Profile	Anomaly	West Flank	East Flank	Total
A	3		5.1	
	2A	4.7	4.4	9.1
	2	3.7	3.6	7.3
	J	3.7	2.6	6.3
	B/M	3.2	2.3	5.5
B	2A	2.9	3.9	6.8
	2	2.4	2.9	5.3
	J	2.8	1.6	4.4
	B/M	2.3	1.3	3.6
C	2A	2.1	3.5	5.6
	2	1.6	2.3	3.9
D	2A		3.2	
	2		2.0	

Rates are in cm/year. B/M, Bruhnes-Matuyama boundary.

Table 2b: Sea Floor Spreading Rates Along the East Ridge Measured During Indicated Anomaly Interval

Profile	Interval	West Flank	East Flank	Total
A	3-2A		6.8	
	2A-2	5.8	5.7	11.5
	2-J	3.7	4.6	8.3
	J-B/M	5.1	3.4	8.5
	B/M-axis	3.2	2.3	5.5
B	2A-2	3.8	5.8	9.6
	2-J	1.9	4.3	6.2
	J-B/M	4.6	2.5	7.1
	B/M-axis	2.3	1.3	3.6
C	2A-2	2.8	5.2	8.0
	2-axis	1.6	2.3	3.9
D	2A-2			4.9
	2-axis			2.0

Rates are in cm/year. B/M, Bruhnes-Matuyama boundary.

TABLE 3: Plate Motion Data: Juan Fernandez Four Plate System

Latitude	Longitude	Datum	Standard Deviation	Weighted Residuals	Importance	Source
<u>Pacific-Antarctic Rates</u>						
-35.60	-110.90	10.60	0.40	0.06	0.16	RM2
-35.80	-110.90	10.30	0.40	-0.79	0.16	RM2
-36.00	-111.00	10.20	0.50	-0.81	0.10	RM2
-42.00	-111.20	9.90	0.40	-0.87	0.12	RM2
-44.40	-112.20	10.00	0.40	-0.16	0.10	RM2
-47.60	-112.90	9.80	0.40	0.00	0.09	RM2
-51.40	-118.10	9.50	0.50	0.26	0.05	RM2
-53.70	-118.00	9.80	0.50	1.31	0.05	RM2
-54.50	-118.70	8.80	0.50	-0.50	0.05	RM2
-55.20	-121.20	9.10	0.50	0.36	0.05	RM2
-54.50	-138.20	8.80	0.50	0.54	0.06	RM2
-56.00	-145.00	8.40	0.50	0.53	0.07	RM2
-58.50	-149.00	8.00	0.50	0.60	0.08	RM2
-59.60	-151.30	7.70	0.60	0.37	0.06	RM2
-60.50	-151.00	7.80	0.50	0.82	0.09	RM2
-63.20	-163.10	6.00	0.70	-0.78	0.06	RM2
-64.10	-169.00	5.60	0.50	-1.11	0.14	RM2
-65.00	-174.00	5.80	0.50	0.00	0.15	RM2
<u>Transforms</u>						
-49.80	-115.00	162.00	5.00	-0.26	0.04	RM2
-53.00	-118.50	160.00	5.00	-0.24	0.04	RM2
-54.50	-119.00	158.00	5.00	-0.53	0.05	RM2
-55.20	-125.00	158.00	3.00	0.04	0.12	RM2
-55.50	-130.00	157.00	3.00	0.44	0.12	RM2
-56.20	-143.00	150.00	3.00	-0.02	0.13	RM2
-58.80	-150.50	153.00	5.00	1.59	0.06	RM2
-64.50	-170.50	138.00	5.00	1.12	0.10	RM2
-64.50	-175.20	124.00	3.00	-0.67	0.43	RM2
<u>Slip Vectors</u>						
-56.00	-123.40	157.00	10.00	-0.14	0.01	RM2
-54.80	-136.00	151.00	10.00	-0.24	0.01	RM2
-56.60	-142.50	151.00	10.00	0.09	0.01	RM2
-65.70	-179.30	141.00	15.00	0.95	0.01	RM2
<u>Nazca-Pacific Rates</u>						
-5.80	-106.80	15.30	0.80	0.19	0.17	RM2
-9.40	-110.00	16.30	0.80	0.83	0.13	RM2
-9.90	-110.10	15.50	0.80	-0.24	0.12	RM2
-10.80	-110.30	16.60	1.00	0.81	0.08	RM2
-11.40	-110.50	16.10	1.00	0.25	0.07	RM2
-12.00	-110.80	15.90	0.60	-0.03	0.19	RM2

TABLE 3. (continued)

Latitude	Longitude	Datum	Standard Deviation	Weighted Residuals	Importance	Source
-19.00	-113.00	16.50	1.00	0.01	0.05	RM2
-20.00	-113.80	16.10	0.60	-0.76	0.15	RM2
-28.00	-112.00	17.50	0.80	0.85	0.11	RM2
<u>Transforms</u>						
-3.70	-102.90	-9.00	3.00	-0.21	0.22	RM2
-4.50	-105.50	-12.00	3.00	-0.71	0.23	RM2
-6.00	-107.00	-17.00	5.00	-1.28	0.08	RM2
-13.50	-112.00	-20.00	10.00	-0.72	0.02	RM2
<u>Slip Vectors</u>						
-4.40	-105.90	-15.00	20.00	-0.24	0.01	RM2
-4.50	-106.00	-14.00	15.00	-0.26	0.01	RM2
-4.60	-105.80	-13.00	15.00	-0.20	0.01	RM2
-13.30	-111.50	-15.00	20.00	-0.12	0.01	RM2
-28.70	-112.70	-28.00	20.00	-0.77	0.00	RM2
<u>Nazca-Antarctic Rates</u>						
-38.20	-94.20	5.80	0.80	-0.58	0.27	H
-44.60	-78.30	6.20	0.80	-0.25	0.42	H
<u>Transforms</u>						
-41.30	-88.50	10.00	10.00	0.04	0.08	RM2
-44.68	-80.00	19.00	10.00	0.30	0.10	H
-45.72	-77.50	19.00	10.00	0.11	0.10	H
-45.90	-76.30	21.00	10.00	0.22	0.11	H
-36.00	-107.50	-12.00	10.00	-0.65	0.08	E
-36.50	-102.50	-8.00	10.00	-0.59	0.07	E
<u>Slip Vectors</u>						
-36.20	-100.90	8.00	15.00	0.55	0.03	RM2
-36.30	-97.20	11.00	15.00	0.55	0.03	RM2
-41.70	-84.00	4.00	15.00	-0.60	0.04	RM2
-36.40	-98.80	8.00	15.00	0.43	0.03	T
-36.00	-102.60	-1.00	15.00	0.04	0.03	T
-36.30	-98.10	4.00	15.00	0.16	0.03	T
-36.50	-97.20	9.00	15.00	0.41	0.03	T
-36.60	-98.20	24.00	15.00	1.46	0.03	T
-36.60	-97.50	10.00	15.00	0.50	0.03	T
-37.20	-95.20	30.00	15.00	1.71	0.03	T
<u>Nazca-Juan Fernandez Rates</u>						
-33.32	-109.17	3.90	0.50	0.76	0.64	T
-33.69	-109.20	5.30	0.50	0.13	0.34	T
-34.25	-109.25	7.30	0.50	-0.73	0.75	T

TABLE 3. (continued)

Latitude	Longitude	Datum	Standard Deviation	Weighted Residuals	Importance	Source
	<u>Transform</u>					
-33.69	-109.20	-5.00	15.00	0.07	0.86	F
	<u>Slip Vectors</u>					
-31.36	-111.06	-134.00	20.00	-0.52	0.09	T
-31.40	-110.84	-153.00	20.00	-1.31	0.11	T
	<u>Pacific-Juan Fernandez Slip Vectors</u>					
-32.80	-111.70	-127.00	20.00	1.55	0.07	T
-34.40	-112.22	-124.00	20.00	0.56	0.17	T

Weighted residuals and importances are those for the inversion using the new poles derived in this study and in the work by Engeln [1985]. Rates are in centimeters per year. Transform fault and slip vector azimuths are in degrees measured counterclockwise from east. Sources: RM2, compiled by Minster and Jordan [1978]; H, Herron et al. [1981]; E, EN-112 (1984 survey); T, this study; F, fictitious transform (assuming orthogonal spreading).



TABLE 4: Euler Vectors: Juan Fernandez  
Four Plate System

---

Plate Pair	Latitude	Longitude	Degrees Per Million Years	Reduced Chi-Squared
---------------	----------	-----------	------------------------------	------------------------

---

Nazca-Juan Fernandez Best Fit Pole:

Anomaly 2 Rates

NZ-JF	-32.23	-109.05	18.37	0.000
-------	--------	---------	-------	-------

All Data: Anomaly 2 Rates

NZ-JF	-32.51	-109.05	22.49	
PA-JF	-36.30	-109.99	22.56	
AN-JF	-33.91	-109.25	22.32	0.510

All Data: Anomaly 2A Rates

NZ-JF	-31.27	-108.48	15.24	
PA-JF	-36.81	-109.72	15.31	
AN-JF	-33.30	-108.73	15.07	1.385

Only Rate Data From JF Plate: Anomaly 2 Rates

NZ-JF	-32.23	-109.05	18.37	
PA-JF	-36.86	-110.15	18.44	
AN-JF	-33.94	-109.31	18.19	0.449

Only Rate Data From JF Plate: Anomaly 2A Rates

NZ-JF	-32.06	-109.03	22.18	
PA-JF	-35.89	-109.93	22.23	
AN-JF	-33.47	-109.24	22.00	0.455

---

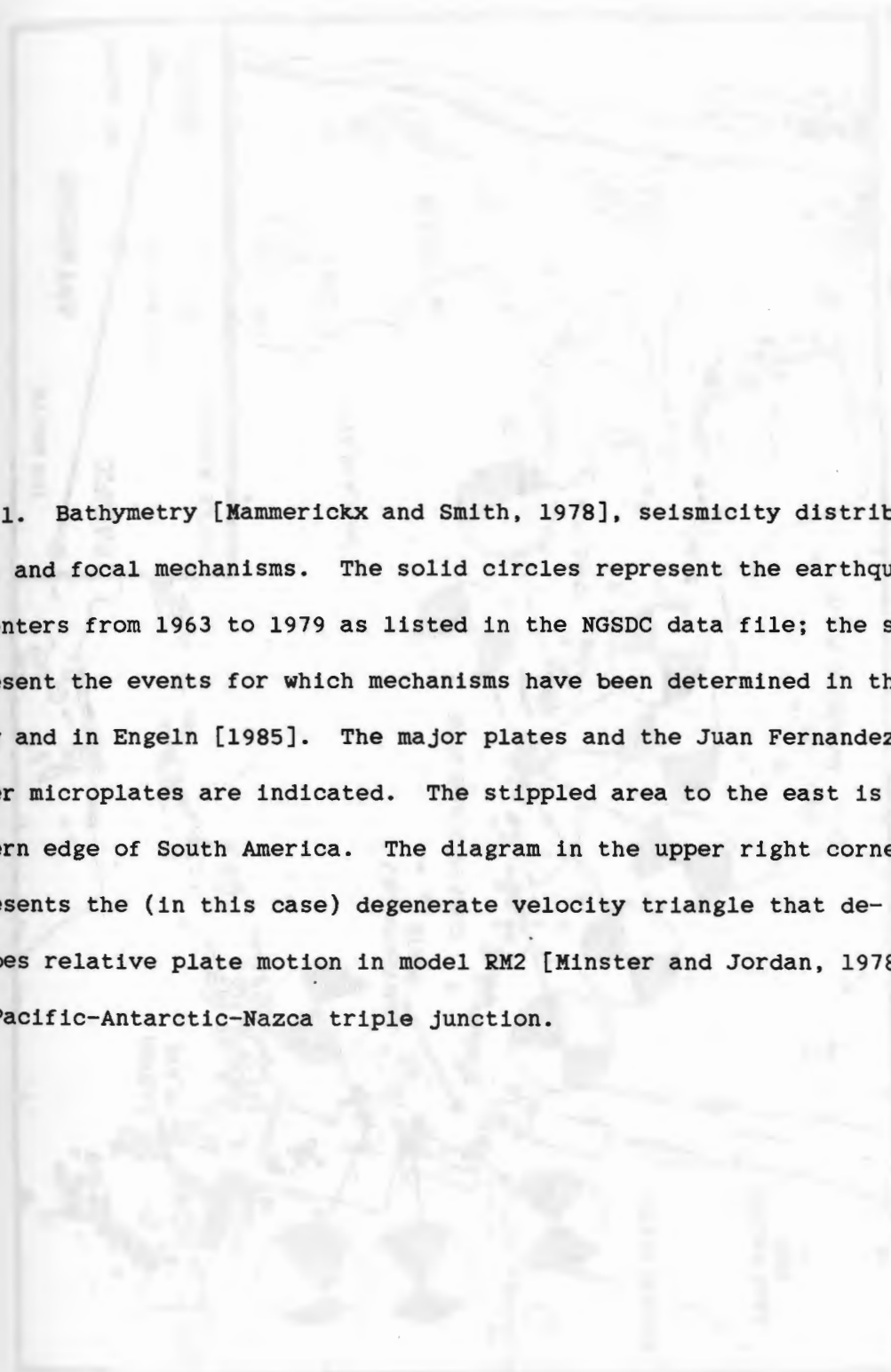
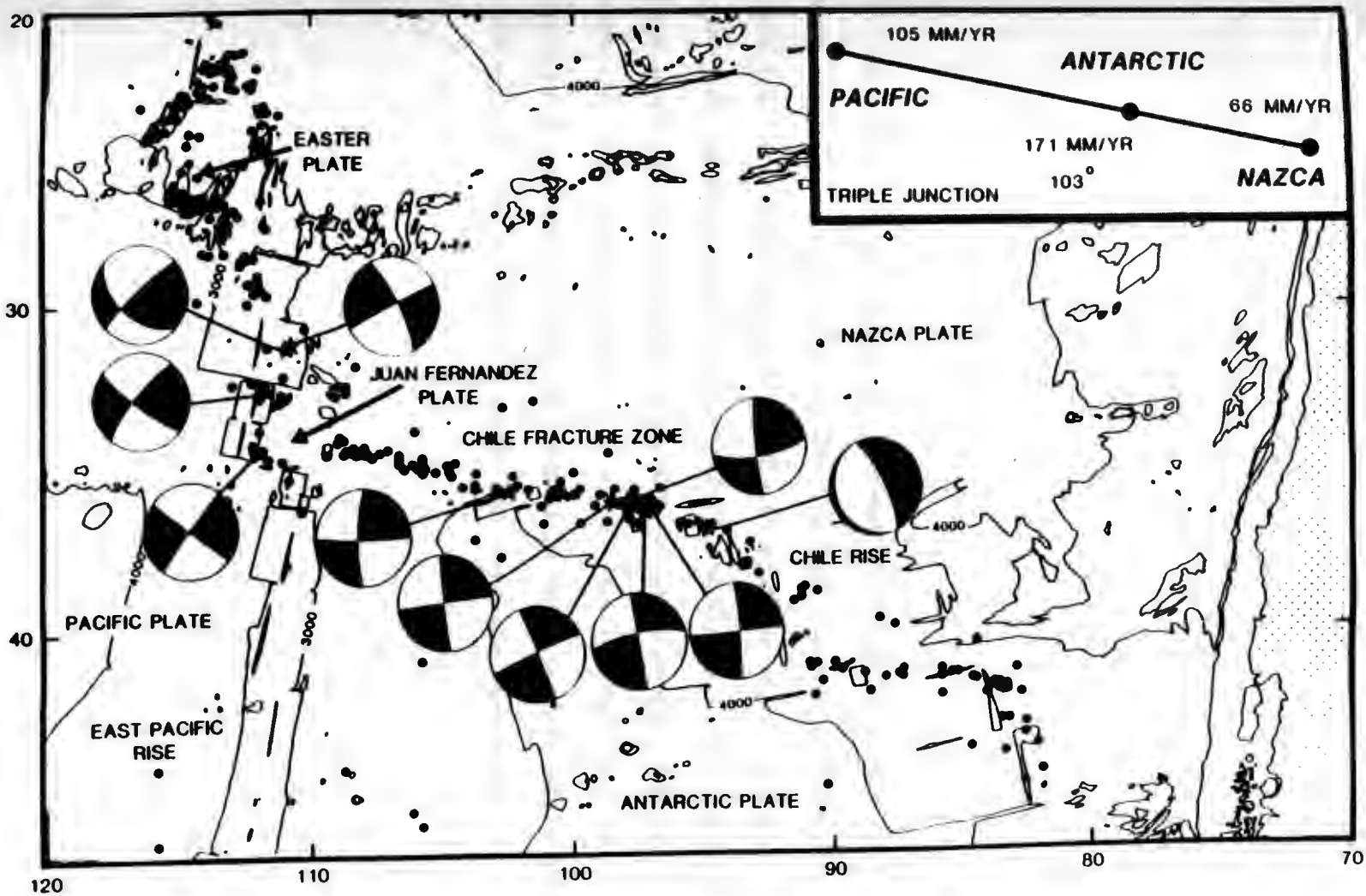
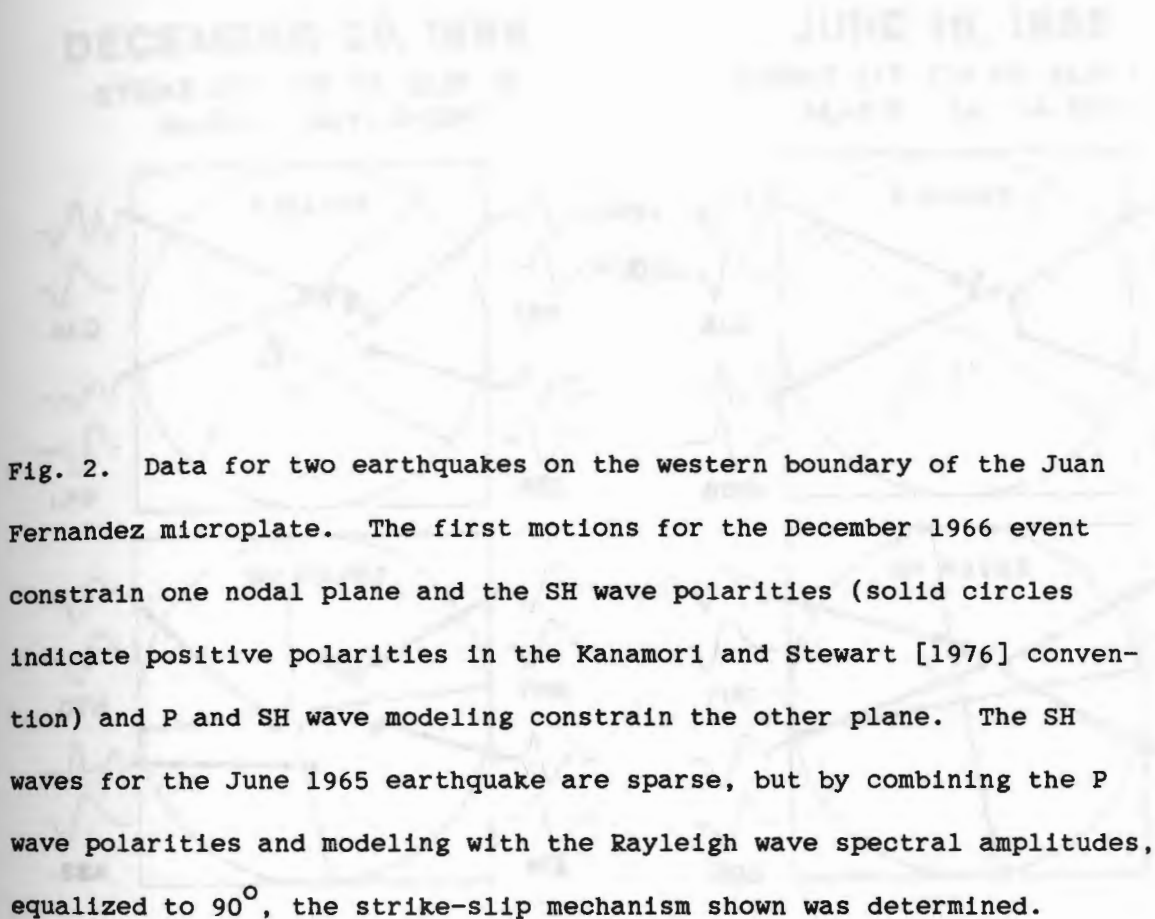


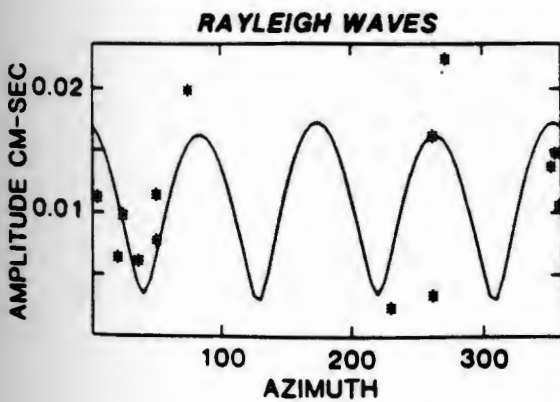
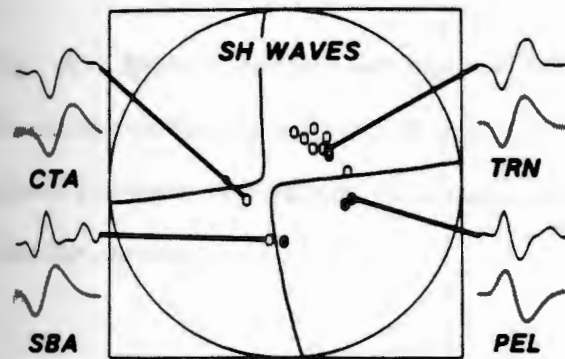
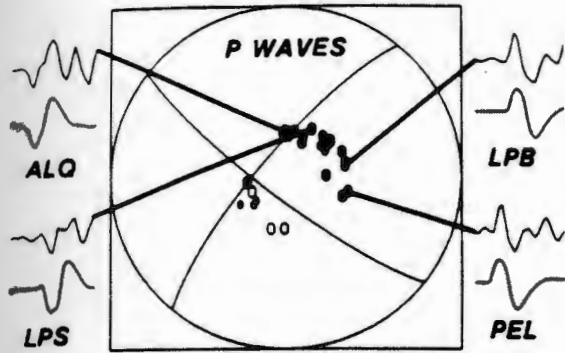
Fig. 1. Bathymetry [Mammerickx and Smith, 1978], seismicity distribution, and focal mechanisms. The solid circles represent the earthquake epicenters from 1963 to 1979 as listed in the NGSDC data file; the stars represent the events for which mechanisms have been determined in this study and in Engeln [1985]. The major plates and the Juan Fernandez and Easter microplates are indicated. The stippled area to the east is the western edge of South America. The diagram in the upper right corner represents the (in this case) degenerate velocity triangle that describes relative plate motion in model RM2 [Minster and Jordan, 1978] at the Pacific-Antarctic-Nazca triple junction.





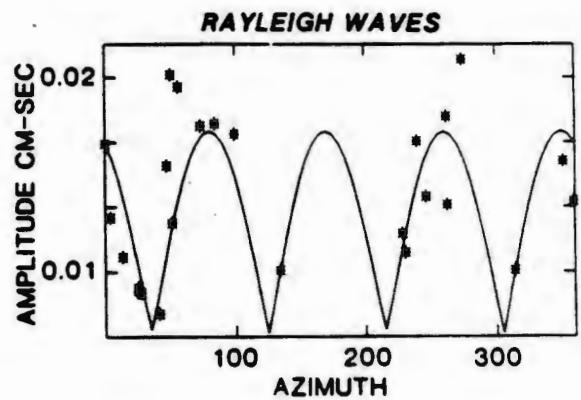
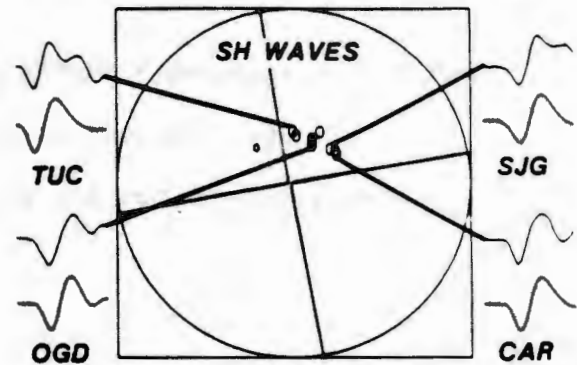
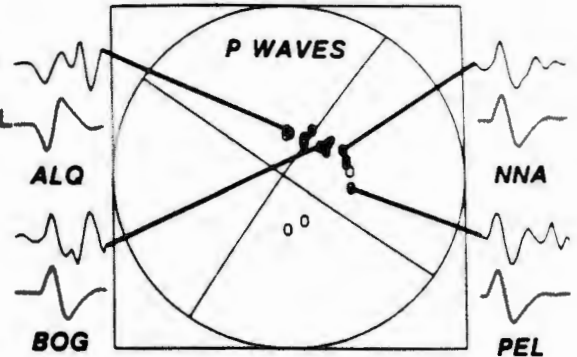
**DECEMBER 29, 1966**

STRIKE 220 DIP 78 SLIP 10  
 $M_S=6.0$   $M_0=1.6 \times 10^{25}$

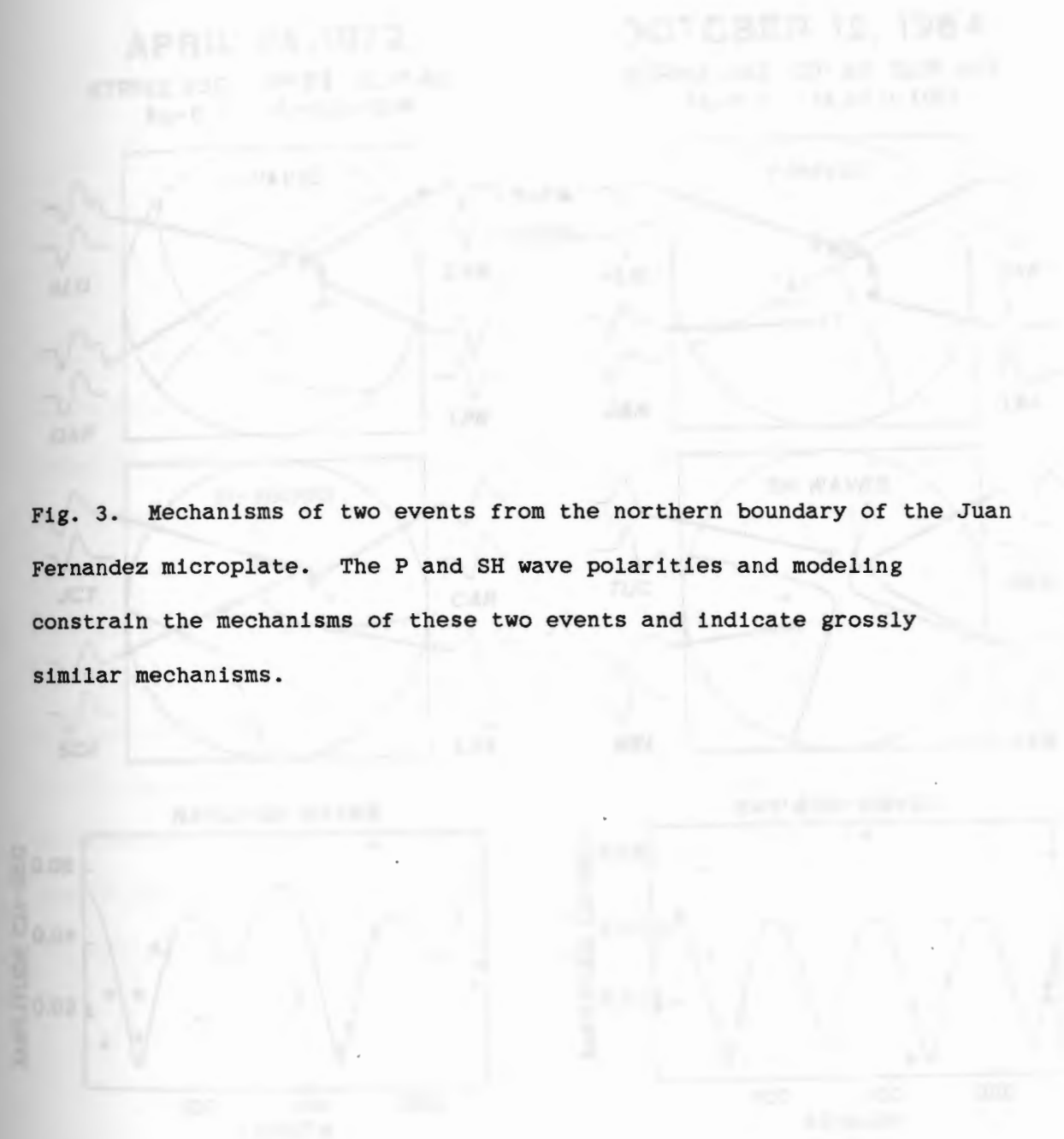


**JUNE 16, 1965**

STRIKE 215 DIP 88 SLIP 1  
 $M_S=5.8$   $M_0=1.4 \times 10^{25}$

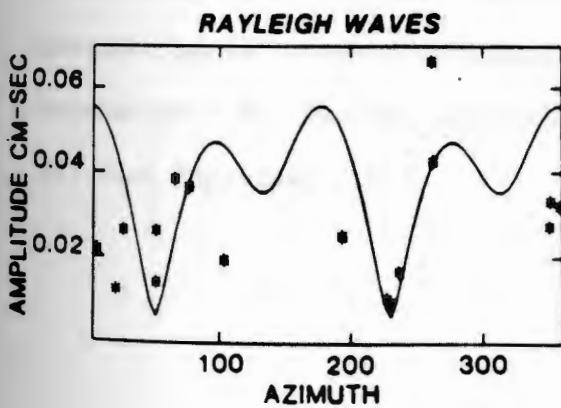
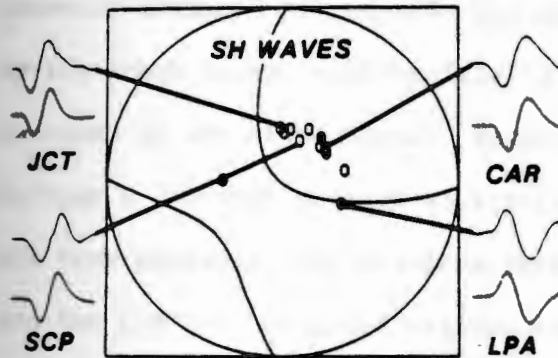
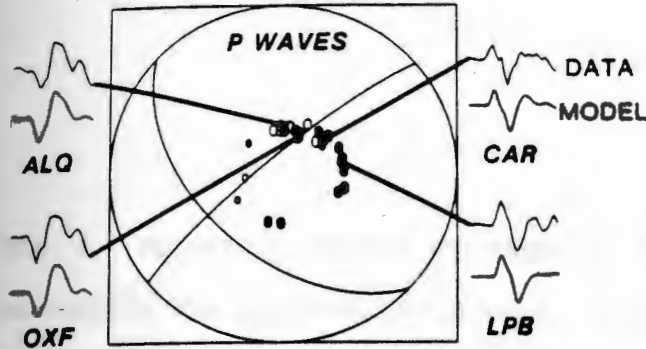






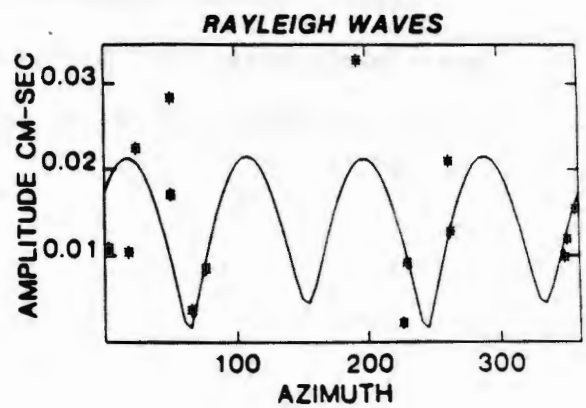
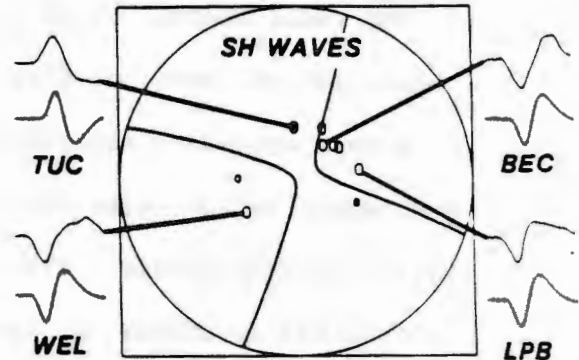
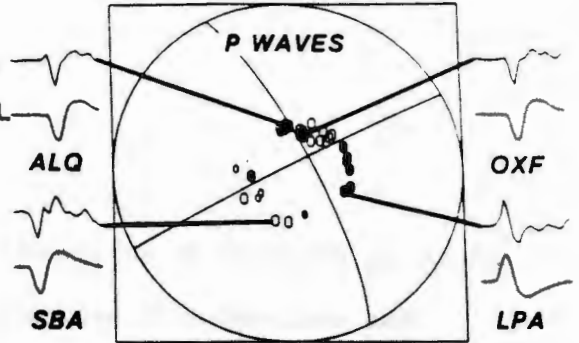
**APRIL 24, 1972**

STRIKE 230 DIP 82 SLIP 40  
 $M_S=6.1$   $M_0=5.3 \times 10^{25}$



**OCTOBER 12, 1964**

STRIKE 243 DIP 88 SLIP 348  
 $M_S=6.1$   $M_0=2.0 \times 10^{25}$



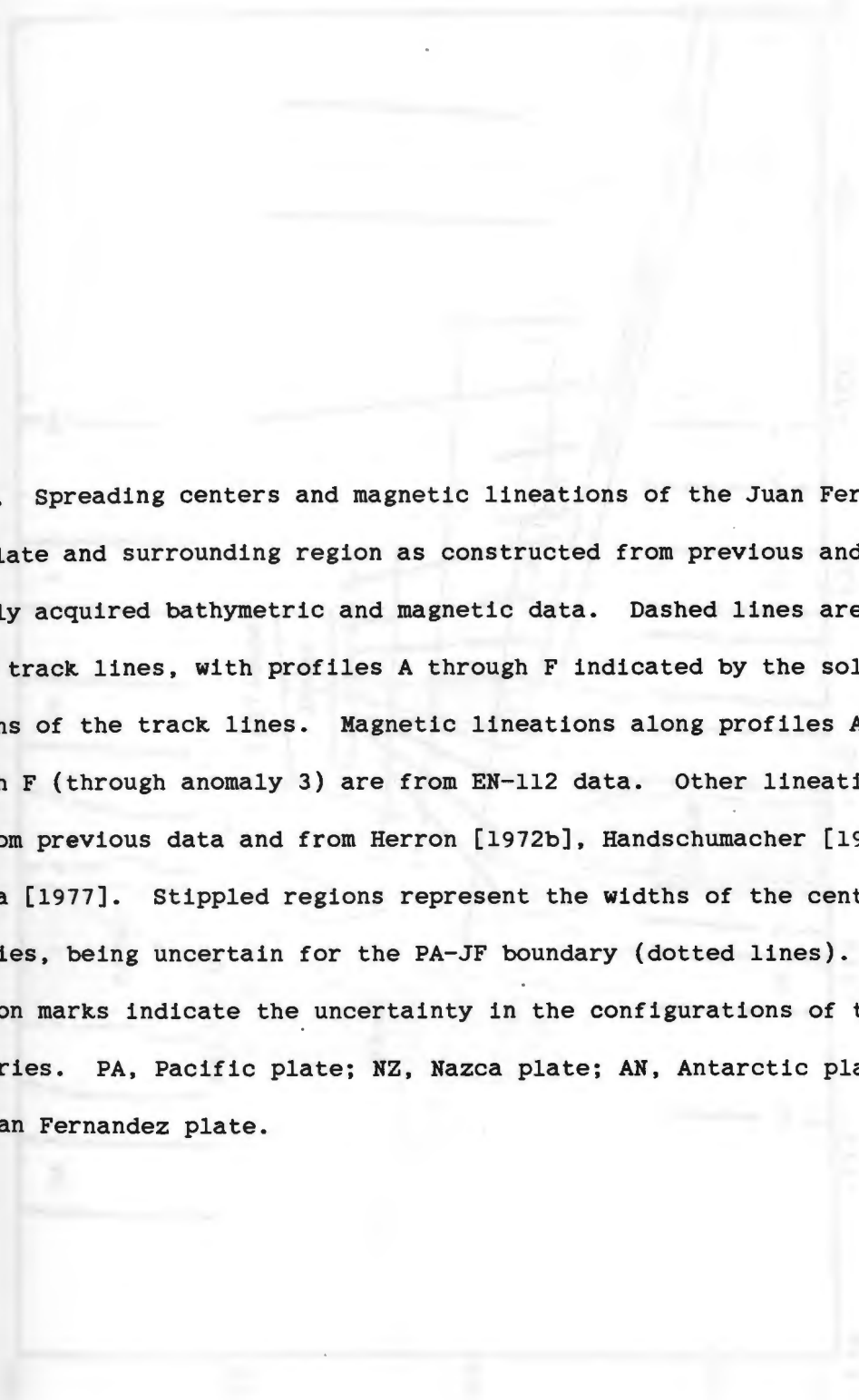


Fig. 4. Spreading centers and magnetic lineations of the Juan Fernandez microplate and surrounding region as constructed from previous and recently acquired bathymetric and magnetic data. Dashed lines are EN-112 track lines, with profiles A through F indicated by the solid sections of the track lines. Magnetic lineations along profiles A through F (through anomaly 3) are from EN-112 data. Other lineations are from previous data and from Herron [1972b], Handschumacher [1976], and Rea [1977]. Stippled regions represent the widths of the central anomalies, being uncertain for the PA-JF boundary (dotted lines). Question marks indicate the uncertainty in the configurations of those boundaries. PA, Pacific plate; NZ, Nazca plate; AN, Antarctic plate; JF, Juan Fernandez plate.

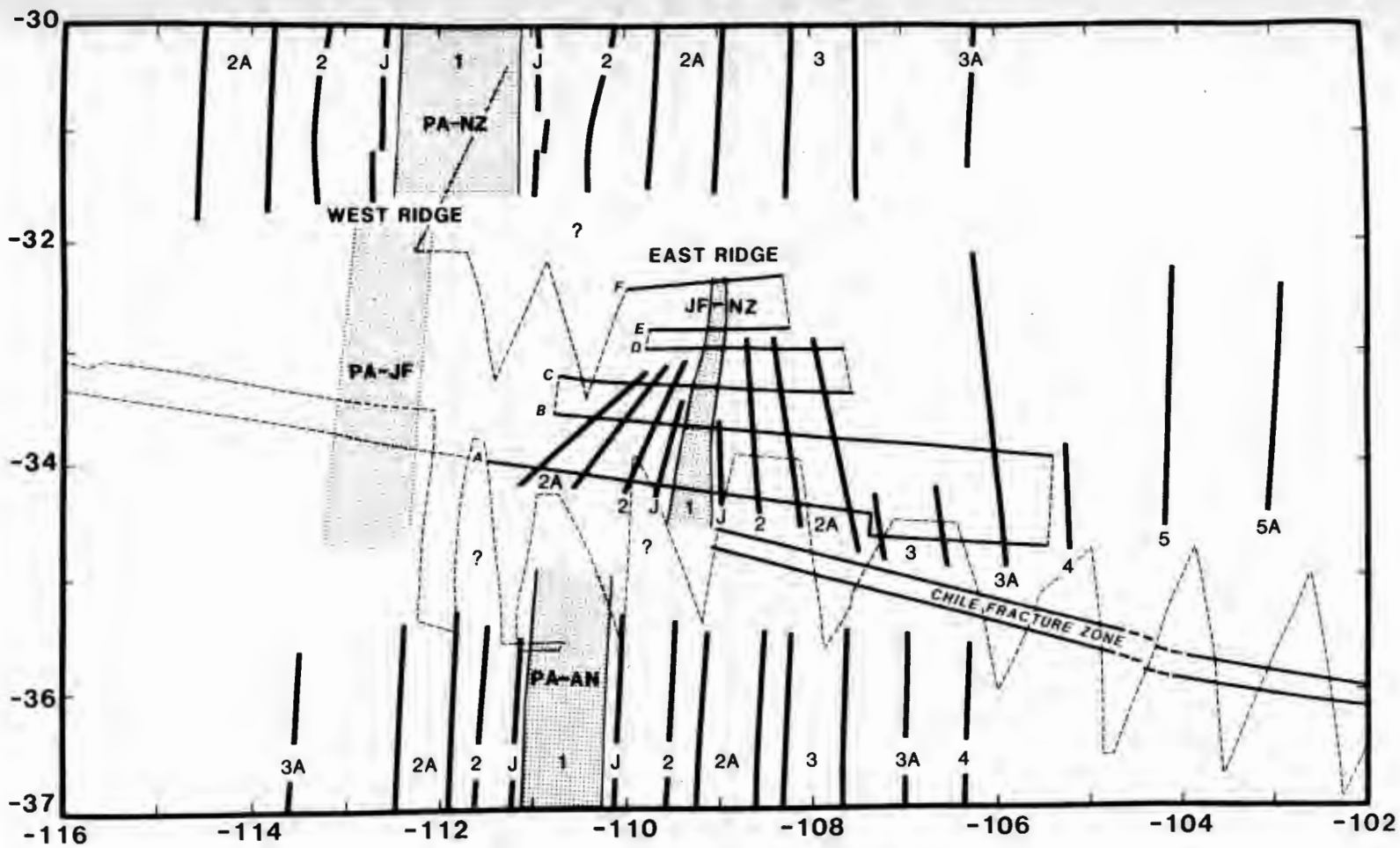


Fig. 5. East Ridge magnetic anomaly profiles projected to an azimuth of  $097^{\circ}$  perpendicular to the spreading axis and aligned along the axial anomaly; see Figure 4 for the locations of the profiles. The model profile is computed from half-spreading rates (S.R.) in cm/year to match profile A and has the following parameters: magnetized layer depth 3.5 to 4.0 km; magnetization 0.015 emu; present day Inc =  $-41^{\circ}$ , Dec =  $17^{\circ}$ ; remanent Inc =  $-52^{\circ}$ , Dec =  $0^{\circ}$ . The black blocks are normally magnetized, white blocks are reversely magnetized. The Jaramillo anomaly is labeled J.



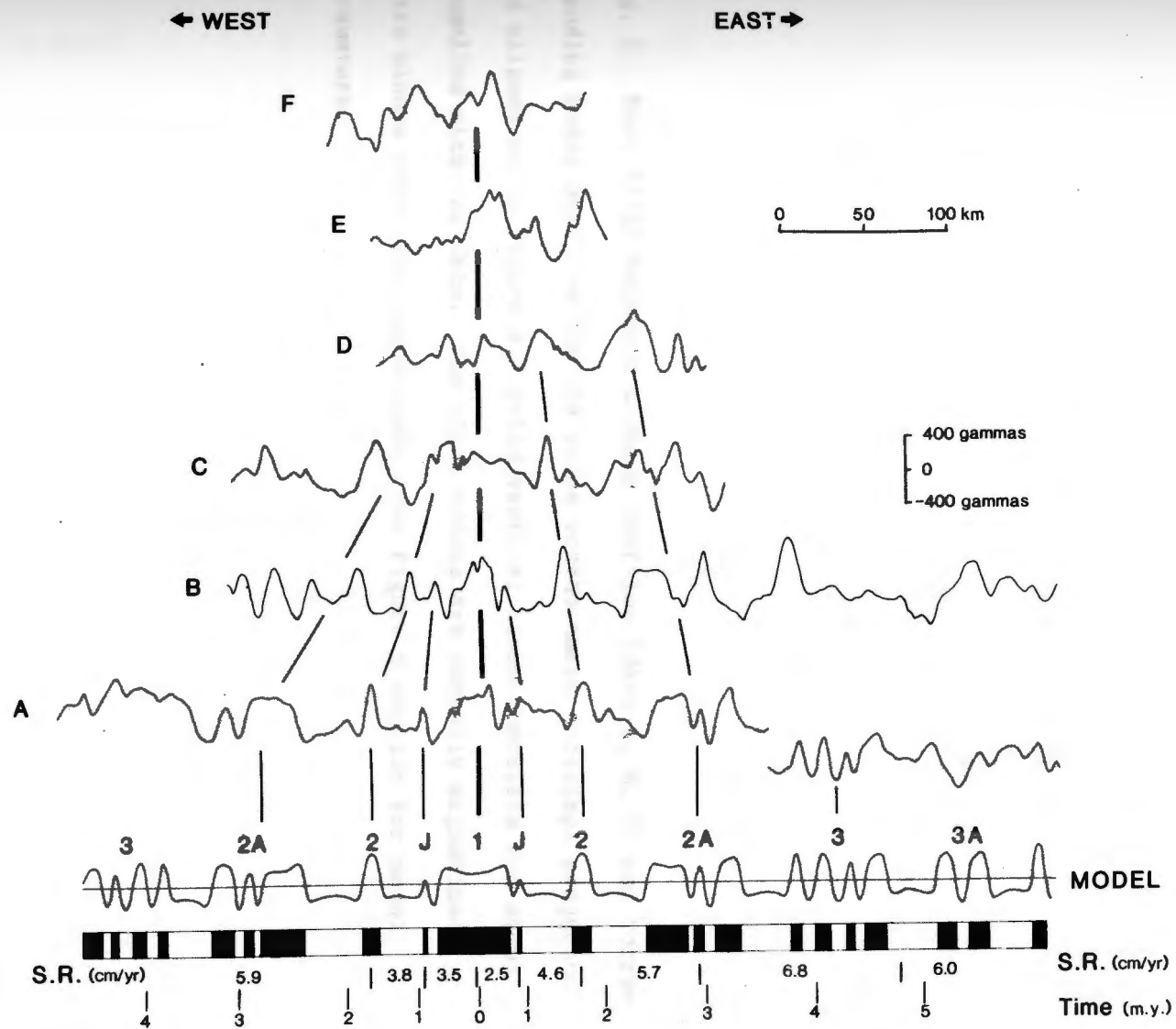
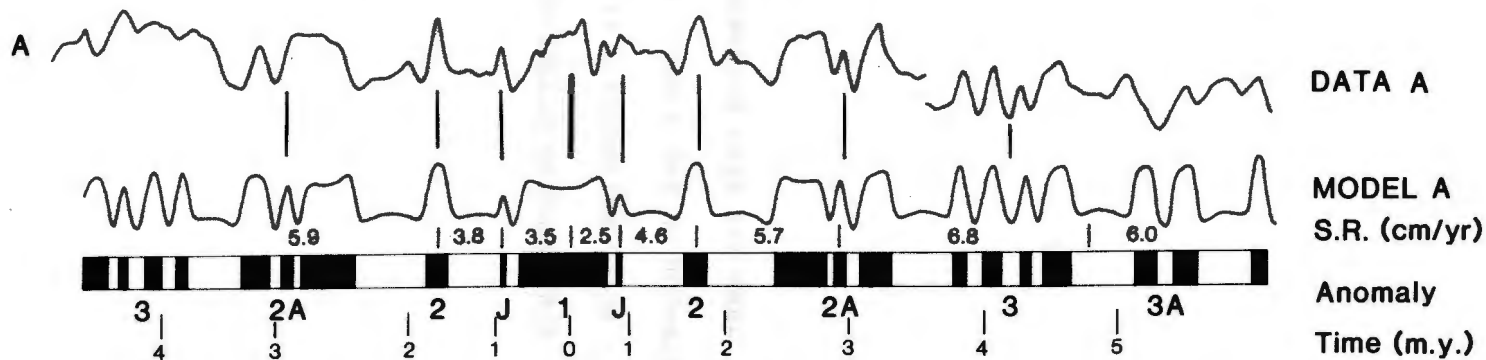
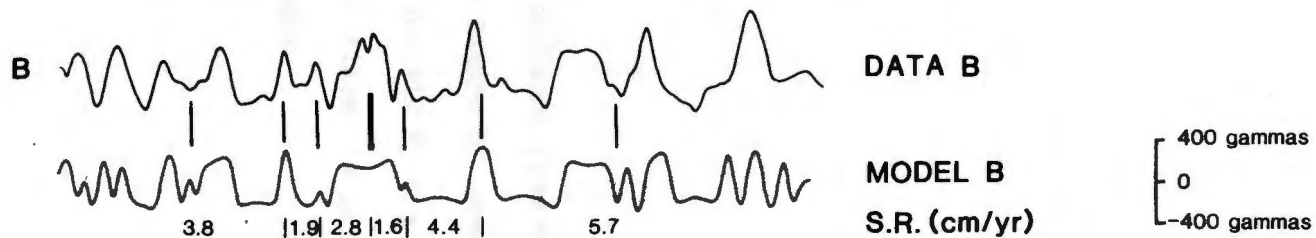
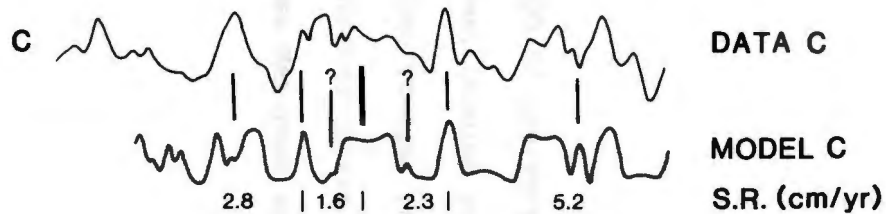


Fig. 6. East Ridge magnetic anomaly profiles (data A, B, C) and corresponding model profiles for the three southernmost crossings projected and aligned as in Figure 5. Solid vertical lines correlate the model anomalies with the data. The black blocks are normally magnetized, white blocks reversely magnetized. See Figure 5 caption for model parameters.

← WEST

EAST →



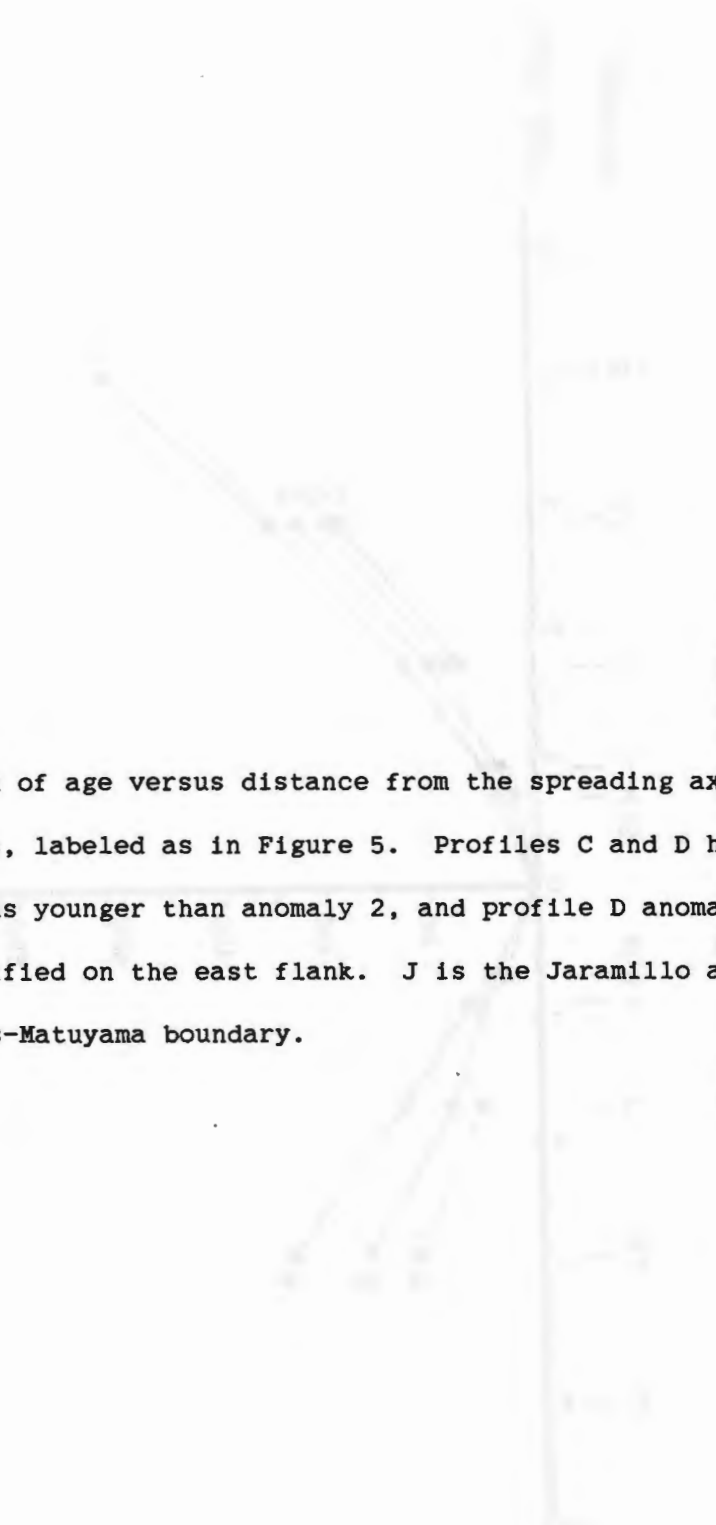
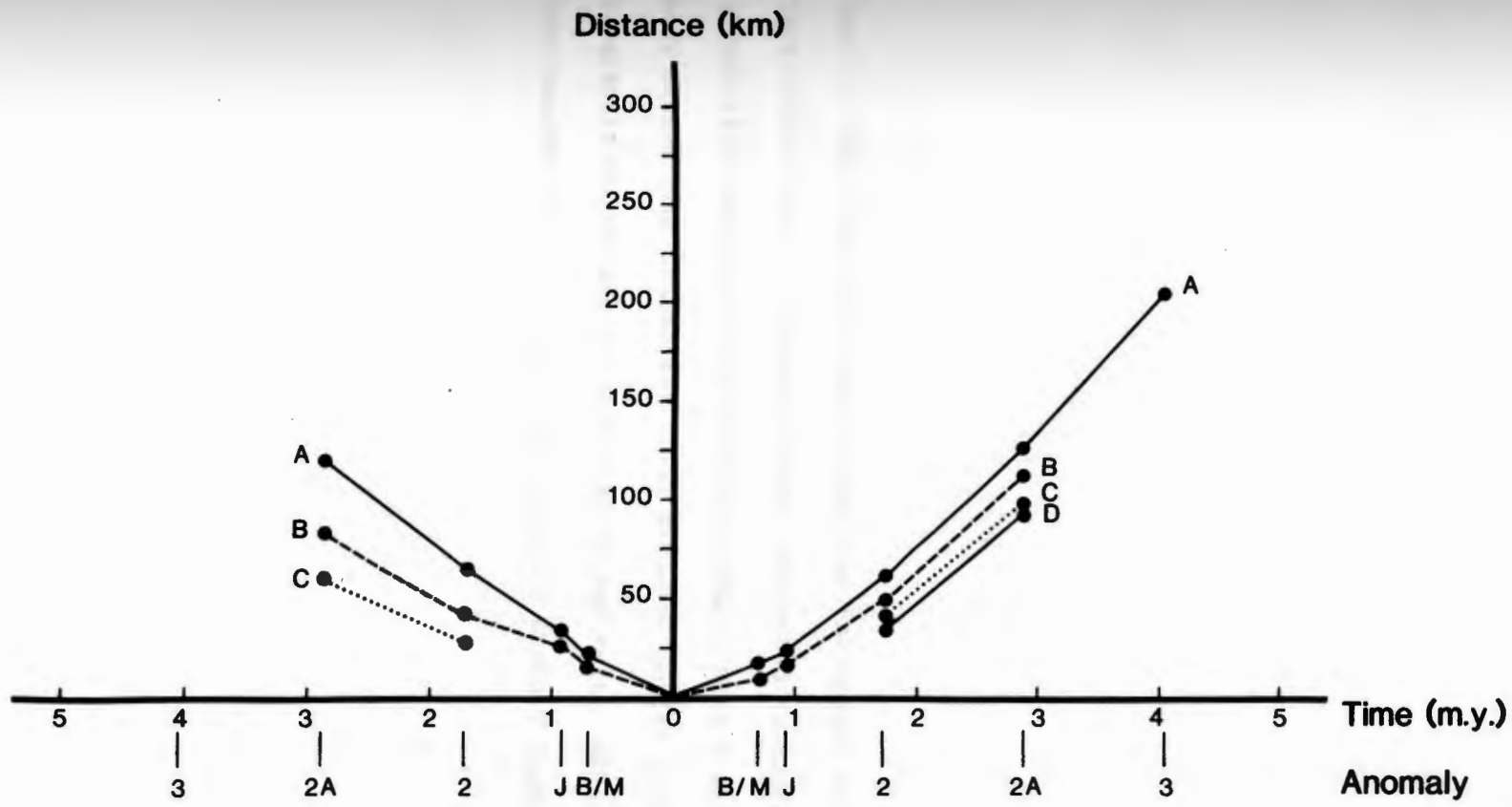


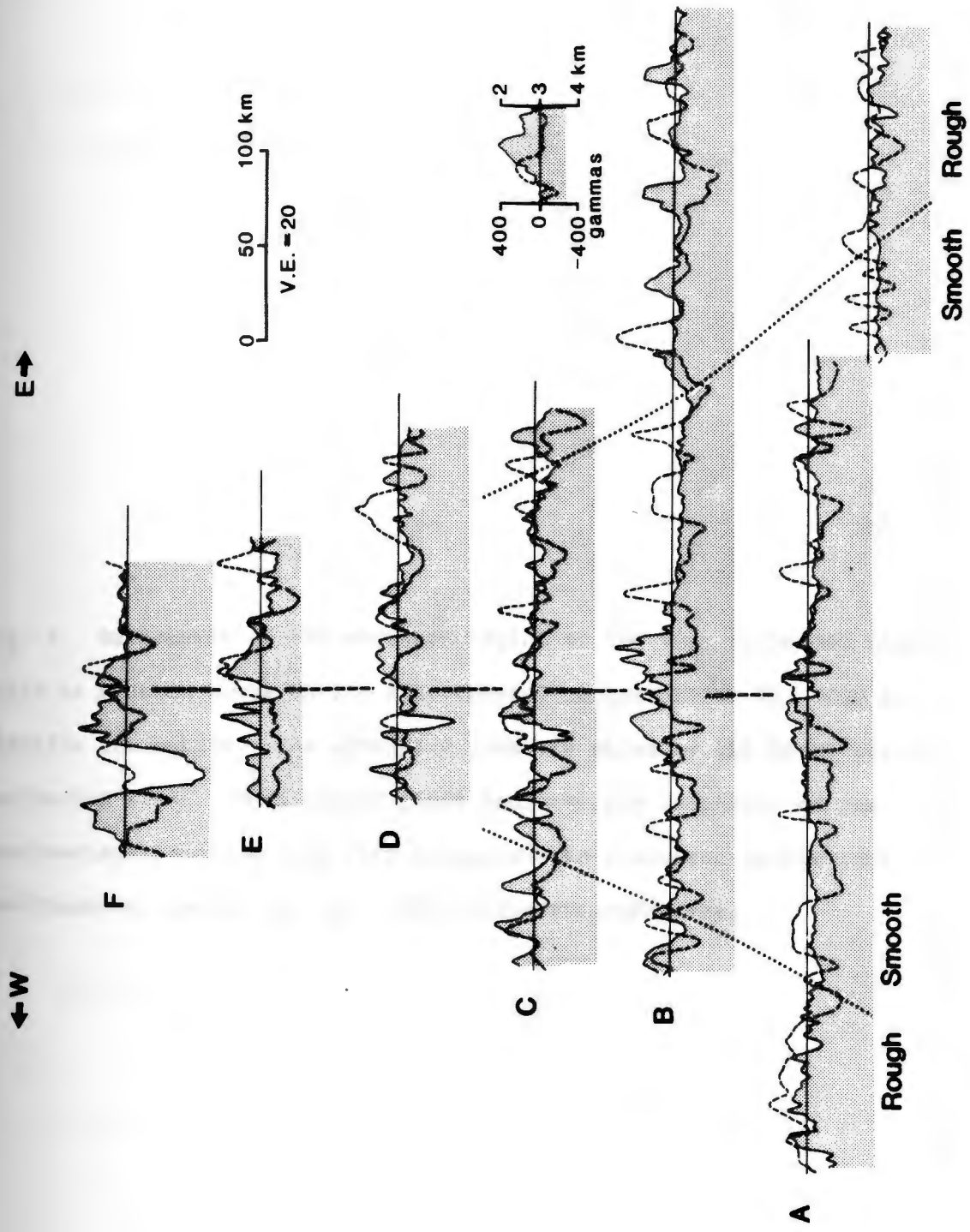
Fig. 7. Graph of age versus distance from the spreading axis for East Ridge profiles, labeled as in Figure 5. Profiles C and D had no anomaly identifications younger than anomaly 2, and profile D anomalies could only be identified on the east flank. J is the Jaramillo anomaly, B/M is the Brunhes-Matuyama boundary.



Age vs. Distance from axis



Fig. 8. East Ridge bathymetric profiles (stippled) and magnetic profiles (from Figure 5, dashed curves) projected to azimuth  $097^{\circ}$  and aligned with respect to the central anomaly, with a baseline of 3000 m. Heavy dashed line traces the axial anomaly; dotted lines trace the topographic boundaries as described in the text. Note the locations of these boundaries relative to the magnetic anomaly locations.



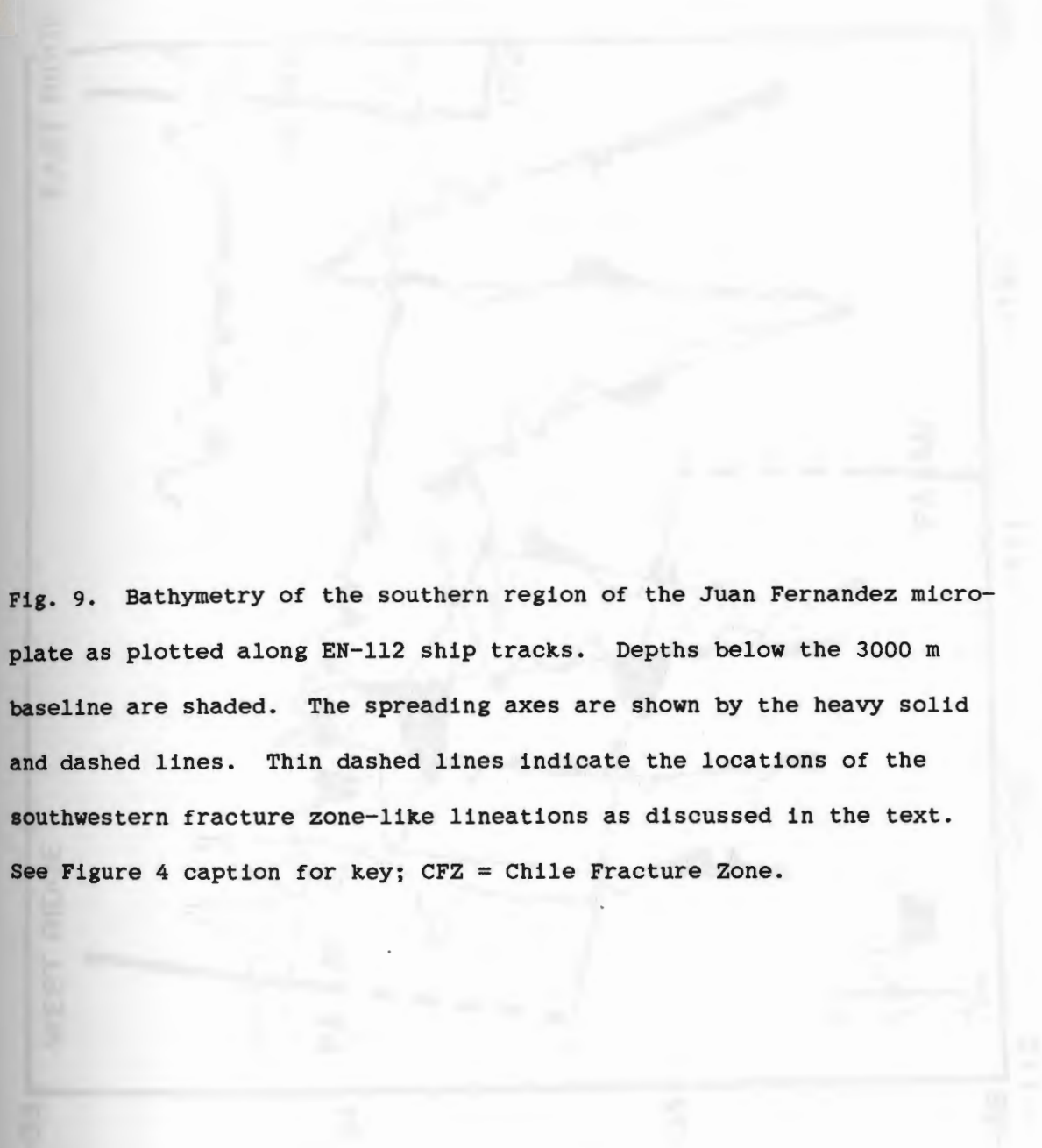
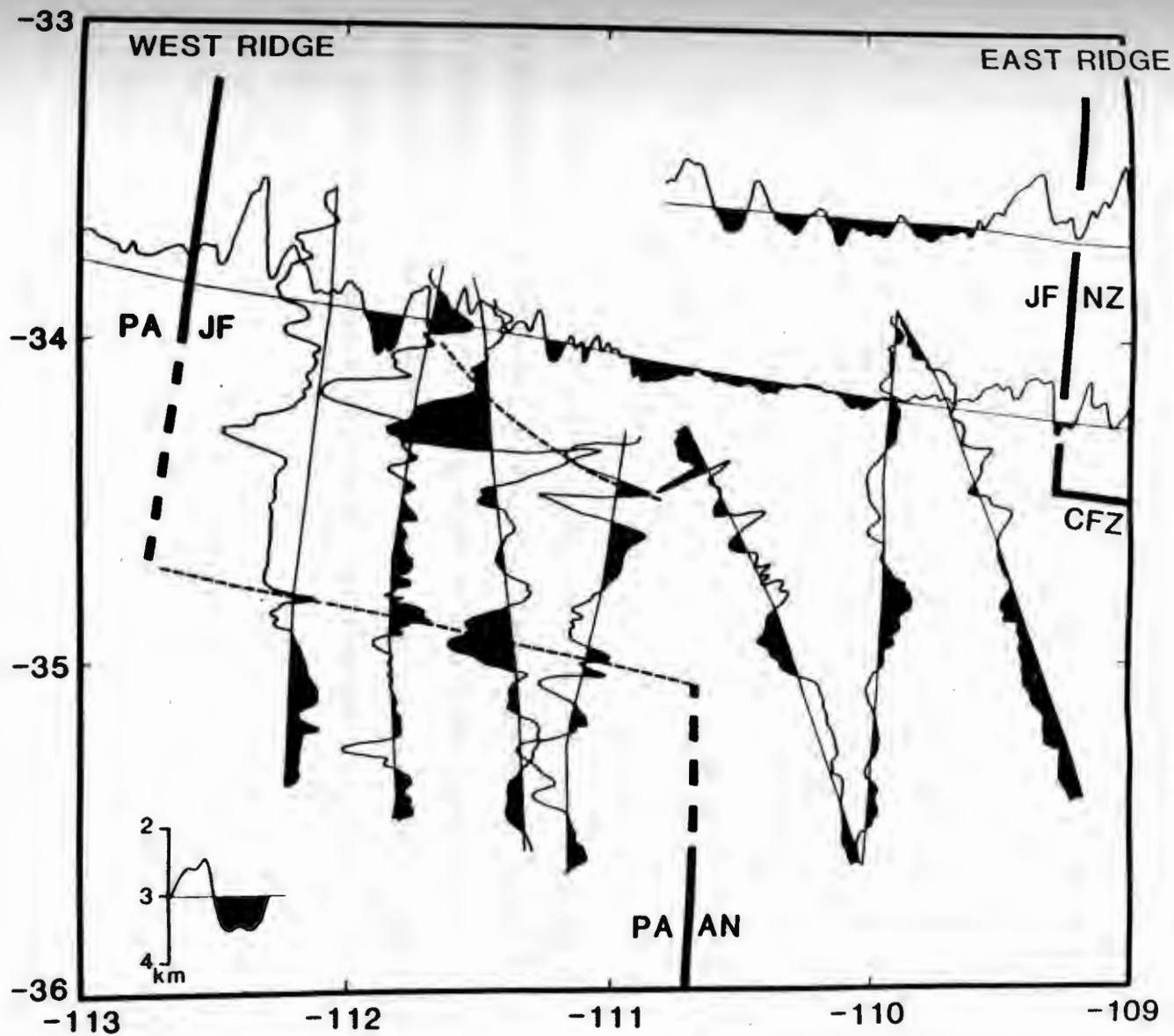


Fig. 9. Bathymetry of the southern region of the Juan Fernandez micro-plate as plotted along EN-112 ship tracks. Depths below the 3000 m baseline are shaded. The spreading axes are shown by the heavy solid and dashed lines. Thin dashed lines indicate the locations of the southwestern fracture zone-like lineations as discussed in the text. See Figure 4 caption for key; CFZ = Chile Fracture Zone.



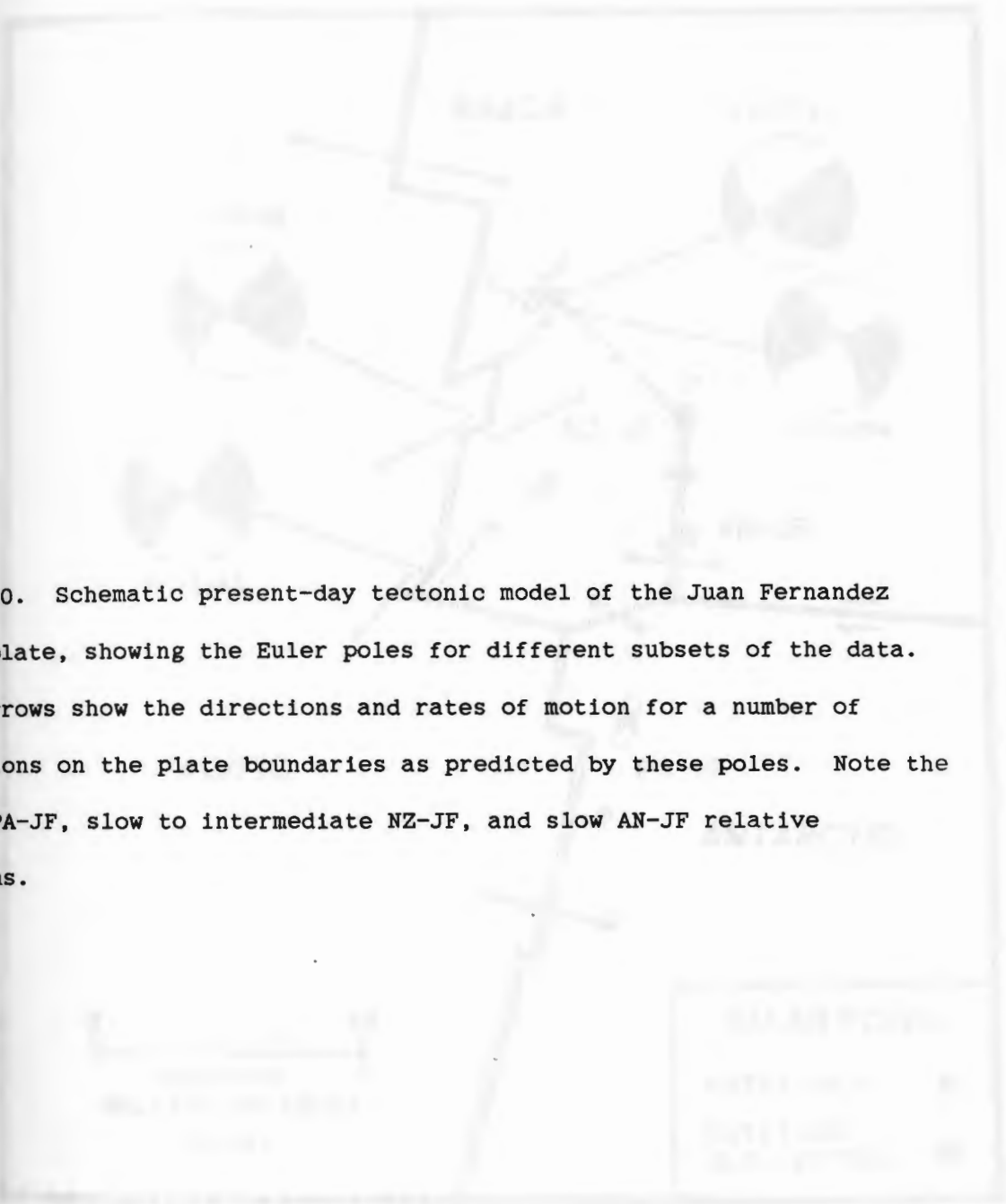
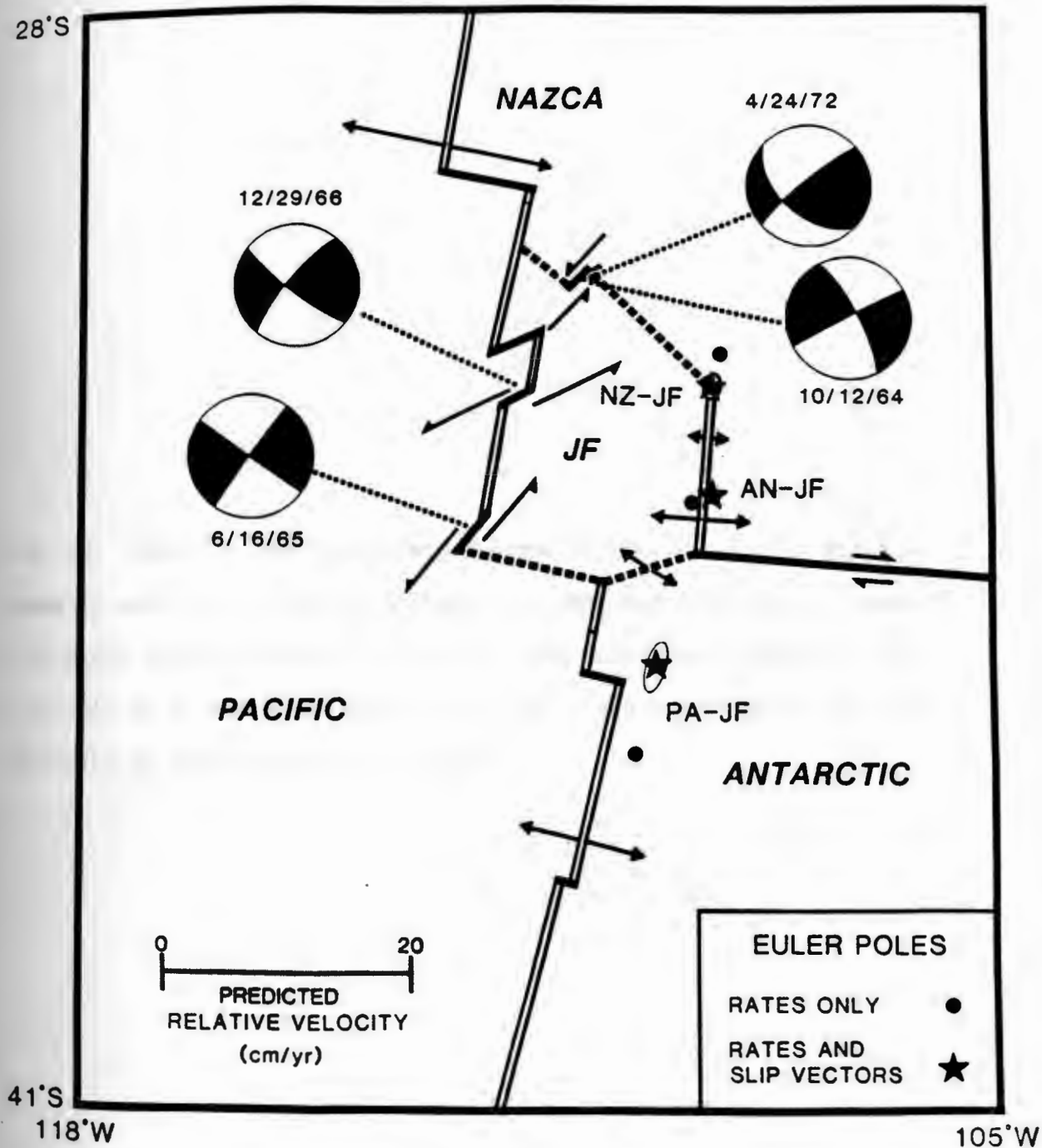


Fig. 10. Schematic present-day tectonic model of the Juan Fernandez microplate, showing the Euler poles for different subsets of the data. The arrows show the directions and rates of motion for a number of locations on the plate boundaries as predicted by these poles. Note the fast PA-JF, slow to intermediate NZ-JF, and slow AN-JF relative motions.



28°S




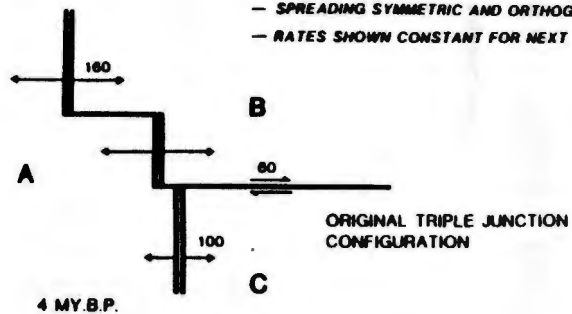


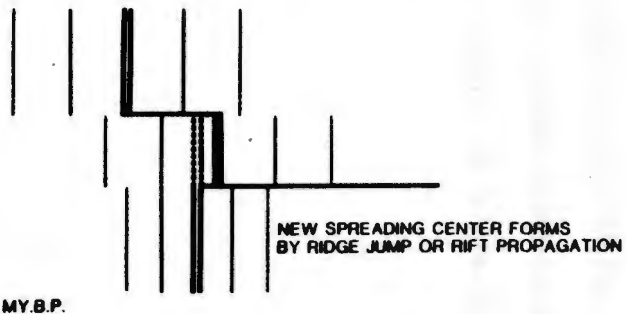
Fig. 11. Possible past evolutionary model for the Pacific (= plate A), Nazca (= plate B), Antarctic (= plate C), and Juan Fernandez (= plate D) four plate system at 1 m.y. intervals. The main simplifications are that this is a flat-plate model (i.e., poles are at infinity) and that spreading is symmetric and orthogonal.

**ASSUMPTIONS**

- POLES AT INFINITY
- SPREADING SYMMETRIC AND ORTHOGONAL
- RATES SHOWN CONSTANT FOR NEXT TIME STEP

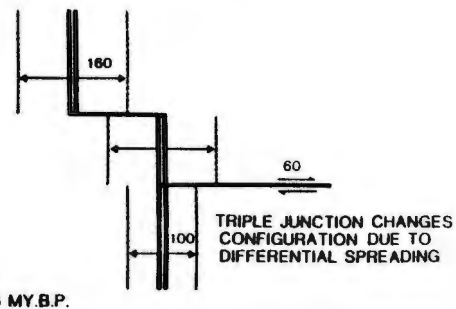


4 MY.B.P.

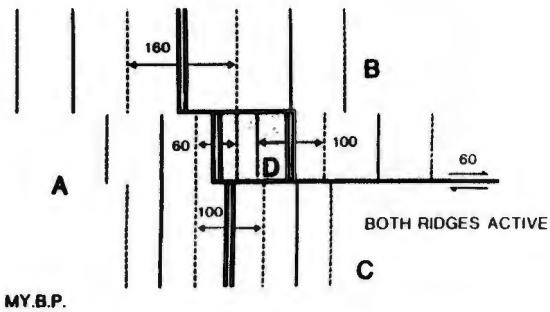


2 MY.B.P.

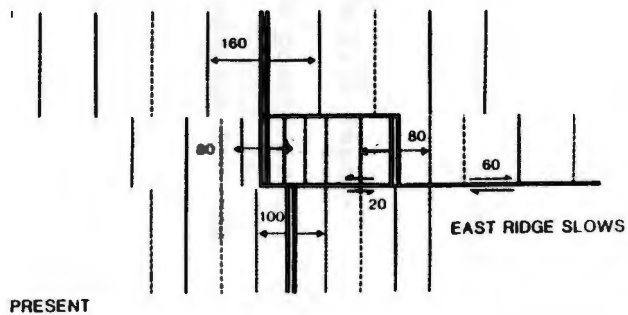
**RATES IN MM/YR**



3 MY.B.P.



1 MY.B.P.



PRESENT

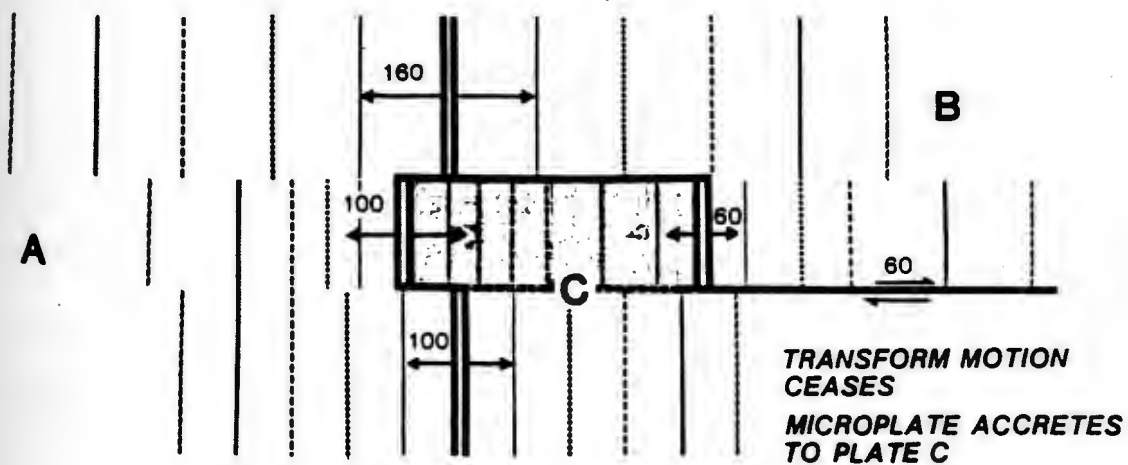
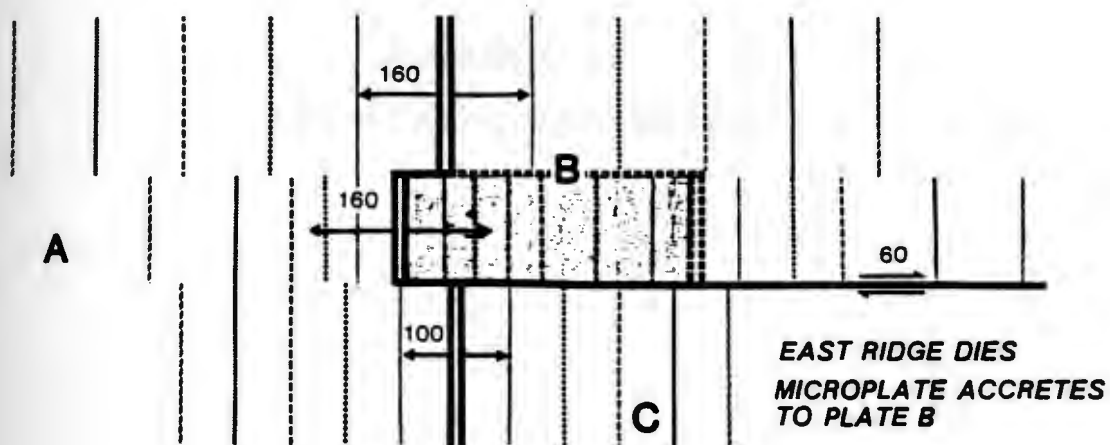
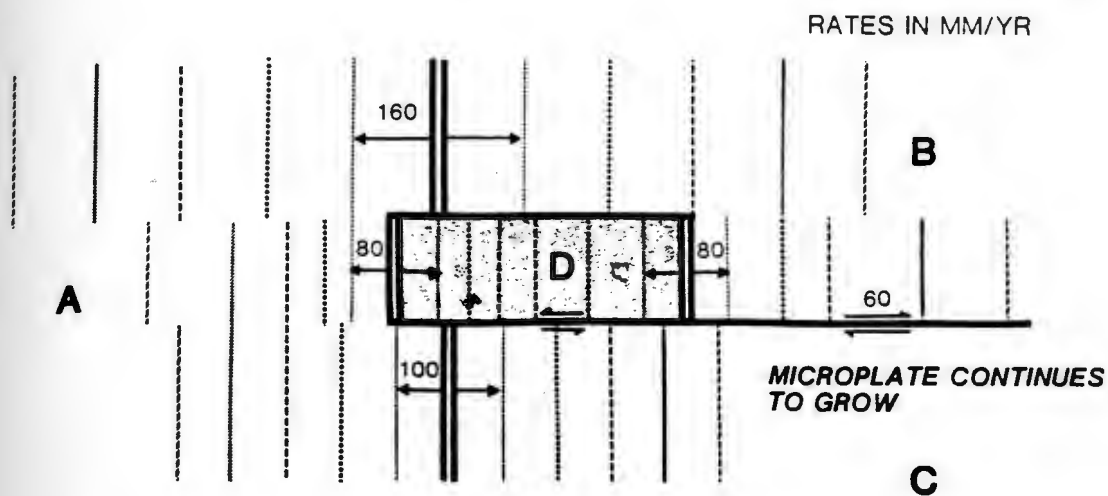
Fig. 12. Possible future evolutionary models for the Pacific-Nazca-Antarctic-Juan Fernandez system. All three examples are possibilities for 1 m.y. in the future. Rates of motion on plate boundaries are the same in all examples.

A



C

EAST PLATE AND  
MIDDLE PLATE ATTACHED  
TO PLATE B





## SUMMARY

In this study we present a new, more detailed tectonic model of part of the Chilean subduction system. We consider the subduction zone from 33°S to 43°S, from 100°W to the intersection with the East Andes of the Juan Fernandez arc, located at 33°S to 35°S, 100°18'W. A possible zone of thrust lines of crust can be followed through the active region, with the transform fault being relatively narrow and well-defined in the western portion from 33°W to approximately 100°18'W. The transform zone then widens to the east, with a probable zone of extensional forces to the south at 100°W.

**TECTONICS OF THE**  
**NAZCA-ANTARCTIC PLATE BOUNDARY**

Along the Chile Transform and the normal faults described near the northern end of the Chile Trench we have compiled a new, larger relative motion data set for the same subduction boundary consisting of three new earthquake and bathymetric data in addition to other data from the western portion of the boundary. We have inverted these data to produce a new best fit pole for the Nazca-Antarctic plate pair, providing tighter constraints on the relative plate motions. This new best fit pole is located farther south and rotates the data better than the best fit pole calculated from old data, though some discrepancies still remain. Additional data, particularly from the western portion of the boundary, are needed to further refine the pole location and improve the agreement between assumed and predicted relative motions along the entire Nazca-Antarctic boundary.

## ABSTRACT

In this study, we present a new, contoured bathymetric chart of part of the Chile transform system, based mainly on bathymetric data from an R/V Endeavor survey, from  $100^{\circ}\text{W}$  to its intersection with the East Ridge of the Juan Fernandez microplate at  $34^{\circ}30'\text{S}$ ,  $109^{\circ}15'\text{W}$ . A generally continuous lineated trend can be followed through the entire region, with the transform valley being relatively narrow and well-defined in the western portion from  $109^{\circ}\text{W}$  to approximately  $104^{\circ}30'\text{W}$ . The fracture zone then widens to the east, with at least two probable en echelon offsets to the south at  $104^{\circ}$  and  $102^{\circ}\text{W}$ . We also present six new strike-slip mechanisms along the Chile Transform and one normal fault mechanism near the northern end of the Chile Rise. We have compiled a new, larger relative motion data set for the Nazca-Antarctic boundary consisting of these new earthquake and bathymetric data in addition to other data from the eastern portion of the boundary. We have inverted these data to produce a new best fit pole for the Nazca-Antarctic plate pair, providing tighter constraints on the relative plate motions. This new best fit pole is located farther south and matches the data better than the best fit pole calculated from old data, though some discrepancies still remain. Additional data, particularly from the western portion of the boundary, are needed to further refine the pole location and improve the agreement between measured and predicted relative motions along the entire Nazca-Antarctic boundary.

## INTRODUCTION

The Chile Fracture Zone in the southeastern Pacific Ocean has been one of the most poorly surveyed sections of the mid-ocean ridge system. It is a major part of the Nazca-Antarctic plate boundary, extending from the Chile Ridge at about  $36^{\circ}\text{S}$ ,  $97^{\circ}30'\text{W}$  to the East Ridge of the recently surveyed Juan Fernandez microplate [1, 2] at  $34^{\circ}30'\text{S}$ ,  $109^{\circ}15'\text{W}$ , a distance of approximately 1300 km (Fig. 1). The geometry of this boundary and the relative motion there have been poorly constrained due to the lack of sufficient geophysical data. Klitgord et al. [3] estimated the half-spreading rate on the Chile Ridge at  $40^{\circ}\text{S}$ ,  $92^{\circ}\text{W}$  to be approximately 40 mm/yr averaged over the past 5 m.y. However, in a later survey Herron et al. [4] collected extensive magnetic data from the eastern section of the Nazca-Antarctic boundary along the Chile Ridge to the Chile Margin triple junction which showed that spreading rates have slowed down over the past 5 m.y. They calculated a present half-spreading rate of no more than 28 mm/yr. Their determination of several transform fault azimuths provided additional constraints on Nazca-Antarctic motion in that area (east of the Chile Fracture Zone).

The limited bathymetric data do not define a lineation direction for the Chile Fracture Zone, but the locations of earthquake epicenters show an overall ESE trend (Fig. 1). However, a limited number of slip directions determined from focal plane mechanisms by Forsyth [5] and Anderson et al. [6] indicate a different slip direction of approximately ENE. These slip directions conflict with those predicted by the world-wide plate motion model of Minster and Jordan [7], while the trend of earth-

quake epicenters from the western portion of the transform (Fig. 1) is nearly parallel to the predicted motion.

The Chile Fracture Zone from  $100^{\circ}\text{W}$  to its termination at the East Ridge of the Juan Fernandez microplate (Figs. 1 and 2) was extensively surveyed for the first time in early 1984 during a marine geophysical cruise of the R/V Endeavor (EN-112). The bathymetric data collected was combined with data from the few previous track lines to construct a new bathymetric contour map of the region (Fig. 2). In this study, we present this new map and discuss the general character and some finer bathymetric features of the transform fault system. In addition, we reconsider the seismicity along the Nazca-Antarctic boundary and present six new strike-slip mechanisms along the Chile Transform. We have compiled a new, larger data set of geophysical information for this plate boundary and use this data set to calculate a new Nazca-Antarctic best fit pole that provides tighter constraints on the relative plate motions.

#### BATHYMETRY AND SEISMICITY

Figure 2 is a contoured bathymetric chart of the Chile transform system based mainly on data from EN-112. The track lines from this cruise follow a sawtooth pattern across the fracture zone from  $100^{\circ}\text{W}$  to its intersection with the East Ridge of the recently surveyed Juan Fernandez microplate [1, 2] at approximately  $109^{\circ}15'\text{W}$ . Additional data were obtained from the National Geophysical Data Center in Boulder, Colorado, and consist of several widely spaced track lines from four



cruises (Fig. 2). The EN-112 conventional echo soundings (uncorrected meters) were positioned with satellite navigation and were plotted at 5 minute (approximately 1.6 km) intervals along track on a Mercator projection at a scale of 4 in.(10 cm)/1° longitude (older soundings at 3 to 5 minute intervals). The juxtaposition of ship tracks on the contours should be noted so the reader is aware of the degree of interpolation between track lines. Soundings along the old track lines were generally in good agreement with the EN-112 data, with positioning cross-over errors less than 7 km. More weight was given to the EN-112 data where the agreement was questionable. The two older tracks (POL7008 and ELT24) that intersect the Chile transform system between 100° and 105°W are very oblique crossings, and by themselves provide little constraint on bathymetric trends. Thus, the EN-112 tracks are crucial in the analysis of the transform's configuration, character, and trend.

Although the interpolation between track lines eliminates some fine bathymetric features, a generally continuous lineated trend can be followed through the entire region. The trend gradually changes from 109° (109° to ~106°45'W) to 102° (106°45' to ~104°W), and from 93° to 91° from ~103°45' to 100°W. At about 104°W, there appears to be a small en echelon offset or change in transform character. West of this location the probably active transform valley, generally deeper than 4000 m, can easily be traced to its termination just west of 109°W (Fig. 2), where the bathymetric lineations curve northward to parallel the Juan Fernandez microplate's East Ridge axis [1, 2]. The width of the fracture zone through this section of the transform varies from approxi-



mately 20 to 50 km from  $109^{\circ}$  to  $105^{\circ}30'W$ . The width then increases significantly from 90 to 130 km eastward. East of  $104^{\circ}W$ , it is difficult to define the active transform valley, though the deepest troughs appear to be shifted southward compared to the deepest trough west of  $104^{\circ}W$ , perhaps indicating the presence of an en echelon offset. Another offset may exist at approximately  $102^{\circ}W$ , though its location is not well-constrained. In this eastern half of the transform, the topography consists of a series of fracture zone-parallel ridges and troughs. On the south side of the intersection of the transform and the East Ridge of the Juan Fernandez microplate, there is a topographic high less than 3000 m in depth (Figure 2). Similar highs, possibly due to lithospheric melting, have also been observed at fast-slipping ridge-transform intersections such as at the Clipperton and Garrett transforms (P.J. Fox, personal communication, 1985; D. Gallo, personal communication, 1985). No topographic deep or nodal basin is observed at the ridge-transform intersection, though some deepening of the East Ridge's rift valley to its intersection with the fracture zone at  $34^{\circ}30'S$ ,  $109^{\circ}30'W$  is probable (<200m).

In Figure 3, we show stacked bathymetric profiles projected orthogonal to the suspected transform trend. The change in morphology along strike is apparent. The possible en echelon offsets are located near profile 7 ( $\sim 104^{\circ}W$ ) and between profiles 3 and 4 ( $\sim 102^{\circ}W$ ). From east (profile 1) to west (profile 13) the profiles show an obvious change from a series of peaks and troughs, with this rough topography up to 150 km wide, to a single, well-defined valley west of profile 9. This val-

ley is from 5 to 10 km wide, with a local relief of approximately 2000 to 2500 m. It is particularly deep and well-defined near its intersection with the East Ridge (profile 13). On profiles 12 and 13, the north side of the transform valley is 400 to 700 m higher than the south side, with the topography both north and south of the valley being particularly smooth on profiles 11, 12, and 13. It becomes more difficult to define the active transform valley east of profile 9 as the rough topography becomes broader, showing a local relief which varies from 500 to 2000 m along the profiles. On profiles 1 and 2, the topography on the Antarctic plate to the south of the fracture zone is noticeably smoother than that to the north on the Nazca plate. Profile 1 again shows a better-defined transform valley with a local relief of approximately 2000 m.

The trend of earthquake epicenters clearly follows the apparent bathymetric trend of the transform system (Fig. 4). From  $100^{\circ}\text{W}$  to approximately  $105^{\circ}\text{W}$ , the epicenters are widely scattered, consistent with the greater width of the fracture zone bathymetry in this eastern section and the lack of a clearly defined active transform valley. West of  $105^{\circ}\text{W}$ , where the transform valley is narrower and better defined, there is significantly less scatter in the epicenter locations which clearly coincide with the valley. Gaps in the seismicity appear to occur near  $104^{\circ}$  and  $102^{\circ}\text{W}$ , the locations of the probable offsets mentioned earlier. The greatest amount of scatter in epicenter locations occurs between  $104^{\circ}$  and  $102^{\circ}\text{W}$ , possibly reflecting the existence of a number of small offsets. The southward shift of epicenter locations

east of  $102^{\circ}\text{W}$  further implies the presence of the offset in the transform there that was ambiguous in the bathymetry. East of  $100^{\circ}\text{W}$ , the available bathymetric data consist only of a few very widely spaced track lines, making it unrealistic to contour the fracture zone to its intersection with the Chile Rise at  $-97^{\circ}30'\text{W}$ . However, the earthquake epicenters continue to follow the projected trend of the fracture zone through this region (Fig. 1).

#### EARTHQUAKE STUDIES

The seismicity of the Chile Rise and Chile transform system also defines the Nazca-Antarctic plate boundary. New mechanisms were determined for six strike-slip earthquakes along the Chile Transform and one normal fault mechanism near the northern end of the Chile Rise (Fig. 1, Table 1). All events were studied using P wave first motions and Rayleigh wave spectral amplitudes. Figure 5 shows the first motions and surface wave amplitude patterns for three of these events. Though the few stations located to the south limit the accurate determination of the fault planes, first motion polarities from all four quadrants were observed, indicating strike-slip motion. For all three events, the north-south nodal plane could be determined using the first motions alone, and both planes of the April 14, 1979, earthquake are constrained. We interpret Rayleigh wave radiation patterns as four-lobed, suggesting strike-slip motion on either north-south or east-west trending fault planes. Data for the other three Chile Transform earthquakes are shown in Figure 6. The September 13, 1965, and July 12, 1979,



events are similar to the other three. However, the strike of the June 26, 1974, earthquake appears to be somewhat different from that of the other events. This apparent difference may be due to poor station coverage.

We also obtained a normal fault mechanism for one event which occurred near the northern end of the Chile Rise (Fig. 7). First motions partially constrain the steeply dipping nodal plane, and the two-lobed Rayleigh wave radiation pattern indicates primarily dip-slip motion on a plane trending  $335^{\circ}$ .

The strike-slip mechanisms show a discrepancy with the apparent trend of the Chile transform system. The east-west nodal plane strike is noticeably more northerly than expected from the morphology. This situation suggests that either a "leaky" component of extension may be present, though no such events were observed, or the region consists of a series of en echelon transform faults [5, 8], though the gross bathymetry suggests only two offsets, both east of  $105^{\circ}\text{W}$ . Unfortunately, no events west of  $102^{\circ}30'\text{W}$  were large enough to be studied. However, it may be significant to note that the slip vector for the event at  $102^{\circ}30'\text{W}$ , calculated to be  $91^{\circ}$  (Table 1), is close to the measured transform azimuth at that location, which is between  $93^{\circ}$  and  $91^{\circ}$ . This may suggest that the discrepancy between slip vector direction and transform (and epicenter) trend is not as great as previously believed [5, 6]. There is clearly a need for additional slip vector data west of  $102^{\circ}\text{W}$  to test this hypothesis.

## TECTONICS OF THE NAZCA-ANTARCTIC BOUNDARY

The relative motion at the Nazca-Antarctic boundary has been poorly constrained, largely due to a lack of data along this boundary. We have compiled a new, larger data set which includes, in addition to RM2 data [7], magnetic and transform azimuth data from Herron et al. [4] and slip vector and transform azimuth data from this study. These data are listed in Table 2 along with their estimated uncertainties and their fit to our newly determined Euler vector. The easterly trending nodal planes of the Chile Transform earthquakes were taken as the fault planes based on the seismicity distribution (Fig. 1) and the earlier determined poles.

Herron et al. [4] had carried out an extensive bathymetric, gravity, heat flow, and magnetic survey of the Chile Rise to the southeast of the area where the mechanisms were determined. The strikes of three transform faults determined by their survey provide greater control over the direction of Nazca-Antarctic motion in this area. We derived spreading rates from their magnetic data using the LaBrecque et al. [9] time scale. The full spreading rates since anomaly 2 time (1.84 Ma) are approximately 60 mm/year, which is slower than the 76 mm/year rate for this ridge calculated by Klitgord et al. [3], whose data were averaged over the past 5 m.y. This discrepancy is in accord with Herron et al.'s [4] suggestion that spreading has slowed with time, implying that 76 mm/year may be an overestimation of present spreading rates. We thus elected to use the lower rates determined from Herron et al.'s [4] data to include in our data set.



Using the Minster et al. [10] algorithm, we inverted this new relative motion data set for the Nazca-Antarctic boundary (Table 2) to determine a new best fit pole for this plate pair. The results of our inversions and a comparison with previous results are summarized in Table 3 and are shown in Figures 8 and 9. Since Minster and Jordan [7] did not publish a best fit pole for this plate pair, we used their data set and algorithm to produce one (Fig. 8, solid circle). The difference between the pole for this plate pair from global model RM2 [7] and the best fit pole produced using their data and algorithm indicates how poorly motion along this boundary was constrained. Our new pole (Fig. 8, star) is closer to the RM2 pole for this plate pair and matches the data better than the previous data's best fit pole (Fig. 9). This suggests that the larger data set is improving the determination of Nazca-Antarctic relative motion, and also that the world data set in RM2 was adequate to model reasonably accurately the Nazca-Antarctic pole location, even though relative motion data from that plate boundary was clearly inadequate when used by itself. Figure 9 summarizes the data and the predictions of the new best fit pole and the other poles. The differences between the predictions of RM2 and the best fit pole produced using Minster and Jordan's [7] data are very pronounced. In particular, the rates predicted by the old best fit pole fall well outside the standard deviations for the observed rates. Also, there is a clear divergence from east to west between the azimuths predicted by the old best fit pole and those predicted by the other poles and measured from the data. This divergence is also evident in Figure 10.

The predictions of the new best fit pole provide a much better fit overall to the data, indicating that our pole is an improvement over that produced by the old data. However, the quality of the fit to the west is apparently poorer than that to the east for our new pole. Also shown in Figure 9 are the Nazca-Antarctic predicted relative motions based on the Pacific-Nazca-Antarctic-Juan Fernandez four-plate inversion from Anderson-Fontana et al. [2]. These predictions are close to those for our new best fit pole, particularly for the azimuths, but don't fit the rate data as well as the new pole.

In Figure 10 we show small circle trends produced by the different rotation poles superimposed on the transform bathymetry of the western portion of the Nazca-Antarctic boundary; only 3500 and 4000 m and greater contours are shown to avoid confusion. The different points of origin are used so several trends can be illustrated, and do not necessarily represent offsets in the transform. East of  $104^{\circ}\text{W}$ , the trends predicted by our new best fit pole are apparently closer to the bathymetric trend than those predicted by the other poles. However, west of  $104^{\circ}\text{W}$  we see a divergence from the fit between the data and transform trends predicted by the new best fit pole, suggesting that the modeled pole location is still in need of improvement.

#### DISCUSSION

The inversion of our new data set for the Nazca-Antarctic plate boundary has produced a new best fit pole for that plate pair. This new pole predicts relative motions that fit the data better and agree more

closely with motions predicted by the RM2 pole than a best fit pole produced by the previous data set used in the derivation of RM2. However, there is a misfit between the data and the relative motion predicted by the new best fit pole in the western portion of the transform (Fig. 10). Inspection of Figure 9 suggests that this results from a moderate amount of incompatibility between the bathymetric trends from  $101^{\circ}$  to  $109^{\circ}$ W and the slip vector azimuths from earthquakes between  $95^{\circ}$  and  $100^{\circ}$ W. One reason for this discrepancy may be that the topography is far more complex than it appears, with numerous en echelon offsets that trend more easterly (in agreement with the predicted trends) although the overall bathymetry and epicenters trend ESE. Another reason may be that the paucity of geophysical data in the western portion of the Nazca-Antarctic boundary limits the accurate determination of a best fit pole. The general lack of focal mechanisms from  $101^{\circ}$  to  $109^{\circ}$ W and, correspondingly, the lack of precise bathymetric surveys from  $95^{\circ}$  to  $100^{\circ}$ W are the main impediments resolving this question.

Our new best fit pole is located much closer to the Nazca-Antarctic boundary than the old pole, and also south of the RM2 pole (Fig. 8). This is consistent with our data which indicates slower spreading rates and more curvature in the boundary than previously believed. It may be argued that finer bathymetric trends in the western portion of the boundary could be more easterly rather than ESE, thus decreasing the curvature and moving the pole farther north. However, present geophysical data seem to indicate that this is not so. First, our bathymetric data show a relatively narrow, well-defined transform valley west of



105°30'W. Although it is possible that some of the finer trends could be overlooked, it is unlikely that there are any major offsets through this section that would significantly change the actual transform azimuth. Second, although the earthquake data is very sparse west of 100°W, events at 102°30'W and 105°W are in good agreement with the bathymetric data. The event at 102°30'W presented in this study has a strike of 90° and slip vector direction of 91°, nearly parallel to the interpreted transform trend at that location. Dziewonski et al. [13] reported an event located in the transform at 105°W, which was recorded by the Global Digital Seismograph Network (GDSN), with a fault plane strike of 100°, also nearly parallel to the transform azimuth. These earthquake data suggest that our reported transform azimuths are accurate and the Euler pole is indeed located further south than previous data suggested, or than we calculate with this present data set.

The fact that the curvature in the boundary appears greater than even the new best fit pole predicts implies that this pole is located even further south. While our data set has significantly improved the calculated location of the best fit pole, thus providing tighter constraints on Nazca-Antarctic relative motions, a weakness exists due to the fact that most of the data are from locations east of 100°W. Additional geophysical data from the western portion of the boundary are still needed to further refine the pole location and improve the agreement between measured and predicted relative motions along the entire Nazca-Antarctic boundary.

## REFERENCES

- 1 H. Craig, K.-R. Kim and J. Francheteau, Active ridge crest mapping on the Juan Fernandez micro-plate: the use of Sea Beam-controlled hydrothermal plume surveys, *Trans. Am. Geophys. Union* 64, 45, 1983.
- 2 S. Anderson-Fontana, J.F. Engeln, P.Lundgren, R.L. Larson and S. Stein, Tectonics and evolution of the Juan Fernandez microplate at the Pacific-Nazca-Antarctic triple junction, *J. Geophys. Res.* 91, 2005-2018, 1986.
- 3 K.D. Klitgord, J.D. Mudie, P.A. Larson and J.A. Grow, Fast sea-floor spreading on the Chile Ridge, *Earth Planet. Sci. Lett.* 20, 93-99, 1973.
- 4 E.M. Herron, S.C. Cande and B.R. Hall, An active spreading center collides with a subduction zone: a geophysical survey of the Chile Margin triple junction, *Geol. Soc. Am. Mem.* 154, 683-702, 1981.
- 5 D.W. Forsyth, Mechanisms of earthquakes and plate motions in the East Pacific, *Earth Planet. Sci. Lett.* 17, 189-194, 1972.
- 6 R.N. Anderson, D.W. Forsyth, P. Molnar and J. Mammerickx, Fault plane solutions on the Nazca Plate boundaries and the Easter Plate, *Earth Planet. Sci. Lett.* 24, 188-202, 1974.



- 7 J.B. Minster and T.H. Jordan, Present-day plate motions, *J. Geophys. Res.* 83, 5331-5354, 1978.
- 8 E.M. Herron, Sea-floor spreading and the Cenozoic history of the East-Central Pacific, *Geol. Soc. Am. Bull.* 83, 1671-1692, 1972.
- 9 J.L. LaBrecque, D.V. Kent and S.C. Cande, Revised magnetic polarity time scale for late Cretaceous and Cenozoic time, *Geology* 5, 330-335, 1977.
- 10 J.B. Minster, T.H. Jordan, P. Molnar and E. Haines, Numerical modeling of instantaneous plate tectonics, *Geophys. J. R. Astron. Soc.* 36, 541-576, 1974.
- 11 H. Kanamori and G.S. Stewart, Mode of the strain release along the Gibbs Fracture Zone, *Phys. Earth Planet. Inter.* 11, 312-333, 1976.
- 12 J. Mammerickx and S.M. Smith, Bathymetry of the Southeast Pacific, *Geol. Soc. Am. Map Chart Ser.*, MC-26 442, 194, 1978.
- 13 A.M. Dziewonski, A. Friedman, D. Giardini and J.H. Woodhouse, Global seismicity of 1982: Centroid-moment tensor solutions for 308 earthquakes, *Phys. Earth Planet. Inter.*, 33, 76-90, 1983.

TABLE 1: Source Parameters of Earthquakes Studied

Date	Time	Latitude	Longitude	$M_s$	$m_b$	$M_o$	Mechanism *
6/18/72	0058:35	-37.20	-95.20	5.5	5.5	$9.8 \times 10^{24}$	335/75/270
10/23/70	1101:28	-36.50	-97.20	5.5	5.4	$6.0 \times 10^{24}$	85/89/185
9/13/65	1615:44	-36.60	-97.50	5.9	5.4	$2.1 \times 10^{25}$	260/75/180
6/26/74	1343:35	-36.60	-98.20	5.6	5.4	$9.6 \times 10^{24}$	246/86/186
7/12/79	2322:17	-36.30	-98.10	5.4	5.7	$8.4 \times 10^{24}$	84/73/174
4/20/75	1140:40	-36.40	-98.80	6.2	5.8	$1.8 \times 10^{26}$	262/89/182
4/14/79	1000:25	-36.00	-102.60	6.6	5.6	$1.0 \times 10^{26}$	90/86/170

\* Strike, dip, and slip angles using Kanamori and Stewart [11] conventions.

TABLE 2: Plate Motion Data: Nazca-Antarctic Plates

Latitude	Longitude	Datum	Standard Deviation	Weighted Residuals	Importance	Source
<u>Rates</u>						
-38.20	-94.20	5.80	0.80	0.01	0.52	H
-44.60	-78.30	6.20	0.80	-0.01	0.58	H
<u>Transforms</u>						
-41.30	-88.50	n80e	10.00	-0.27	0.12	RM2
-44.60	-80.00	n71e	10.00	-0.15	0.20	H
-45.72	-77.50	n71e	10.00	-0.37	0.23	H
-45.90	-77.30	n69e	10.00	-0.18	0.23	H
-34.90	-108.00	s75e	10.00	-0.77	0.24	T
-35.25	-106.00	s78e	10.00	-0.69	0.19	T
-35.90	-103.00	s84e	10.00	-0.41	0.13	T
-36.18	-101.00	s89e	10.00	-0.12	0.11	T
<u>Slip Vectors</u>						
-36.20	-100.90	n82e	15.00	0.51	0.05	RM2
-36.30	-97.20	n79e	15.00	0.45	0.04	RM2
-41.70	-84.00	n86e	15.00	-0.87	0.07	RM2
-36.40	-98.80	n82e	15.00	0.37	0.04	T
-36.00	-102.60	s89e	15.00	0.03	0.06	T
-36.30	-98.10	n86e	15.00	0.05	0.04	T
-36.50	-97.20	n81e	15.00	0.32	0.04	T
-36.60	-98.10	n66e	15.00	1.38	0.04	T
-36.60	-97.50	n80e	15.00	0.41	0.04	T
-37.20	-95.30	n60e	15.00	1.59	0.04	T

Weighted residuals and importances are those for the inversion using the new pole derived in this study. Rates are in centimeters per year; transform fault and slip vector azimuths are measured in degrees. Sources: RM2, compiled by Minster and Jordan [7]; H, Herron et al. [4]; T, this study.

TABLE 3: Euler Vectors: Nazca-Antarctic Motion

Latitude	Longitude	Degrees Per Million Years	Reduced Chi-Squared
<u>New Best Fit Pole</u>			
23.80	-102.20	0.589	0.446
<u>RM2 Pole</u>			
43.21	-95.02	0.605	1.067
<u>Best Fit Pole From Previous Data</u>			
83.56	-131.40	0.839	0.275

Reduced chi-squared is the value for the Nazca-Antarctic motion only.

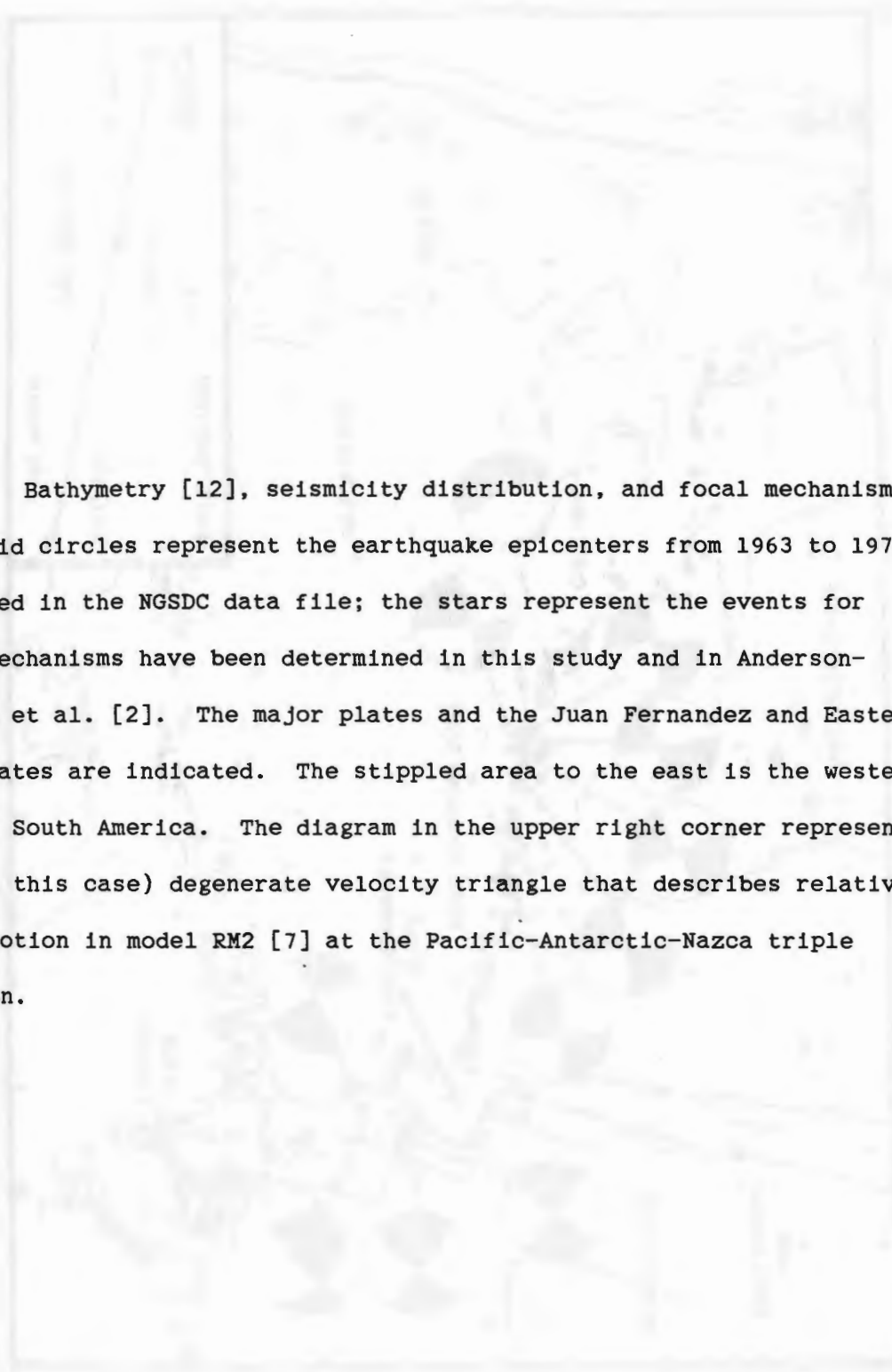
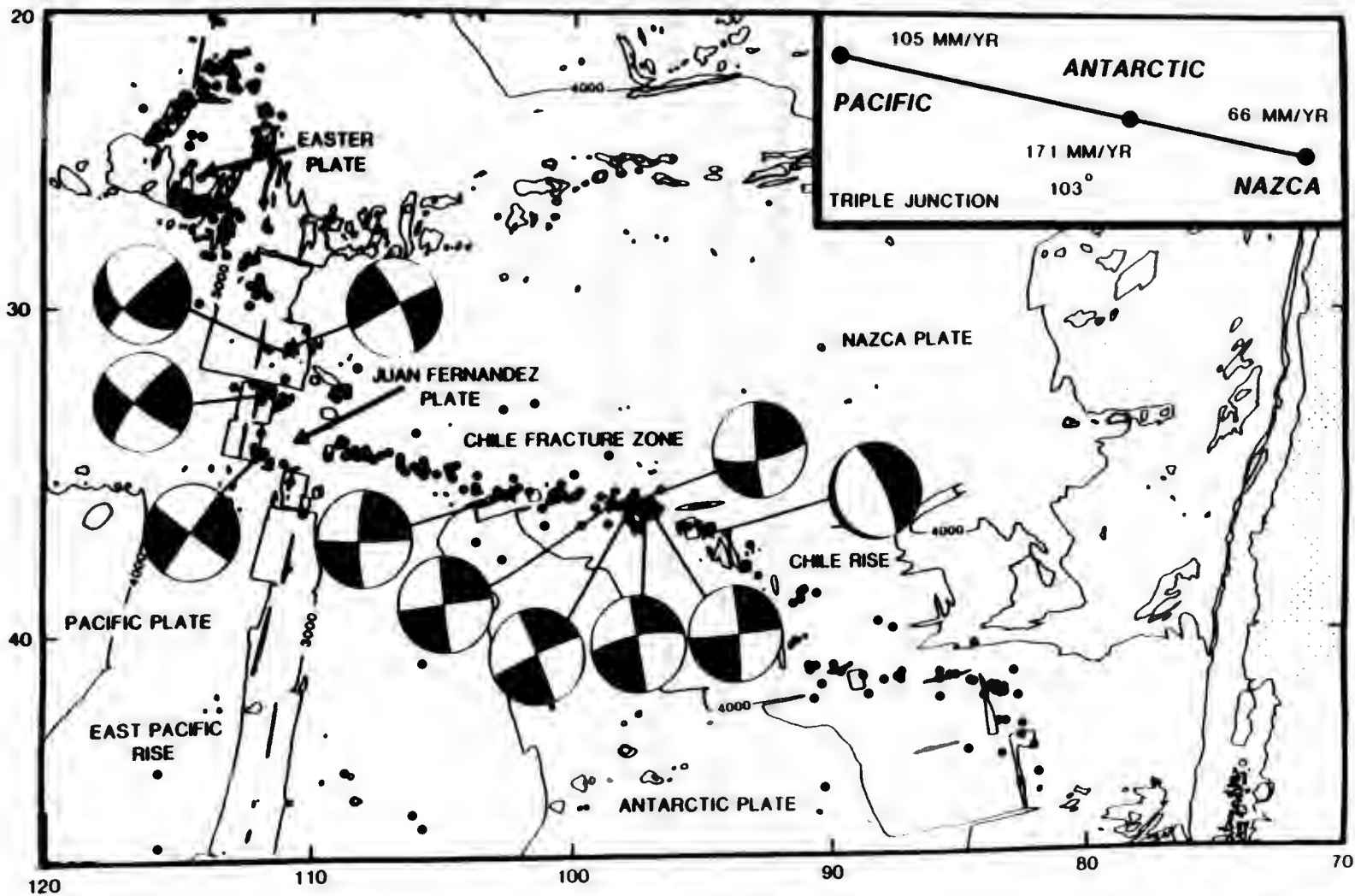


Fig. 1. Bathymetry [12], seismicity distribution, and focal mechanisms. The solid circles represent the earthquake epicenters from 1963 to 1979 as listed in the NGSDC data file; the stars represent the events for which mechanisms have been determined in this study and in Anderson-Fontana et al. [2]. The major plates and the Juan Fernandez and Easter microplates are indicated. The stippled area to the east is the western edge of South America. The diagram in the upper right corner represents the (in this case) degenerate velocity triangle that describes relative plate motion in model RM2 [7] at the Pacific-Antarctic-Nazca triple junction.





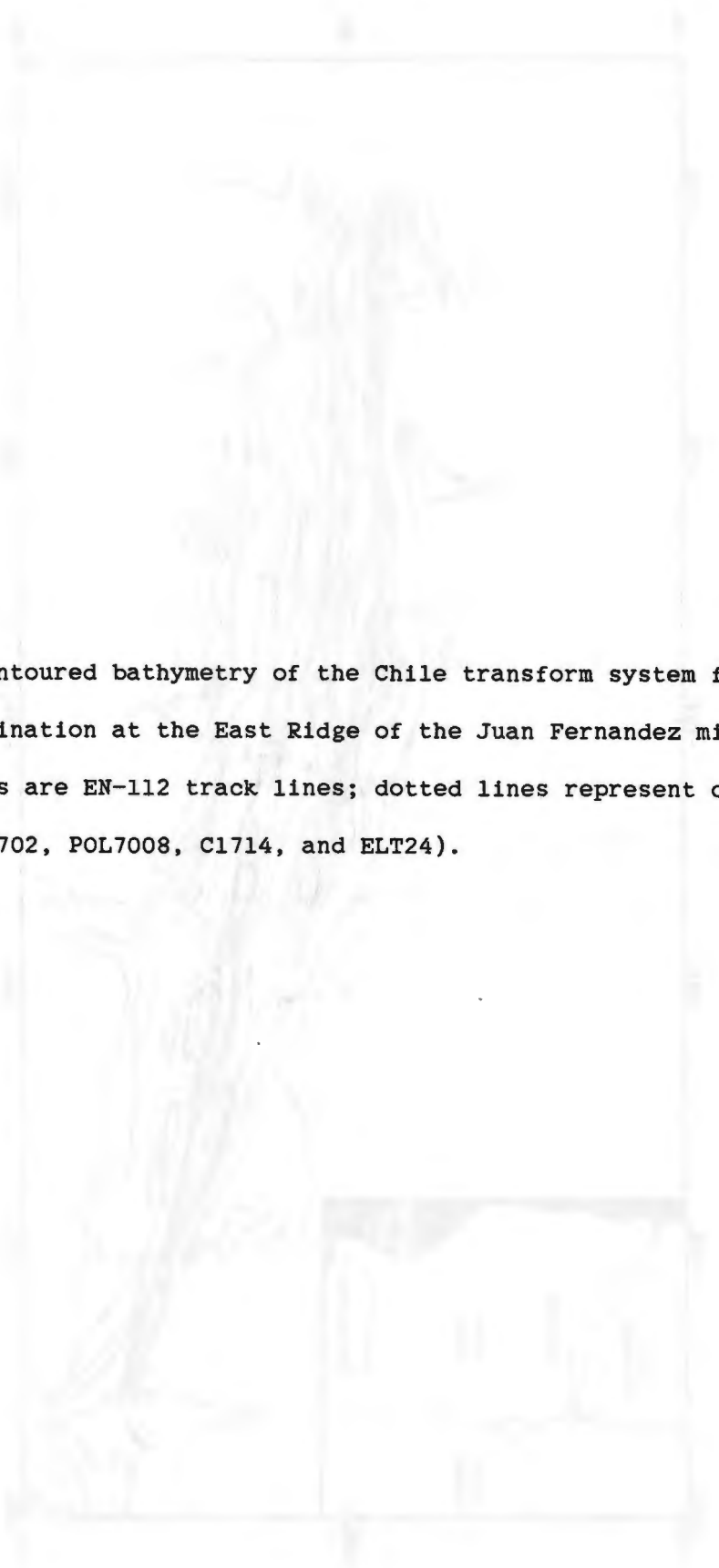
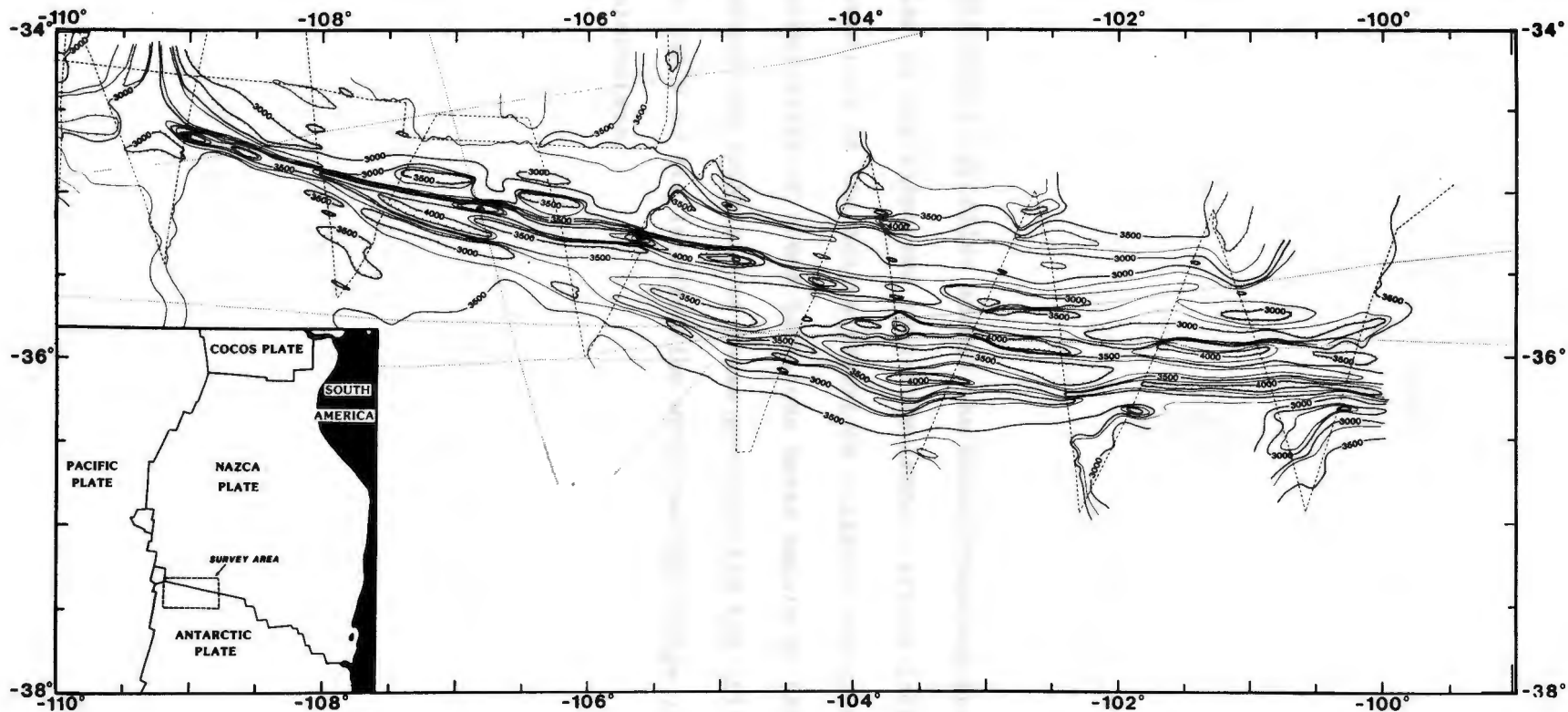


Fig. 2. Contoured bathymetry of the Chile transform system from  $100^{\circ}\text{W}$  to its termination at the East Ridge of the Juan Fernandez microplate. Dashed lines are EN-112 track lines; dotted lines represent older track lines (POL6702, POL7008, C1714, and ELT24).




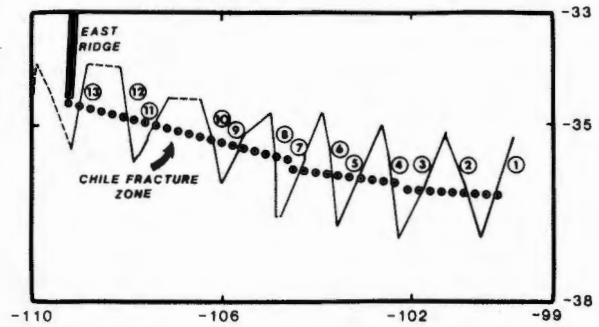
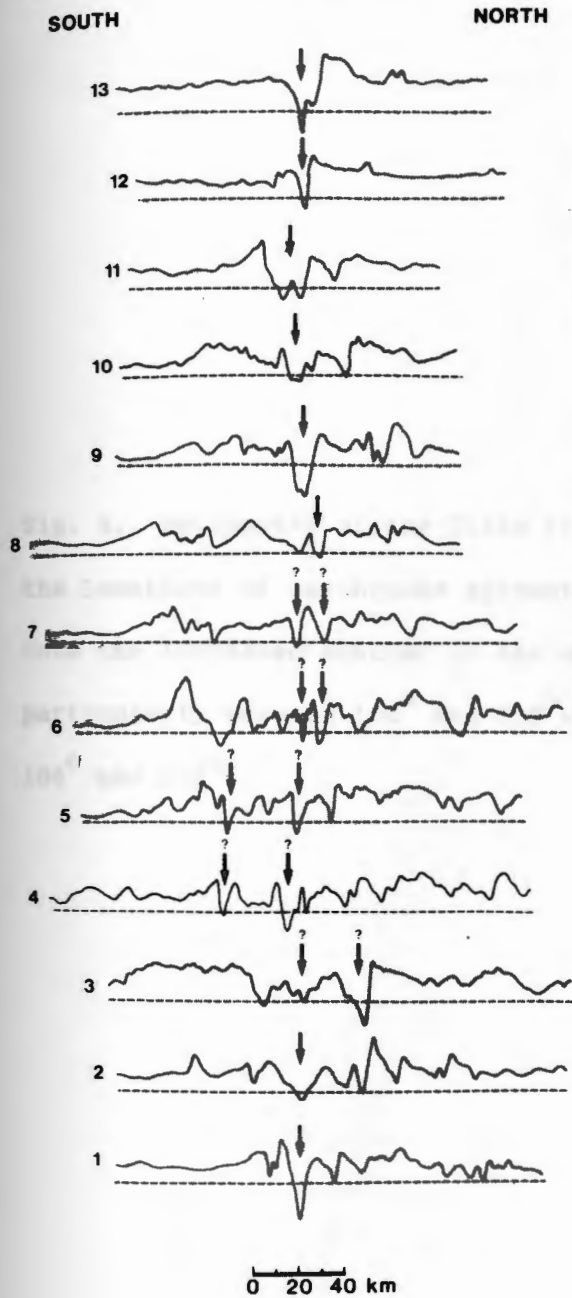


Fig. 3. Bathymetric profiles across the Chile Transform projected perpendicular to the suspected transform trend. Arrows indicate the probable locations of the active transform valleys; the question marks imply the uncertainty of these locations based solely on the bathymetry. The inset shows the locations of these profiles and the Chile transform system from  $100^{\circ}\text{W}$  to its intersection with the East Ridge of the Juan Fernandez microplate.

# PROJECTED BATHYMETRIC PROFILES



V.E. = 13.3



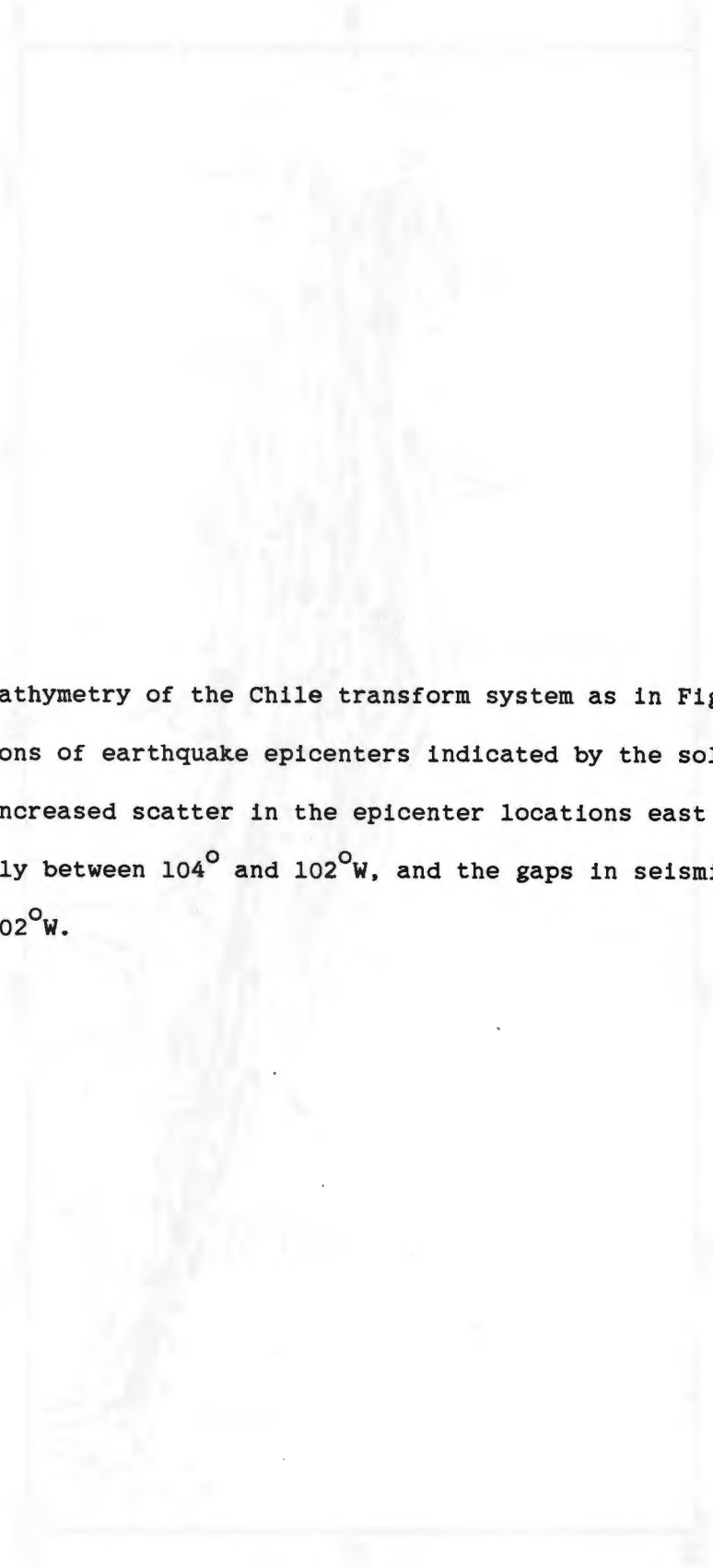


Fig. 4. Bathymetry of the Chile transform system as in Figure 2 with the locations of earthquake epicenters indicated by the solid circles. Note the increased scatter in the epicenter locations east of  $104^{\circ}30'W$ , particularly between  $104^{\circ}$  and  $102^{\circ}W$ , and the gaps in seismicity also at  $104^{\circ}$  and  $102^{\circ}W$ .

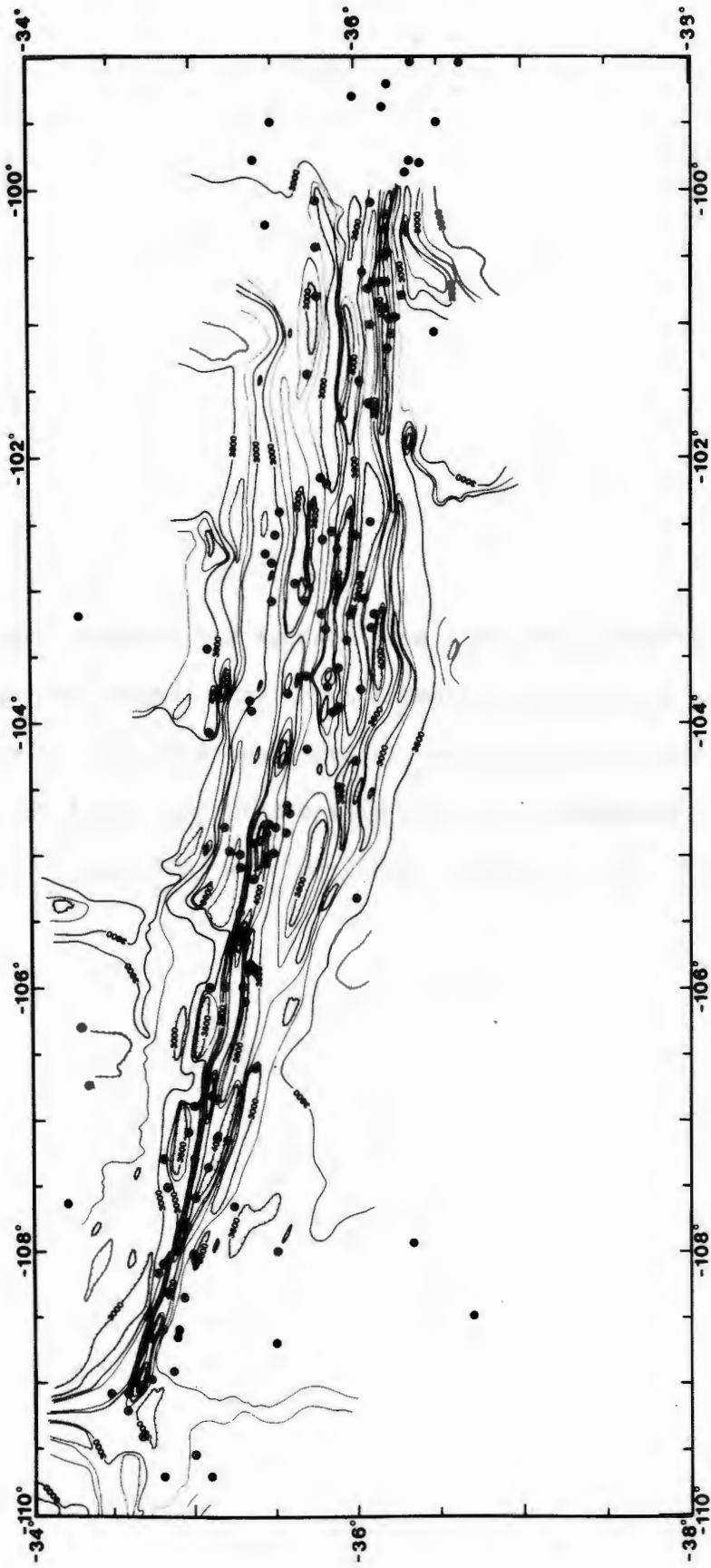
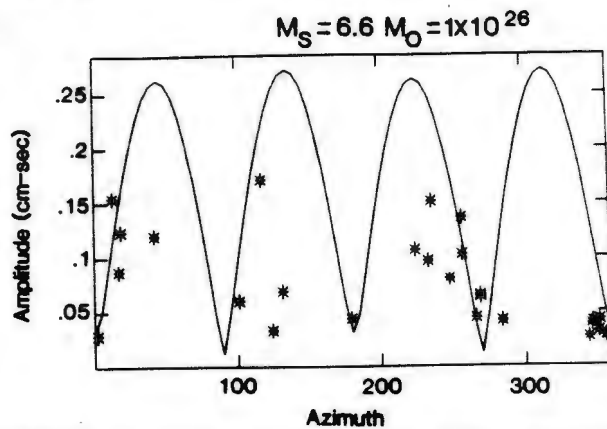
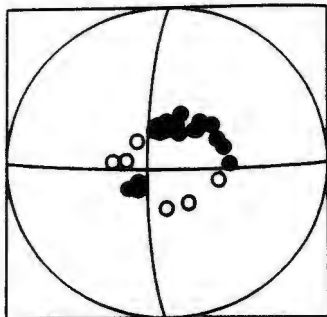


Fig. 5. First motions and surface wave amplitude patterns for three Chile Transform events. The north trending nodal planes are well constrained by first motions, with closed circles representing compressional arrivals, and strike-slip motion is suggested. Rayleigh wave patterns are interpreted as four-lobed, consistent with strike-slip motion.

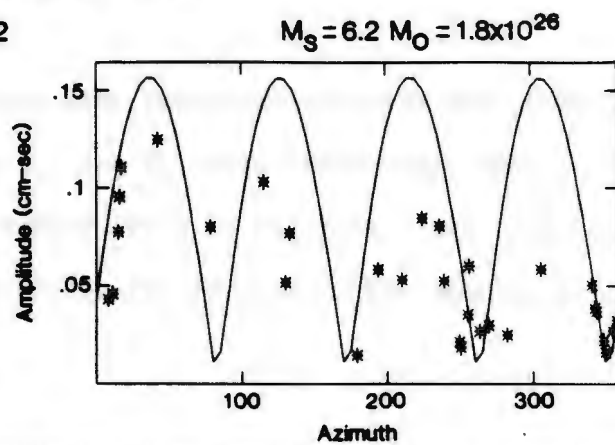
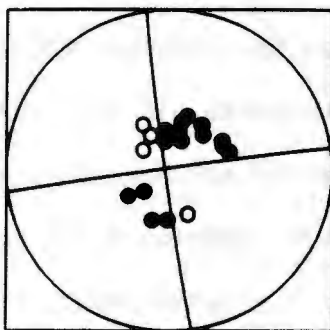
APRIL 14, 1979

STRIKE 90 DIP 86 SLIP 170



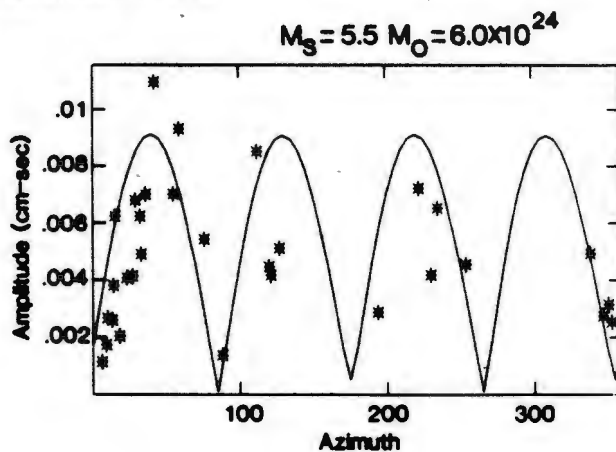
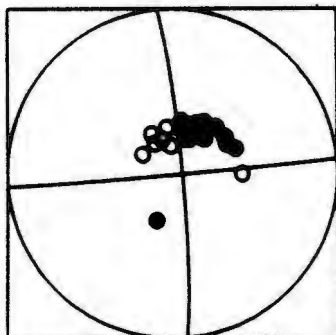
APRIL 20, 1975

STRIKE 262 DIP 89 SLIP 182



OCTOBER 23, 1970

STRIKE 85 DIP 89 SLIP 185



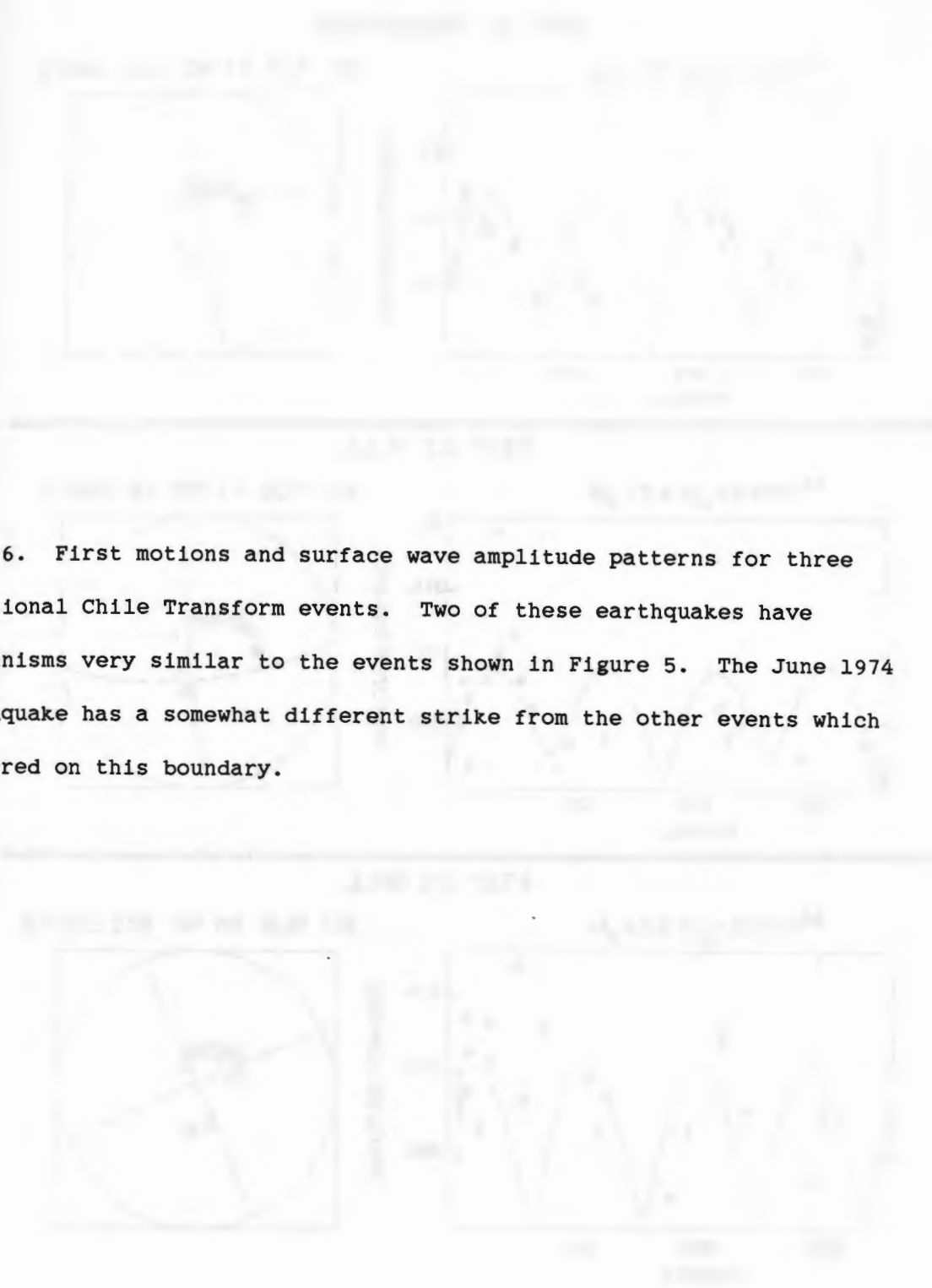
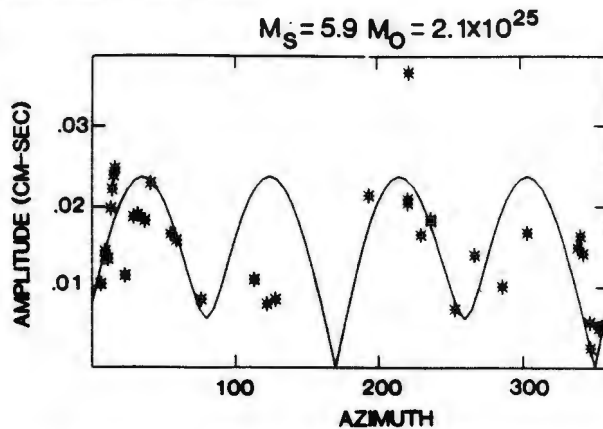
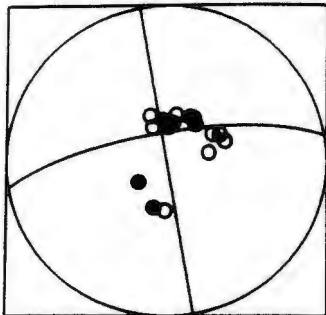


Fig. 6. First motions and surface wave amplitude patterns for three additional Chile Transform events. Two of these earthquakes have mechanisms very similar to the events shown in Figure 5. The June 1974 earthquake has a somewhat different strike from the other events which occurred on this boundary.



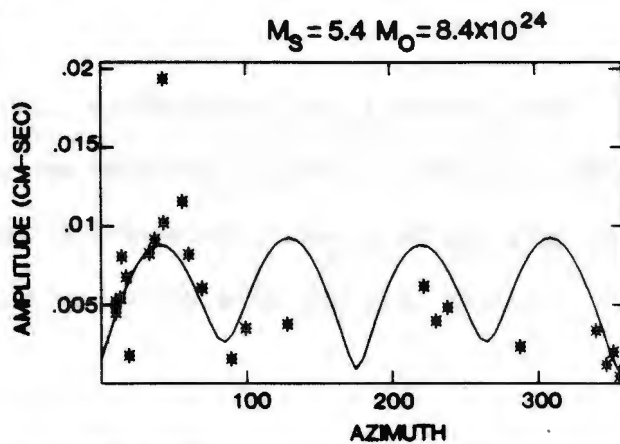
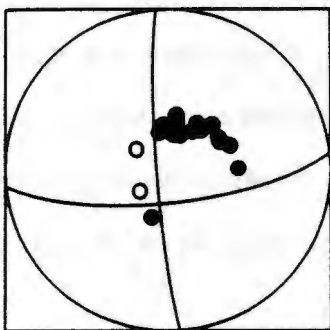
SEPTEMBER 13, 1965

STRIKE 260 DIP 75 SLIP 180



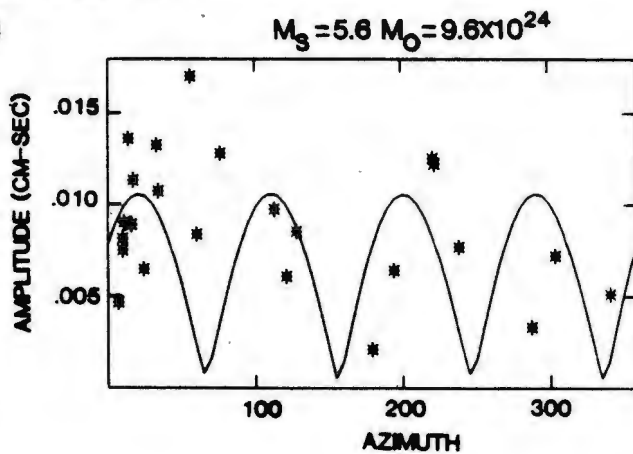
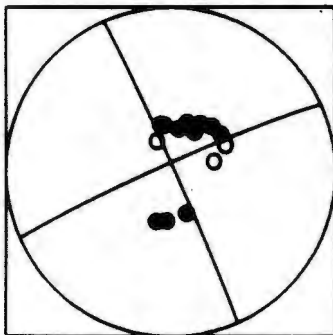
JULY 12, 1979

STRIKE 84 DIP 73 SLIP 174



JUNE 26, 1974

STRIKE 246 DIP 86 SLIP 186



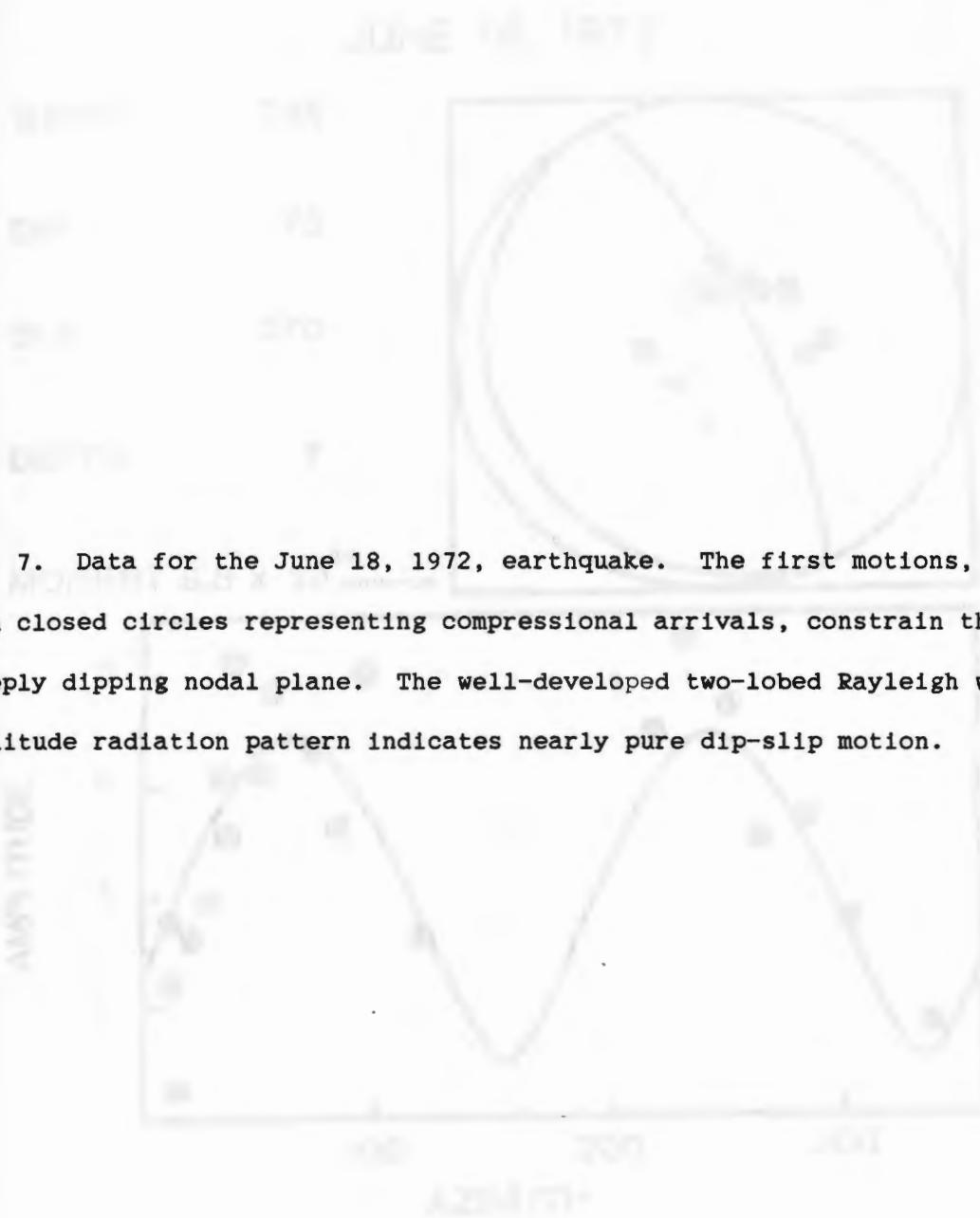
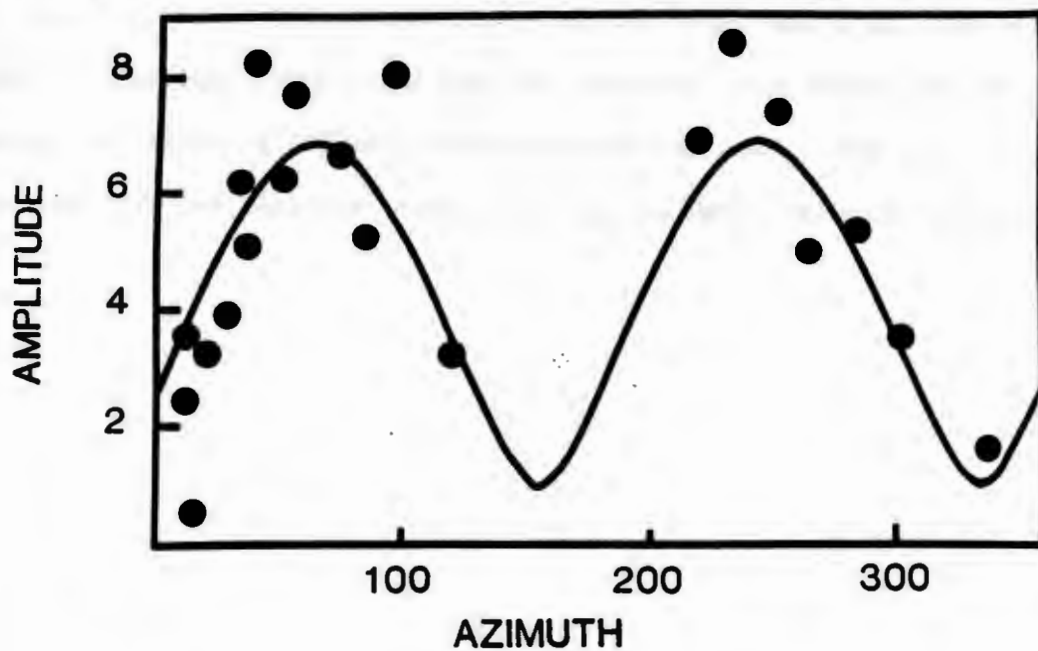
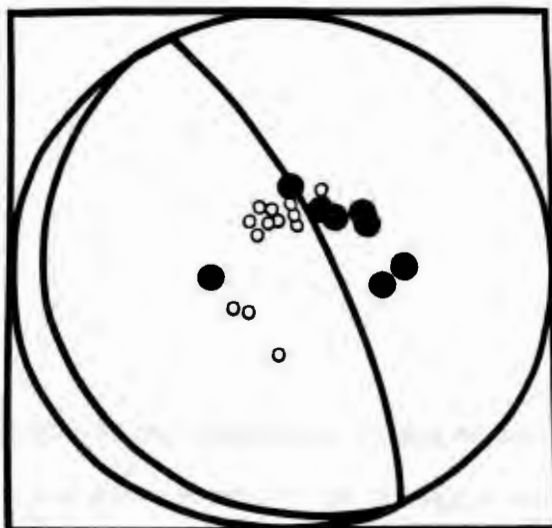


Fig. 7. Data for the June 18, 1972, earthquake. The first motions, with closed circles representing compressional arrivals, constrain the steeply dipping nodal plane. The well-developed two-lobed Rayleigh wave amplitude radiation pattern indicates nearly pure dip-slip motion.

JUNE 18, 1972

STRIKE 335  
 DIP 75  
 SLIP 270  
 DEPTH 7  
 MOMENT  $9.8 \times 10^{24}$  dyne-cm



## NAZCA-ANTARCTIC EULER POLES

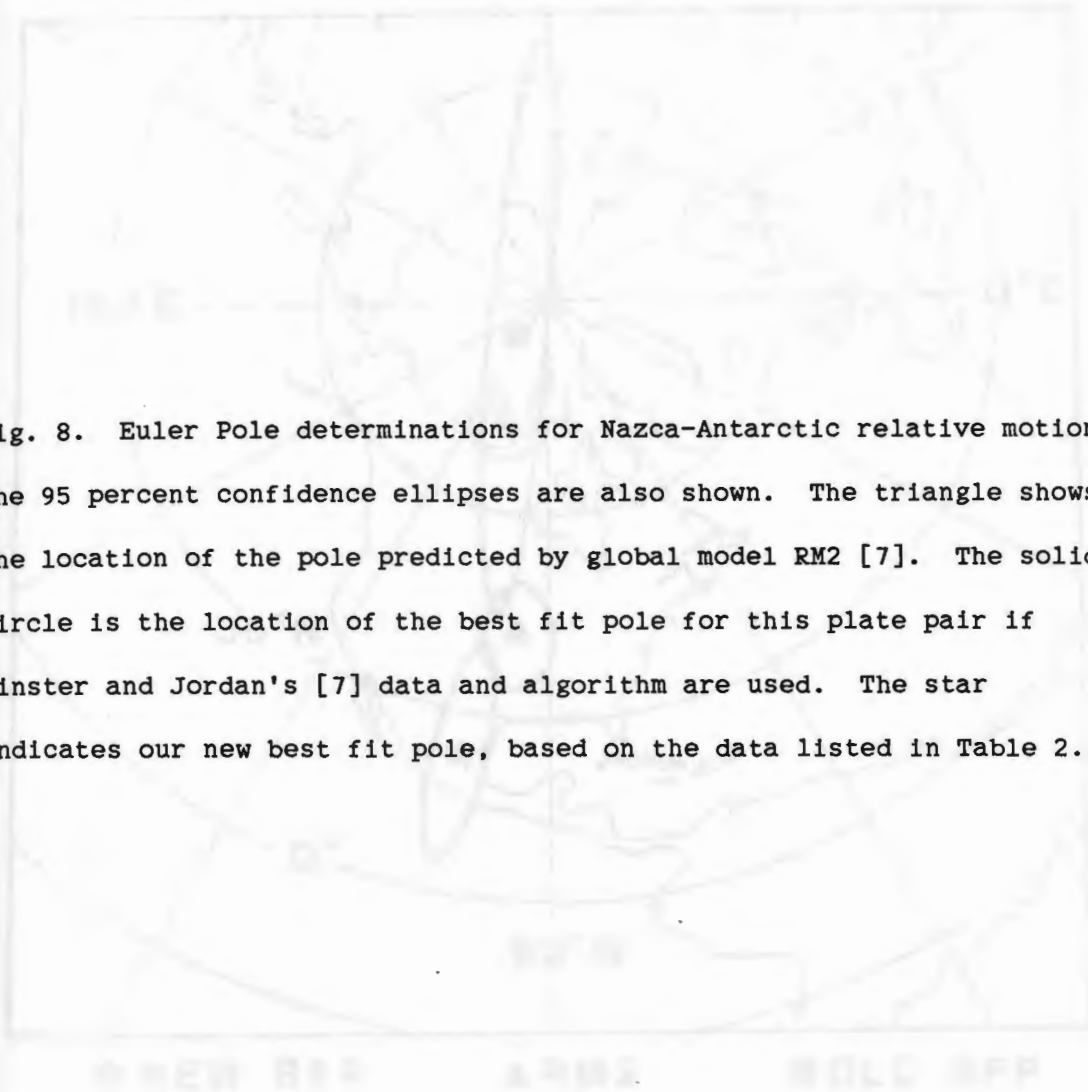
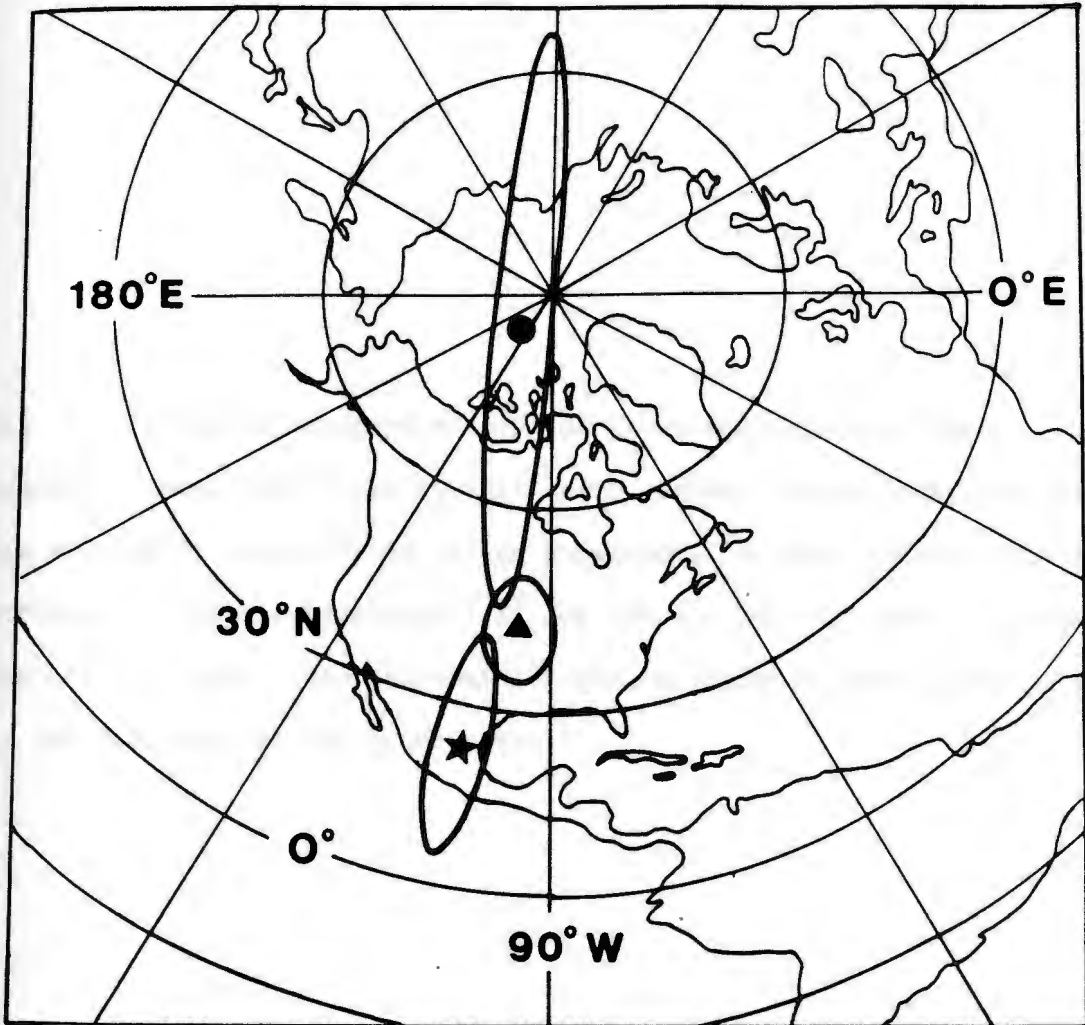


Fig. 8. Euler Pole determinations for Nazca-Antarctic relative motion. The 95 percent confidence ellipses are also shown. The triangle shows the location of the pole predicted by global model RM2 [7]. The solid circle is the location of the best fit pole for this plate pair if Minster and Jordan's [7] data and algorithm are used. The star indicates our new best fit pole, based on the data listed in Table 2.

## NAZCA-ANTARCTIC EULER POLES



★ NEW BFP

▲ ARM2

● OLD BFP



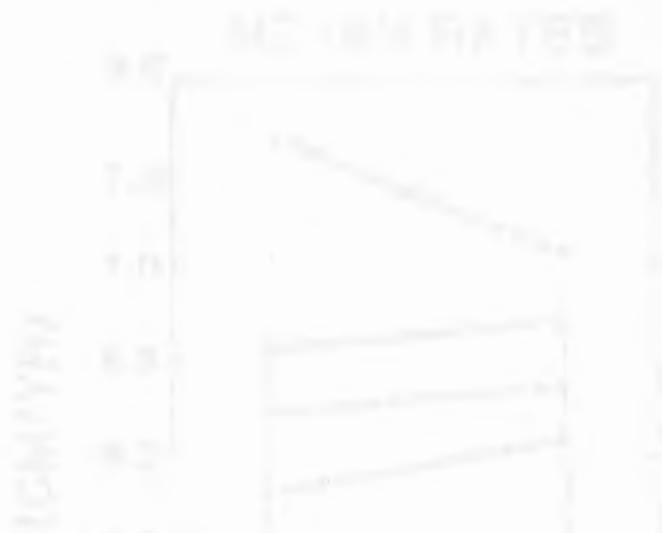
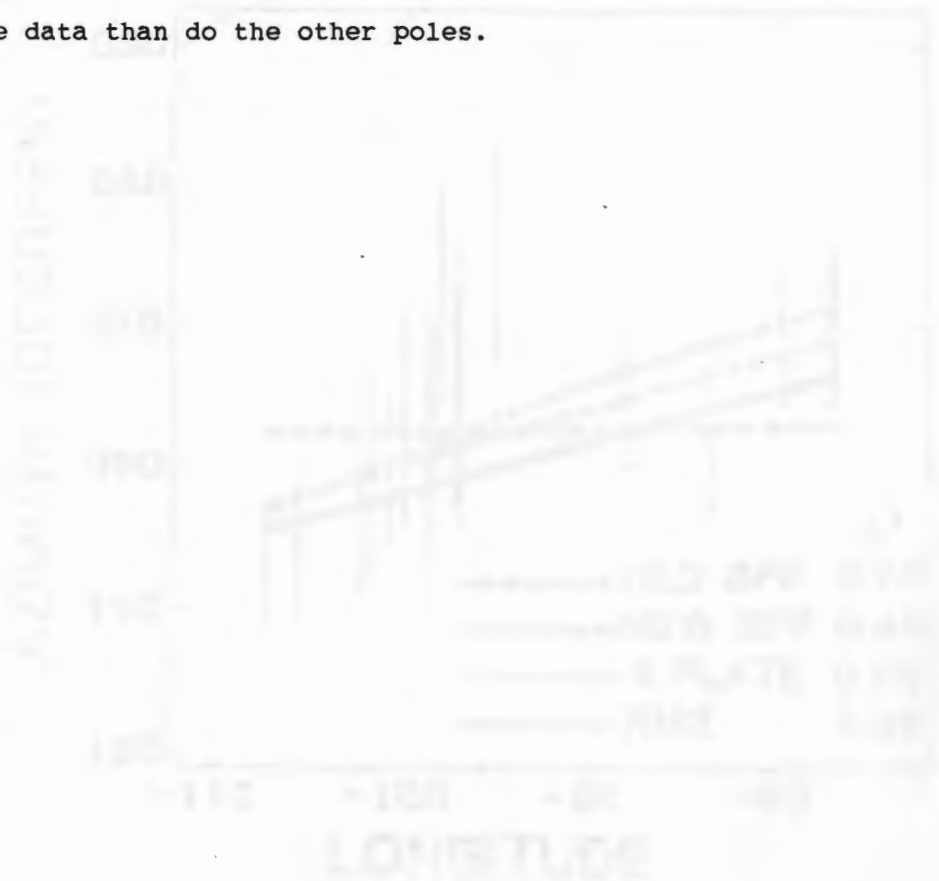
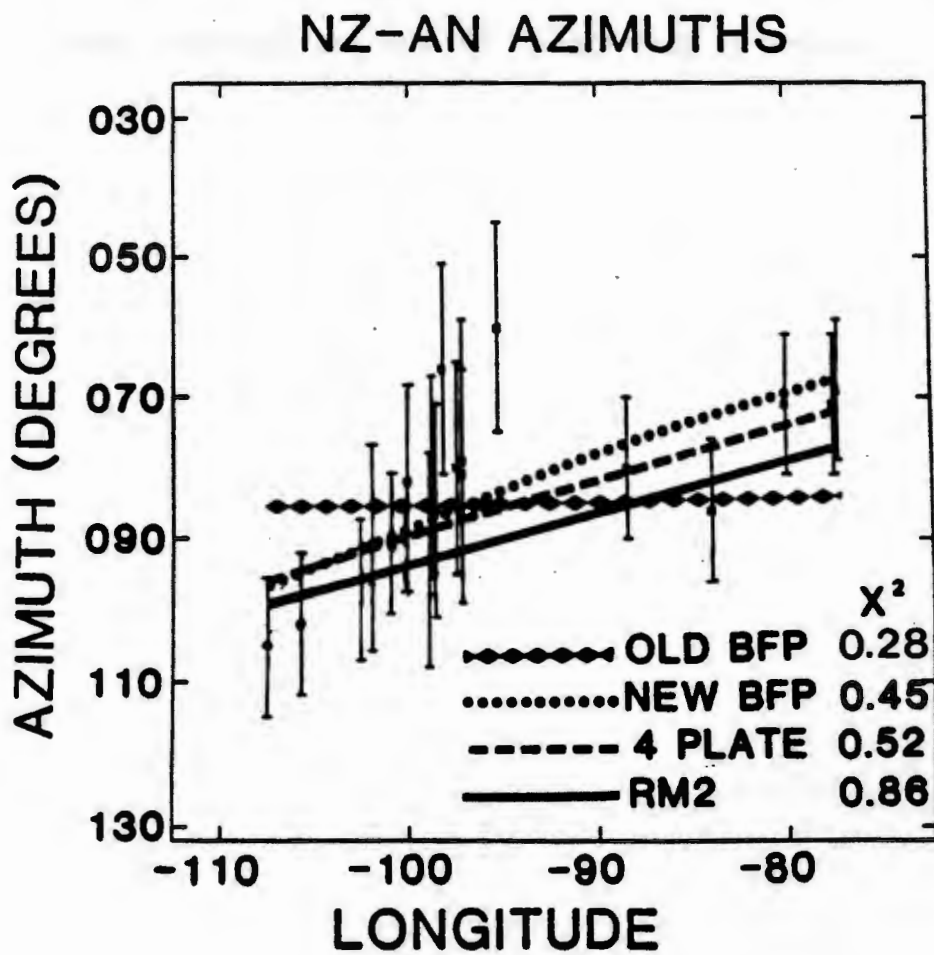
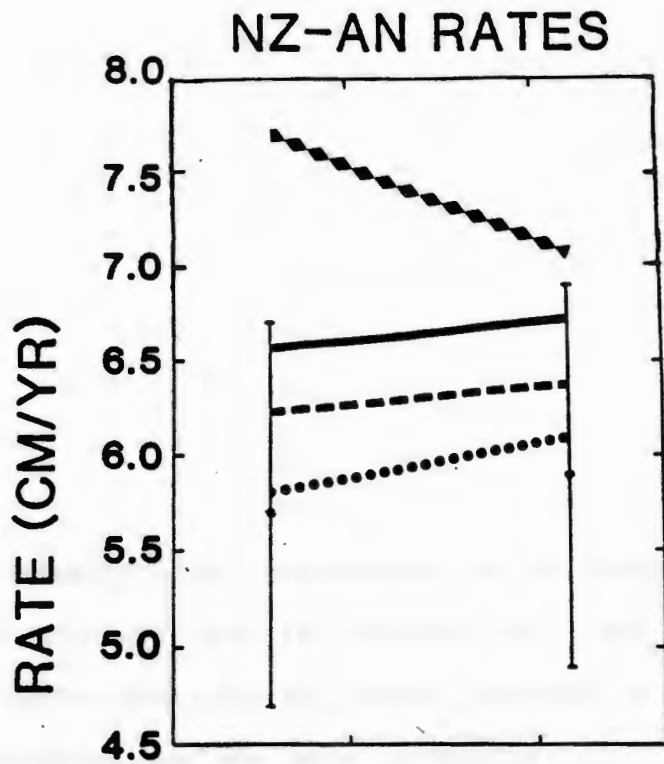


Fig. 9. Predicted relative motions on the Nazca-Antarctic plate boundary. Data from Table 2, with their standard deviations shown by the error bars, are plotted versus longitude. Motions predicted by the different poles are indicated.  $\chi^2$  for the old best fit pole is based on the RM2 data only. The new best fit pole provides a better overall fit to the data than do the other poles.





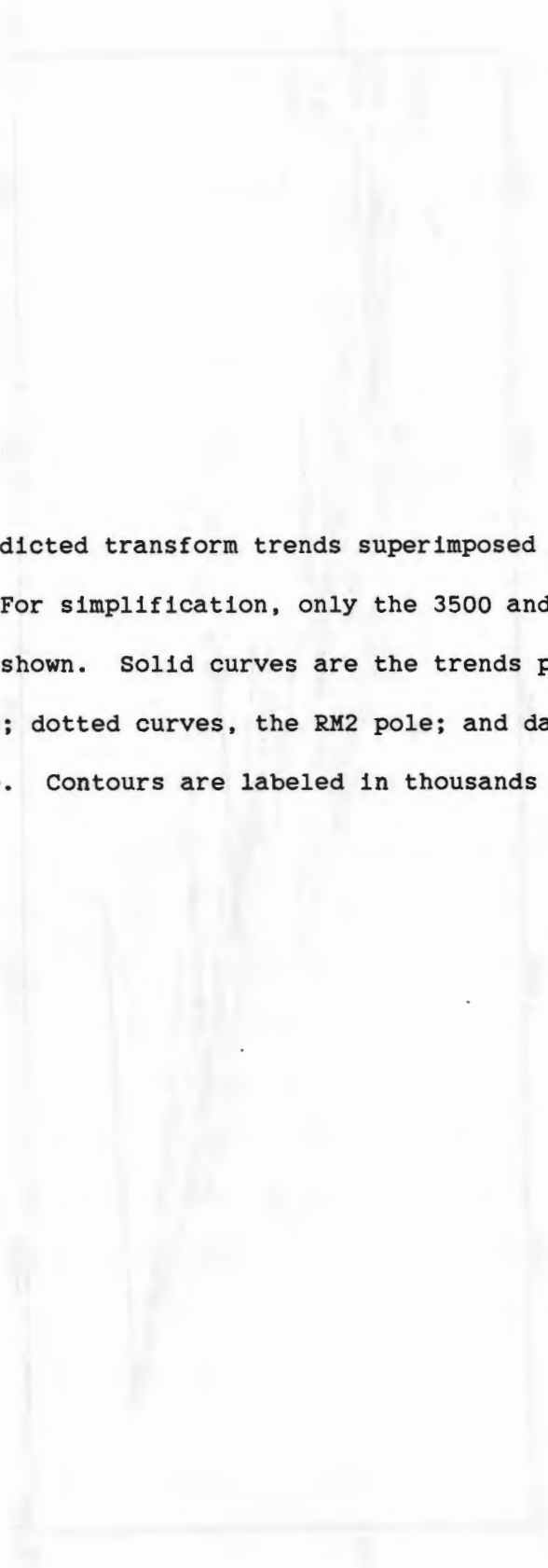
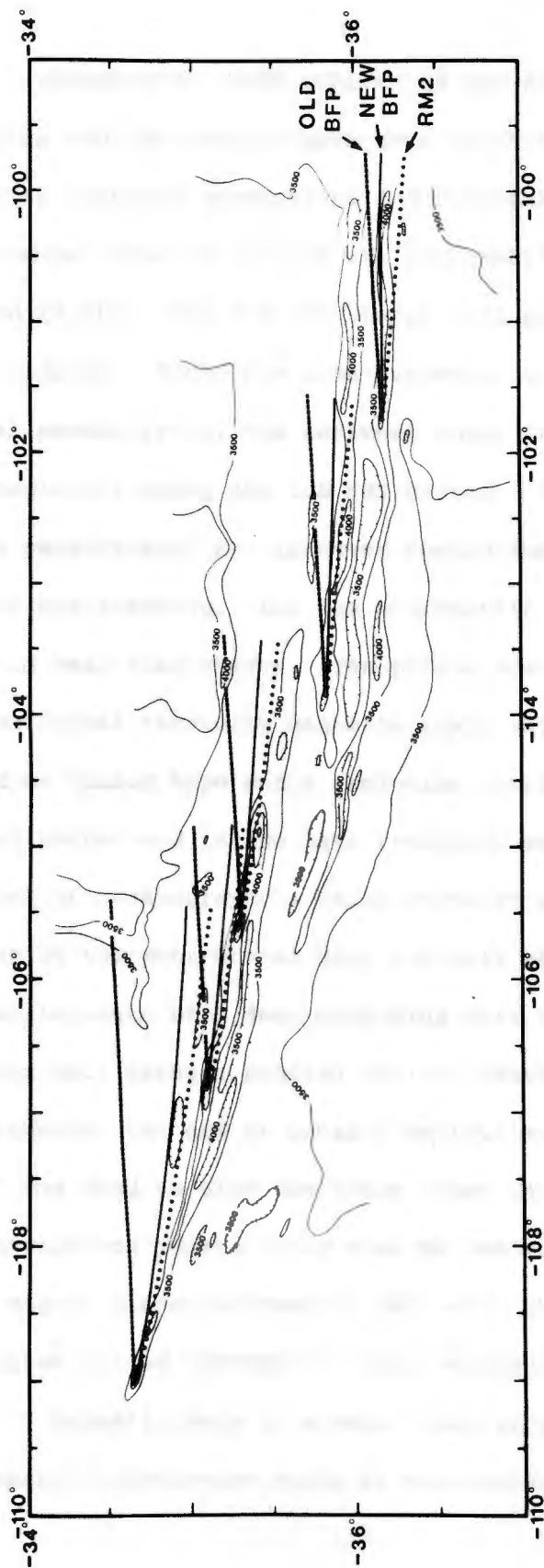


Fig. 10. Predicted transform trends superimposed on the Chile Transform bathymetry. For simplification, only the 3500 and 4000 m and greater contours are shown. Solid curves are the trends predicted by our new best fit pole; dotted curves, the RM2 pole; and dashed curves, the old best fit pole. Contours are labeled in thousands of meters.



## APPENDIX A: DATA COLLECTION AND REDUCTION

The magnetic and bathymetric data were collected on R/V Endeavor cruise 112 using standard geophysical instrumentation. Endeavor's echo sounding system was used to collect the bathymetric data at frequencies of 3.5 kHz and 12 kHz. The 3.5 kHz energy will penetrate through thin sediments to bedrock. Since the area surveyed is relatively young with low biological productivity, the sediment cover is thin enough to be penetrated completely using the 3.5 kHz system. The 12 kHz frequency provides less penetration, but improved resolution, facilitating on-board analyses and planning. All the bathymetric data were recorded on analog tape and real-time charts. The proton precision magnetometer was used to collect total intensity magnetic field data. These data were also recorded on analog tape and a real-time chart.

All the software used in the data reduction are available on the Graduate School of Oceanography's PRIME computer under BOBD>GEOPHYSLIB. The first step in the post-cruise data analysis was to combine the satellite position data with dead reckoning data to produce a best fit navigation data set, using a program called "CNAV". The remoteness of the region prevented the use of Loran C navigation. The program "CRUISETRACK" was used to plot the track lines on a Mercator projection. Obvious bad navigation points could then be removed. The next step was to merge the magnetic and bathymetric data with the navigational data using the program called "MERGE80". This included the reduction of the total intensity magnetic data to anomaly form by subtracting the International Geomagnetic Reference Field at each point [Peddie, 1982]. The



magnetic anomaly and bathymetric data were then plotted along track on a Mercator projection using the program "MERCPROF".

The next step was to select magnetic and bathymetric profiles for projection using the program "BTMAGPRJ". This program allows for projection of profiles along track, to a specified azimuth, or to a small circle through a specified point based on a given pole of rotation. In the projection process, magnetic anomaly profiles are zero-meaned, and both magnetic and bathymetric profiles are smoothed by a cubic spline fitting technique after interpolation to a 0.5 km spacing. Initial identifications of magnetic anomalies can then be made, along with calculations of spreading rates. Comparisons with the corresponding bathymetric profiles can also be made. This is followed by magnetic block modeling ("MDLMAG") to verify magnetic anomaly identifications, to further quantify spreading rates, and to summarize the recent spreading history. The completed two-dimensional block model consists of a continuous string of rectangles with a constant specified magnetization and layer thickness that are magnetized parallel or antiparallel to the earth's present-day magnetic field at that latitude. Paleofield directions can be used if the age of the model warrants it. The vertical boundaries of these rectangles are calculated from the chronology of geomagnetic field reversals at specific times (e.g., LaBrecque et al., 1977) and the estimated spreading velocities. Also specified in the model are present day and remanent magnetic field inclination and declination, and spreading center azimuth. The model magnetic anomaly profile is then computed from the block model and compared to the observed profile. Values of any of the input parameters can be changed

if necessary to calculate a model profile which best matches the observed profile.

The data used were only from the all-derivative data obtained from the relative velocity vectors obtained from the direction of relative motion derived from the relative velocity vectors and particularly the velocity.

According to the Euler theory, the instantaneous velocity of a rigid plate on the surface of a sphere can be completely determined by an initial position, an angular velocity vector  $\omega$  and a direction vector  $\mathbf{r}$ . In the corner problem, the components of relative velocity between the plates are the same as those between the plates and the sphere. If the components of the angular velocity vector are known, then the procedure for the determination of the relative velocity vectors is the same as that for the determination of the components of relative velocity vectors. The procedure involves iterative determination of a model starting from an initial guess and convergence is attained.

## APPENDIX B: PLATE MOTION INVERSION

The plate motion inversion program used in this study to obtain the Euler poles was written by Richard Gordon and Seth Stein (Northwestern University) using the Minster et al. [1974] relative plate motion inversion algorithm. The basic assumption made is that the specified plates are rigid. The fact that Minster et al. [1974] and Minster and Jordan [1978] produced rigid plate models that satisfactorily explained all the data (RM1 and RM2, respectively) argues in favor of this basic assumption. Symmetric and orthogonal spreading is also assumed. The data used were only from well-defined plate boundaries and included relative spreading rates calculated from magnetic anomaly profiles and directions of relative motions derived from transform fault trends and earthquake slip vectors.

According to the Euler theorem, the instantaneous motion of a rigid plate on the surface of a sphere can be completely and uniquely described by an axial rotation, or angular velocity vector [Minster et al., 1974]. In the forward problem, the components of relative velocity between two plates at any point on their common boundary can be computed if the parameters of the angular velocity vector are known. These parameters are rate of rotation and latitude and longitude of the rotation pole. In the inversion technique (or inverse problem) of Minster et al. [1974] and Minster and Jordan [1978] that was used in this study, we use observations of the components of relative velocities at plate boundaries to obtain the best representation of instantaneous motions in the form of angular velocity vectors. The procedure involves iterative perturbation of a chosen starting model until convergence is attained.

It is actually a least squares fitting technique in which the solution converges until a change in the model no longer makes the error function smaller. Minster et al. [1974] adapted the linear theory of maximum likelihood for use in their inversions which allowed them to statistically weight the data based on the level of uncertainty (a subjective evaluation of data quality), and to estimate the uncertainty attached to the model induced by errors in the data. They also developed the concept of data importances which depends on the nature and distribution of the data, and on the data uncertainties.

Since a linear technique is being applied to a nonlinear problem, it is important to construct a reasonably accurate starting model so the iterative procedure does not converge to a local minimum. Minster et al. [1974] demonstrated that the proximity of the final model to the starting model justified the use of a linear theory. They did local studies before constructing their global model (RM1), starting with published angular velocity vectors, and found that poles for the global model did not differ much from those obtained from the local studies. Minster and Jordan [1978] constructed their relative plate motion model, RM2, using a revised data set and RM1 as the starting model.

In the first part of this study (Manuscript I), we determined best fit and closure poles for the respective plate pairs in the Juan Fernandez four-plate system, and used these poles (angular velocity vectors) as the starting model in the four plate inversions. As described in Manuscript I, new data from this study and Engeln [1985] were used in addition to RM2 data (Table 3). A present day tectonic model could then be constructed for the Juan Fernandez microplate. In

the second part of this study (Manuscript II), a new data set from the Nazca-Antarctic plate boundary was inverted to produce a new best fit Euler pole for that plate pair.

- Leahy, J.L., *ibid.*, p. 119-124, 1974.
- Anderson-Daniels, G., J.P. English, S. Imagawa, S. A. Jordan, and R. Stein, *Estimation and prediction of the East Pacific rise: a test of the hot-spot-ridge-trench triple junction*, *J. Geophys. Res.*, **81**, 1987-1998, 1976.
- Cande, S.C., S.H. Haxel, and S.E. Hill, *The early Cenozoic history of the southern Pacific*, *Earth Planet. Sci. Lett.*, **26**, 17-24, 1975.
- Craig, A., R. S. Jay, and J. VandenBerg, *Graben ridge axial spreading at the East Pacific Rise*, *J. Geophys. Res.*, **81**, 1987-1998, 1976.
- Dunbar, N.W., *Introduction to Geophysical Astronomy*, McGraw-Hill, Inc., United States of America, 4th ed., 1979.
- Leahy, J.L., A. Friedman, H. Haxel, and J.H. VanDusen, *Geophysical evidence of 1960-1961 Cenozoic-terrestrial tectonic evolution for the Pacific region*, *J. Geophys. Res.*, **76**, 1970-1971, 1971.
- English, J.P., *Geological evidence on the separation of divergent plate boundaries*, Ph.D. thesis, 120 pp., Massachusetts Inst., Cambridge, 1973.
- English, J.P., *and co-workers, Separation of the Pacific plates*, *Earth Planet. Sci. Lett.*, **21**, 257-270, 1974.
- Frederick, P.W., *Geophysical evidence of plate motion in the East Pacific*, *Earth Planet. Sci. Lett.*, **21**, 189-194, 1974.



## BIBLIOGRAPHY

- Anderson, R.N., D.W. Forsyth, P. Molnar, and J. Mammerrickx, Fault plane solutions on the Nazca Plate boundaries and the Easter Plate, Earth Planet. Sci. Lett., 24, 188-202, 1974.
- Anderson-Fontana, S., J.F. Engeln, P. Lundgren, R.L. Larson, and S. Stein, Tectonics and evolution of the Juan Fernandez microplate at the Pacific-Nazca-Antarctic triple junction, J. Geophys. Res., 91, 2005-2018, 1986.
- Cande, S.C., E.M. Herron, and B.R. Hall, The early Cenozoic history of the southeast Pacific, Earth Planet. Sci. Lett., 56, 63-74, 1982.
- Craig, H., K.-R. Kim, and J. Francheteau, Active ridge crest mapping on the Juan Fernandez micro-plate: The use of SEABEAM-controlled hydrothermal plume surveys, Eos Trans. AGU, 64, 45, 1983.
- Dobrin, M.B., Introduction to Geophysical Prospecting, McGraw-Hill, Inc., United States of America, 630 pp., 1976.
- Dziewonski, A.M., A. Friedman, D. Giardini, and J.H. Woodhouse, Global seismicity of 1982: Centroid-moment tensor solutions for 308 earthquakes, Phys. Earth Planet. Inter., 33, 76-90, 1983.
- Engeln, J.F., Seismological studies of the tectonics of divergent plate boundaries, Ph.D. thesis, 138 pp., Northwestern Univ., Evanston, Ill., 1985.
- Engeln, J.F., and S. Stein, Tectonics of the Easter plate, Earth Planet. Sci. Lett., 68, 259-270, 1984.
- Forsyth, D.W., Mechanisms of earthquakes and plate motions in the East Pacific, Earth Planet. Sci. Lett., 17, 189-194, 1972.

- Fox, P.J., and D.G. Gallo, A tectonic model for ridge-transform-ridge plate boundaries: Implications for the structure of oceanic lithosphere, Tectonophysics, 104, 205-242, 1984.
- Fukao, Y., Focal process of a deep-focus earthquake as deduced from long period P and S waves, Bull. Earthquake Res. Inst., 48, 707-727, 1970.
- Handschumacher, D.W., Post-Eocene tectonics of the Eastern Pacific, in The Geophysics of the Pacific Ocean Basin and Its Margin, Geophys. Monogr. Ser., vol. 19, edited by G.H. Sutton, M.H. Manghnani, and R. Moberly, pp. 117-202, AGU, Washington, D.C., 1976.
- Herron, E.M., Two small crustal plates in the South Pacific near Easter Island, Nature Phys. Sci., 240, 35-37, 1972a.
- Herron, E.M., Sea-floor spreading and the Cenozoic history of the East-Central Pacific, Geol. Soc. Am. Bull., 83, 1671-1692, 1972b.
- Herron, E.M., S.C. Cande, and B.R. Hall, An active spreading center collides with a subduction zone: A geophysical survey of the Chile Margin triple junction, Geol. Soc. Am. Mem., 154, 683-702, 1981.
- Hey, R.N., A new class of "pseudofaults" and their bearing on plate tectonics: A propagating rift model, Earth. Planet. Sci. Lett., 37, 321-325, 1977.
- Hey, R.N., and D.S. Wilson, Propagating rift explanation for the tectonic evolution of the northeast Pacific--The pseudomovie, Earth. Planet. Sci. Lett., 58, 167-188, 1982.
- Hey, R.N., D.F. Naar, M.C. Kleinrock, W.J. Phipps Morgan, E. Morales, and J.-G. Schilling, Microplate tectonics along a superfast seafloor spreading system near Easter Island, Nature, 317, 320-325, 1985.

- Hilde, T.W.C., S. Uyeda, and L. Kroenke, Tectonic history of the Western Pacific, in Geodynamics Progress and Prospects, edited by C.L. Drake, pp. 1-15, AGU, Washington, D.C., 1976.
- Kanamori, H., and G.S. Stewart, Mode of the strain release along the Gibbs Fracture Zone, Phys. Earth Planet. Inter., 11, 312-332, 1976.
- Kennett, J.P., Marine Geology, Prentice-Hall, Inc., Englewood Cliffs, N.J., 813 pp., 1982.
- Klitgord, K.D., J.D. Mudie, P.A. Larson, and J.A. Grow, Fast sea-floor spreading on the Chile Ridge, Earth Planet. Sci. Lett., 20, 93-99, 1973.
- LaBrecque, J.L., D.V. Kent, and S.C. Cande, Revised magnetic polarity time scale for Late Cretaceous and Cenozoic time, Geology, 5, 330-335, 1977.
- Lancelot, Y., and R.L. Larson, Sedimentary and tectonic evolution of the Northwestern Pacific, in Initial Reports of the Deep-Sea Drilling Project, vol. 32, edited by R.L. Larson et al., pp. 925-939, 1975.
- Langston, C.A., and D.V. Helmsberger, A procedure for modelling shallow dislocation sources, Geophys. J. R. Astron. Soc., 42, 117-130, 1975.
- Macdonald, K.D., K. Kastens, S. Miller, and F.N. Spiess, Deep-tow studies of the Tamayo transform fault, Mar. Geophys. Res., 4,
- Mammerickx, J., and S.M. Smith, Bathymetry of the Southeast Pacific, Geol. Soc. Am. Map Chart Ser., MC-26 442, 194, 1978.
- Mammerickx, J., E. Herron, and L. Dorman, Evidence for two fossil spreading ridges in the southeast Pacific, Geol. Soc. Am. Bull., 91, 263-271, 1980.

- McElhinny, M.W., Paleomagnetism and Plate Tectonics, Cambridge Univ. Press, London, 358 pp., 1973.
- Mendenhall, W., R.L. Scheaffer, and D.D. Wackerly, Mathematical Statistics with Applications, Wadsworth, Inc., Belmont, Calif., 686 pp., 1981.
- Minster, J.B., and T.H. Jordan, Present-day plate motions, J. Geophys. Res., 83, 5331-5354, 1978.
- Minster, J.B., T.H. Jordan, P. Molnar, and E. Haines, Numerical modeling of instantaneous plate tectonics, Geophys. J. R. Astron. Soc., 36, 541-576, 1974.
- Peddie, N.W., International geomagnetic reference field: The third generation, J. Geomag. Geoelec., 34, 309-326, 1982.
- Rea, D.K., Analysis of a fast-spreading rise crest: The East Pacific Rise,  $9^{\circ}$  to  $12^{\circ}$  South, Mar. Geophys. Res., 2, 291-313, 1976a.
- Rea, D.K., Changes in the axial configuration of the East Pacific Rise near  $6^{\circ}$ S during the past 2 m.y., J. Geophys. Res., 81, 1495-1504, 1976b.
- Rea, D.K., Local axial migration and spreading rate variations, East Pacific Rise,  $31^{\circ}$ S, Earth Planet. Sci. Lett., 34, 78-84, 1977.
- Rea, D.K., Evolution of the East Pacific Rise between  $3^{\circ}$ S and  $13^{\circ}$ S since the middle Miocene, Geophys. Res. Lett., 5, 561-564, 1978.
- Rea, D.K., Tectonics of the Nazca-Pacific divergent plate boundary, Geol. Soc. Am. Mem., 154, 27-62, 1981.
- Stover, C.W., Seismicity and tectonics of the East Pacific Ocean, J. Geophys. Res., 78, 5209-5220, 1973.

Tamaki, K., M. Joshima, and R.L. Larson, Remanent Early Cretaceous spreading center in the Central Pacific Basin, J. Geophys. Res., 84, 4501-4510, 1979.

Vacquier, V., Geomagnetism in Marine Geology, Elsevier Publishing Co., Amsterdam, 185 pp., 1972.

Weissel, J.K., D.E. Hayes, and E.M. Herron, Plate tectonics synthesis: the displacements between Australia, New Zealand, and Antarctica since the late Cretaceous, Mar. Geol., 25, 231-277, 1977.